TECHNICAL REPORT RG-CR-84-2

(12)

GRADIENT INDEX LENS RESEARCH

Prepared by:
Duncan T. Moore
The Institute of Optics
University of Rochester
Rochester, New York 14627

Prepared for:
Guidance and Control Directorate
US Army Missile Laboratory

November 1982

U.S. ARMY MISSILE COMMAND
Redstone Arsenal, Alabama 35898

Cleared for public release; distribution unlimited.

DISPOSITION INSTRUCTIONS

DESTROY THIS REPORT WHEN IT IS NO LONGER NEEDED. DO NOT RETURN IT TO THE ORIGINATOR.

DISCLAIMER

THE FINDINGS IN THIS REPORT ARE NOT TO BE CONSTRUED AS AN OFFICIAL DEPARTMENT OF THE ARMY POSITION UNLESS SO DESIGNATED BY OTHER AUTHORIZED DOCUMENTS.

TRADE NAMES

USE OF TRADE NAMES OR MANUFACTURERS IN THIS REPORT DOES NOT CONSTITUTE AN OFFICIAL INDORSEMENT OR APPROVAL OF THE USE OF SUCH COMMERCIAL HARDWARE OR SOFTWARE.

UNCLASSIFIED

SECURITY CLASSIFICATION OF THIS PAGE *(When Data Entered)*

REPORT DOCUMENTATION PAGE		READ INSTRUCTIONS BEFORE COMPLETING FORM
1. REPORT NUMBER TR-RG-CR-84-2	2. GOVT ACCESSION NO. AD-A145544	3. RECIPIENT'S CATALOG NUMBER
4. TITLE *(and Subtitle)* Gradient Index Lens Research		5. TYPE OF REPORT & PERIOD COVERED Final Report, 8/1/81 to 8/30/82 6. PERFORMING ORG. REPORT NUMBER
7. AUTHOR(s) Duncan T. Moore		8. CONTRACT OR GRANT NUMBER(s) 81 DAAH01-C-BC42
9. PERFORMING ORGANIZATION NAME AND ADDRESS The Institute of Optics University of Rochester Rochester, New York 14627		10. PROGRAM ELEMENT, PROJECT, TASK AREA & WORK UNIT NUMBERS
11. CONTROLLING OFFICE NAME AND ADDRESS Commanding General, US Army Missile Command ATTN: DRSMI-RPT Redstone Arsenal, AL 35898		12. REPORT DATE November 25, 1982 13. NUMBER OF PAGES
14. MONITORING AGENCY NAME & ADDRESS*(if different from Controlling Office)*		15. SECURITY CLASS. *(of this report)* UNCLASSIFIED 15a. DECLASSIFICATION/DOWNGRADING SCHEDULE

16. DISTRIBUTION STATEMENT *(of this Report)*

Cleared for public release; distribution unlimited.

17. DISTRIBUTION STATEMENT *(of the abstract entered in Block 20, if different from Report)*

18. SUPPLEMENTARY NOTES

19. KEY WORDS *(Continue on reverse side if necessary and identify by block number)*

Gradient Index	Infrared Materials
Optics	Infrared Measurements
Ellipsometry	Optical Design
Optical Measurements	

20. ABSTRACT *(Continue on reverse side if necessary and identify by block number)*

This contract has been divided into four major tasks. A method for non-destructive testing of any gradient index sample independent of a base index of refraction has been developed. The method is based on ellipsometry and permits the index of refraction to be measured for both visible and infrared wavelengths in a semi-automatic way. The technique, called Phase Lock Ellipsometry, measures the surface index of refraction. A number of indices of refraction can be measured with this, particularly those that transmit only in the infrared portion of the spectrum. These include zinc selenide, cadmium

DD FORM 1 JAN 73 1473 EDITION OF 1 NOV 65 IS OBSOLETE (Over)

SECURITY CLASSIFICATION OF THIS PAGE *(When Data Entered)*

sulfide, zinc sulfide and glass samples.

A gradient index germanium component has been fabricated using a gradient of silicon and germanium. The index change in the sample is 0.13 and the depth of the gradient is approximately 10 mm. This type of sample is well suited for FLIR-type optics.

An f/2 imaging system with a field of view of 20 degrees has been designed for infrared imagery. Finally, the techniques for manufacturing large radial gradients have been investigated. Two general techniques were investigated. Electric field assisted diffusions and phase separated glasses. Neither technique was completely successful and more work needs to be done on each of them. A brief summary of the problems of each is included.

Table of Contents

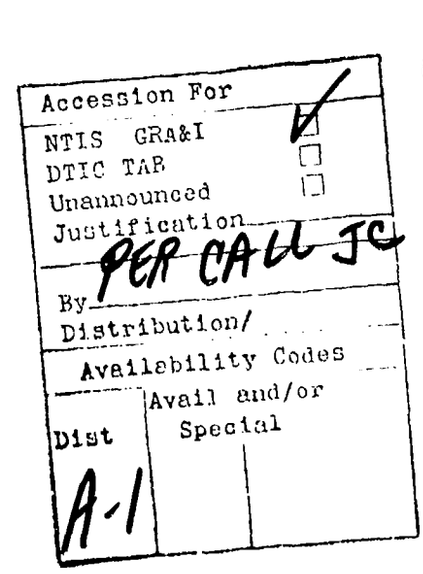

ABSTRACT

This Contract has been divided into four major tasks. A method for non-destructive testing of any gradient index sample independent of a base index of refraction has been developed. The method is based on ellipsometry and permits the index of refraction to be measured for both visible and infrared wavelengths in a semi-automatic way. The technique, called Phase Lock Ellipsometry, measures the surface index of refraction. A number of indices of refraction can be measured with this, particularly those that transmit only in the infrared portion of the spectrum. These include zinc selenide, cadmium sulfide, zinc sulfide and glass samples.

A gradient index germanium component has been fabricated using a gradient of silicon and germanium. The index change in the sample is 0.13 and the depth of the gradient is approximately 10 mm. This type of sample is well suited for FLIR-type optics.

A f/2 imaging system with a field of view of 20 degrees has been designed for infrared imagery. Finally, the techniques for manufacturing large radial gradients have been investigated. Two general techniques were investigated. Electric field assisted diffusions and phase separated glasses. Neither technique was completely successful and more work needs to be done on each of them. A brief summary

of the problems of each is included.

INTRODUCTION

This report has been divided into six main sections designated by their tasks. The first two sections give the theory of a new type of instrument based on the concepts of phase-lock interferometry and ellipsometry. In conventional ellipsometry, the angle of polarization is measured after reflection from an absorbing surface. These techniques do not, generally, work very well for dielectrics where the absorption is fairly low. However, by employing the techniques of phase-lock interferometry developed over the last ten years at The Institute of Optics, the index of refraction can be measured even for dielectric materials. The advantage of this method is that it can work not only for materials with an index of refraction of 1.5 but for those of any index at any wavelength band. The method is a reflection technique and, therefore, all that is necessary is a source operating at that wavelength. This method also provides absolute index of refraction rather than relative index of refraction as was the case with standard interferometry. Sections I and II describe the theory of this instrument.

The third section describes the design of a mapping lens operating at f/2. This is a design that is an extension of work which was done previously for the visible portion of the spectrum. The most significant differences are the change of base index of refraction which lowered the index of refraction

gradient.

The fourth and fifth sections describe the technique for making gradient index germanium and, in particular, a sample which is being delivered as a portion of this contract. The method is that of Czochralski crystal growth using a seed of germanium and using silicon as a dopant. The index of refraction change is .13 and the depth of the gradient is 10 mm. The exact index of refraction profile is also given. This measurement has been confirmed by other techniques, including laser beam deflection.

The final section is devoted to a short analysis of the technique for making large geometry radial gradients. There have been two methods proposed for this - that of phase separated glasses and electric field assisted diffusions. The original orientation in this work was to see if phase separated glasses could be used for this technique. However, as work progressed, it became more and more difficult to obtain the necessary materials to perform the work and an alternative technique was studied - that of electric field assisted diffusions. This was far more successful. A short analysis of the two techniques is given with suggestions for future research.

Section 1

Introduction - Ellipsometry

While the commercial applications of gradient index optics are still limited to GRIN rod lenses in photocopier arrays and medical endoscopes, and gradient index fibers for communication, recent work strongly suggests increased usefulness of gradients in the near future.

A historical view of the development of gradient index optics is given by Marchand[1] and Moore.[2] A recent overview of this subject is presented by Moore.[3] A number of applications of GRIN rod lenses in optical fiber communication systems have been described, such as connectors, attenuators, directional couplers, switches, isolators and wavelength-division multiplexers[4] and some are beginning to come into use. Feasibility of GRIN rods as imaging relay systems in the one to three meter range in the visible and IR has been shown theoretically.[5] A radial gradient singlet was shown to have enough degrees of freedom to meet the specifications of a 4 element homogeneous binocular objective and to correct the paraxial axial color and axial secondary spectrum.[6] A two-element photographic objective was designed using radial gradients to give comparable performance to a standard 6-element homogeneous system.[7]

In order to utilize gradient index components in an optical system, accurate characterization of the index of refraction as a function of position is necessary. It is important to know both the index of the base glass and the profile of the gradient. In general these can be considered separate measurement problems. The base index can be measured either prior to diffusion or subsequently within a homogeneous portion of the glass. The change in index as a function of position can then be measured to determine the gradient profile.

There exist cases in which the base index cannot be well characterized. For example, in order for a radial gradient to be useful, the gradient must exist all the way to the center of the lens. Because of the diffusion process, it is likely that the index at the center will differ from the original base index. In addition, IR transmitting materials such as ZnS and ZnSe are difficult to measure because the base index of refraction is large. A technique which would allow measurement of both absolute index of refraction at one position and the change of index across the gradient would be advantageous.

Many methods exist to measure profiles of refractive index gradients. These can be broadly classified as interferometric and non-interferometric techniques.

References 2 and 8-13 describe a few of the recent interferometric systems applied to various types of gradient index measurement problems. All are capable of generating highly accurate relative refractive index profiles. A number of non-interferometric and non-destructive methods[14-18] have been developed to characterize gradient profiles in a radial geometry, i.e., optical fibers, preforms and GRIN rod lenses. In addition, the maximum slope of the gradient has been successfully measured using a schlieren technique.[19]

While the above systems are quite well suited for their respective requirements, none are capable of measuring absolute index of refraction. In a method described by Johnson[20] absolute index of refraction profiles are obtained non-destructively for gradients along the optical axis. A Gaussian gradient profile is assumed. The sample is oriented in a modified Mach-Zehnder interferometer such that the gradient is colinear with the direction of light propagation. The change in optical phase is measured as the sample is rotated about an axis perpendicular to the direction of propagation. A computer ray-tracing program is used to analyze the data and determine the Gaussian coefficients and the sample thickness. While this approach is relatively straightforward for an axially oriented gradient,

application to a gradient of radial symmetry would be quite complex. In addition, data reduction cannot be performed without the aid of a computer.

Some thought must be given to standard techniques of refractive index measurement in homogeneous glass and their possible extension to gradients. The Pulfrich refractometer measures index of refraction by finding the critical angle of a prism of glass of known index characteristics used in conjúnction with the sample. The viewing angle of the boundary separating light and dark is related to the critical angle. If a gradient index sample is used, one would expect this boundary line to appear curved rather than straight, with the shape of the curve corresponding to the shape of the gradient. Because the light incident on the sample is not collimated, the rays will not travel along lines of constant index and the resulting crossover will cause substantial ambiguity in the normally sharp boundary[21]. This problem could be solved by using cylindrical lenses such that the light is focused in the planes of constant index and collimated in the planes of the gradient. But this method does not address itself to the problem of radial geometries or IR samples.

Other methods of refractive index measurement based on refraction would be unsuitable for gradients for more obvious reasons. A prism spectrometer, for instance, would be impractical in any situation where glass fabrication or

modification was done on an individual element basis, even if other problems could be resolved.

Another method of refractive index measurement of homogeneous materials is ellipsometry. Ellipsometry is an optical technique for characterizing a surface or bulk material by observing the change in the state of polarization of incident light due to interaction with the material. This interaction can be reflection, transmission, or scattering but the term ellipsometry generally refers to the reflection type. Ellipsometry measures the complex index of refraction of an absorbing material and is commonly used for characterizing thin films or other surface phenomena and for measuring the optical properties of metals. The two parameters which are measured are the azimuth of linear polarization of the reflected light, ψ, which is a measure of the relative differential reflection of light plane polarized parallel and perpendicular to the plane of incidence, and the relative phase shift, Δ, between the two components which causes a change in the ellipticity of the light.

Ellipsometers can be divided into two general categories, null ellipsometers and photometric ellipsometers. In the simplest nulling configuration, a compensator is used to eliminate the phase shift between the two orthogonal components of the light so that an analyzer may then be used to locate the azimuth of polarization by extinction.

Photometric ellipsometry uses known variation of detected intensity as a function of azimuth angle, phase retardation, or angle of incidence to measure the ellipsometric parameters. Null or compensating ellipsometers necessitate low light level detection but tend to be more accurate because they are not sensitive to intensity fluctuations. Non-compensating systems are subject to errors from intensity variation but are generally faster and are capable of providing more diverse polarization state information. Azzam and Bashara[22] provide descriptions of the many variations of ellipsometric techniques.

There have been many modifications to the basic ellipsometer to either improve the sensitivity of the instrument or to increase the speed or both. Since ellipsometry is highly sensitive to surface conditions, it is important to be able to make rapid measurements. Providing some sort of modulation to the system generally increases the accuracy of the measurements and also lends itself to fully automating the procedure.

One method is to vary the intensity of the output signal by rotating the analyzer at a constant speed. Many such systems have been employed. Aspnes and Studna[23] report a photometric ellipsometer of this type which determines complex reflectance ratios as functions of wavelength. Another possibility is to modulate the state of the polari-

zation of light incident on a sample. Jasperson and Schnatterly[24] describe a system in which a block of fused quartz acts as a photo-elastic modulator. A piezoelectric transducer induces a sinusoidal strain which produces a change in index along the strain axis. The ellipse of polarization is modulated sinusoidally due to the oscillating birefringence of the quartz. This introduces a modulation in intensity of the output signal which can be used to determine the optical constants of the sample.

An example of an automatic nulling ellipsometer is that of Takasaki[25]. Two ADP cells are used as modulators and are mounted respectively to the polarizer and analyzer. The detector signals due to each are used as feedback to servomoters which rotate the analyzer and polarizer to the null condition.

A Faraday rotator can also serve as a modulator in a nulling ellipsometer. In a scheme proposed by Monin and Boutry[26] and described in the book by Azzam and Bashara[22], an AC current of frequency ω is used to drive the Faraday rotator. When the transmission axis of the analyzer is parallel to either the major or minor axis of the ellipse of polarization of the emerging light, the amplitude of the fundamental frequency of the detected signal goes to zero. The orientation of the ellipse of polarization is dependent upon both the reflectance ratio of the orthogonal components

of the linearly polarized input light and their relative phase differences after reflection. Thus, by taking null readings corresponding to two input polarizations, both ellipsometric parameters can be determined without the use of a compensator.

A self-compensating ellipsometer using Faraday cell modulation has been constructed by Mathieu, McClure, and Muller[27]. Two modulation cells are used to enable phase sensitive detection of both ellipsometric parameters ψ and Δ. The Faraday cells, in addition to providing an AC modulation, provide a DC offset for the polarizer and analyzer azimuths so that manual adjustment to a null is not necessary. Feedback from the amplitude of the fundamental frequency is used to drive this offset until a null is achieved.

Ellipsometry has traditionally been used for determining optical constants of absorbing materials. To calculate the complex index of refraction, two ellipsometric parameters, $\tan \psi$, the relative reflectance ratio and Δ, the relative phase shift, are measured. Alternatively θ, the azimuth of the ellipse of polarization and the ellipticity, ε, are measured or θ is measured at two points. If a non-absorbing material and therefore real index of refraction is assumed, then only $\tan \psi$ need be measured. The value of Δ is either 0 or π, depending upon whether the angle of incidence is greater or less than the Brewster angle. The angle θ becomes the azimuth of linear polarization ψ, modified only in sign depending

upon the value of Δ. This eliminates the need for a compensator for the determination of Δ or ϵ and allows all information to be obtained from one azimuth measurement.

In some of the previously mentioned ellipsometers, the optical properties of a surface, which are altered by environmental conditions, were measured as a function of time. Ellipsometry applied to refractive index gradients necessitates measuring index as a function of position. This creates two problems: monitoring very small changes in index (and therefore azimuth angle) across the sample, which can be considered equivalent to monitoring small changes in time, and resolution across the sample.

A reflection technique for measuring absolute index of refraction profiles based upon ellipsometric theory will be described. The purpose of this system is not to improve on the already high accuracy and resolution of the better relative profile measurement systems, but rather to provide additional information. Its usefulness will lie primarily in the capability of providing absolute index information in situations where this would be otherwise difficult to obtain. In addition, because this technique is inherently better suited to strong and deep gradients, it complements existing interferometric techniques which more easily measure weaker and shallower profiles. The usefulness of large Δn in lens design has been demonstrated and much effort is being put into developing the capability of manu-

facturing such materials. An easy method of measuring large index of refraction gradients is therefore a second objective of this work.

References

1. Erich W. Marchand, Gradient Index Optics, (New York: Academic Press, 1978).

2. Duncan T. Moore, Gradient Index Optics: Aspects of Design, Testing, Tolerancing, and Fabrication, Ph.D. Thesis, University of Rochester, 1974.

3. Duncan T. Moore, "Gradient-index optics: a review," Appl. Opt., 19, 1035, (1980).

4. W. J. Tomlinson, "Applications of GRIN-rod lenses in optical fiber communication systems," Appl. Opt., 19, 1127, (1980).

5. L. G. Atkinson, D. T. Moore and N. J. Sullo, "Imaging capabilities of a long gradient-index rod," Appl. Opt., 21, 1004, (1982).

6. P. O. McLaughlin, J. J. Miceli, D. T. Moore, D. P. Ryan and J. M. Stagaman, "Design of a gradient index binocular objective," 1980 International Lens Design Conference, Oakland, California.

7. L. G. Atkinson, S. N. Houde-Walter, D. T. Moore, D. P. Ryan and J. M. Stagaman, "Design of a gradient-index photographic objective," Appl. Opt., 21, 993, (1982).

8. D. C. Leiner and D. T. Moore, "Real-time phase microscopy using a phase-lock interferometer," Rev. Sci. Instrum., 49, 1701, (1978).

9. G. W. Johnson, D. C. Leiner and D. T. Moore, "Phase-locked interferometry," Opt. Engr., 18, 46, (1979).

10. Danette P. Ryan, Measurement of the Chromatic Dispersion of Gradient Index Materials by Multiple Wavelength A.C. Interferometry, M.S. Thesis, University of Rochester, 1980.

11. Y. Kokubun and K. Iga, "Refractive-index profile measurement of preform rods by a transverse differential interferogram," Appl. Opt. 19, 846, (1980).

12. Y. Ohtsuka and Y. Koike, "Determination of the refractive-index profile of light-focusing rods:

accuracy of a method using Interphako interference microscopy," Appl. Opt., 19, 2866, (1980).

13. M. J. Saunders and W. B. Gardner, "Nondestructive interferometric measurement of the delta and alpha of clad optical fibers," Appl. Opt. 16, 2368, (1977).

14. D. Marcuse and H. M. Presby, "Focusing method for nondestructive measurement of optical fiber index profiles," Appl. Opt., 18, 14, (1974).

15. C. Saekeang, P. L. Chu and T. W. Whitbread, "Nondestructive measurement of refractive-index profile and cross-sectional geometry of optical fiber preforms," Appl. Opt., 19, 2025, (1980).

16. L. S. Watkins, "Laser beam refraction traversely through a graded-index preform to determine refractive index ratio and gradient profile," Appl. Opt., 18, 2214, (1979).

17. C. Saekeang and P. L. Chu, "Nondestructive determination of refractive index profile of an optical fiber: backward light scattering method," Appl. Opt., 18, 1110, (1979).

18. N. Yamamoto and K. Iga, " Evaluation of gradient-index rod lenses by imaging," Appl. Opt., 19, 1101, (1980).

19. Lisa Gregorka, Measurement of the Chromatic Dispersion of Gradient Refractive Index Glass Using a Schlieren Technique, M.S. Thesis, University of Rochester, 1978.

20. Glen W. Johnson, Measurement of Strongly Refracting Three-Dimensional Index Distributions, Ph.D. Thesis, University of Rochester, 1979.

21. Danette P. Ryan, private communication.

22. R. M. A. Azzam and N. M. Bashara, Ellipsometry and Polarized Light, (New York: North-Holland Publishing Co., 1977).

23. D. E. Aspnes and A. A. Studna, "High precision scanning ellipsometer," Appl. Opt., 14, 220, (1975).

24. S. N. Jasperson and S. E. Schnatterly, "An improved method for high reflectivity ellipsometry based

on a new polarization modulation technique," Rev. Sci. Instrum., 10, 761,(1969).

25. H. Takasaki, "Automatic ellipsometer. Automatic polarimetry by means of an ADP polarization modulator III," Appl. Opt.,5, 759, (1966).

26. J. Monin and G. A. Boutry, "Conception, réalisation et fonctionnement d'un nouvel ellipsomètre," Nouv. Rev. Optique, 4, 159, (1973).

27. H. J. Mathieu, D. E. McClure, and R. H. Muller, "Fast self-compensating ellipsometer," Rev. Sci. Instrum., 45, 798, (1974).

28. Max Born and Emil Wolf, Principles of Optics, 6th ed., (Oxford: Pergamon Press, 1980), pp. 619-620.

Section II

Theory - Ellipsometry

Refractive index profiles of gradient index materials have been accurately measured by a variety of interferometric and non-interferometric techniques[2, 8-20]. For the most part these are limited to relative profile measurements. Many, particularly the interferometric methods, are best suited to measure small changes in index. A modified version of ellipsometry will be investigated as a means of absolute index profile measurement, which, in addition, is applicable to the measurement of large changes in index.

2.1 ELECTROMAGNETIC BASIS OF ELLIPSOMETRIC MEASUREMENTS

Ellipsometric measurements are based on changes in the state of polarization of light upon reflection from the sample under study. The effect on electromagnetic radiation which is incident upon a boundary between two different media may be described in terms of the changes in the two orthogonal components, radiation linearly polarized parallel and perpendicular to the plane of incidence. The two components of the reflected radiation in general undergo both amplitude and phase changes. This indicates that if the incident radiation is linearly polarized, the reflected radiation will be elliptically polarized, the azimuth and the ellipticity being determined

by the relative amplitude and relative phase between the two components.

The Fresnel reflection equations describe the complex amplitude ratio between reflected and incident light for each of the components. In the case where both media are dielectrics, these simplify to

$$r_p = \frac{n_2\cos\theta_i - n_1\cos\theta_t}{n_2\cos\theta_i + n_1\cos\theta_t} = \frac{\tan(\theta_i-\theta_t)}{\tan(\theta_i+\theta_t)}$$

$$r_s = \frac{n_1\cos\theta_i - n_2\cos\theta_t}{n_1\cos\theta_i + n_2\cos\theta_t} = \frac{-\sin(\theta_i-\theta_t)}{\sin(\theta_i+\theta_t)}$$

where r_p refers to the component with electric field vibration parallel to the plane of incidence and r_s to that perpendicular to the plane of incidence. The angles of incidence and refraction are given as θ_i and θ_t respectively. If $n_1 < n_2$ (i.e., an air-glass interface), r_s is always negative, indicating a phase shift of π on reflection. Under the same conditions, r_p is positive for $\theta_i + \theta_t < \pi/2$ and negative for $\theta_i + \theta_t > \pi/2$. The incident angle for which $\theta_i + \theta_t = \pi/2$ is called the Brewster angle, θ_B; it is the angle at which the phase shift on reflection for the parallel component changes from 0 to π and the amplitude of r_p goes to zero.

The ellipsometric parameters ψ and Δ are defined by the following relationships

$$\tan\psi = \frac{|r_s|}{|r_p|} \qquad (2.1)$$

$$\Delta = \delta_p - \delta_s \qquad (2.2)$$

where δ_p is the phase change associated with r_p and δ_s the phase change associated with r_s. Since

$$r_s = |r_s| e^{i\delta_s}$$

$$\text{and } r_p = |r_p| e^{i\delta_p}$$

and with $$\rho = \frac{r_s}{r_p}$$

then $$\tan\psi = \frac{r_s e^{-i\delta_s}}{r_p e^{-i\delta_p}}$$

or

$$\tan\psi = \rho e^{i\Delta} . \qquad (2.3)$$

For the general case of an absorbing surface, equations have been derived relating the dielectric constants to ψ and Δ.[28]

$$\varepsilon_1 = n^2(1-\kappa^2) = \sin^2\theta_i + \frac{\sin^2\theta_i \tan^2\theta_i (\cos^2 2\psi - \sin^2 2\psi \sin^2\Delta)}{(1+\sin 2\psi \cos\Delta)^2}$$

$$\varepsilon_2 = 2n^2\kappa = \frac{\sin^2\theta_i \tan^2\theta_i (2\sin 2\psi \cos 2\psi \sin\Delta)}{(1+\sin 2\psi \cos\Delta)^2}$$

An analogous derivation yields the simplified result for the case of a non-absorbing dielectric ($\kappa=0$, $n_{complex}= n(1+i\kappa)=n$).

$$n^2 = \sin^2\theta_i + \frac{\sin^2\theta_i \tan^2\theta_i (\cos^2 2\psi)}{(1\mp\sin 2\psi)^2} \qquad (2.4)$$

where the top sign applies for $\theta_i < \theta_B$ ($\Delta=-\pi$) and the bottom sign for $\theta_i > \theta_B$ ($\Delta=0$). Measurement of ψ at a known θ_i will therefore directly yield n.

The ellipsometric azimuth ψ must be related to the actual azimuth of linear polarization.

$$(\tan\psi)e^{-i\Delta} = \frac{r_s}{r_p} = \frac{E_{rs}/E_{is}}{E_{rp}/E_{ip}}$$

where the E's are the electric field amplitudes of the incident and reflected light for the perpendicular and parallel components. Defining $\tan\alpha = \frac{E_{is}}{E_{ip}}$ and $\tan\psi_r = \frac{E_{rs}}{E_{rp}}$ to be the incident and reflected azimuths of polarization,

$$\tan\psi = \frac{\tan\psi_r\, e^{i\Delta}}{\tan\alpha} \,. \qquad (2.5)$$

If the incident light is polarized at 45^{o}, $\tan\alpha = 1$ and $\tan\psi_r = \pm\tan\psi$.

2.2 FARADAY EFFECT MODULATION ELLIPSOMETRY

In order to provide more sensitive determination of ψ, a Faraday rotator is used to modulate the polarization. The rotator makes use of the Faraday magneto-optic effect; when a magnetic field is applied in the direction of light propagation, the plane of vibration of linearly polarized light rotates according to

$$\theta = VHl \tag{2.6}$$

where θ is the angle of rotation

H the magnetic field strength

l the length of the medium displaying the Faraday effect

and V the Verdet constant - a measure of the strength of this effect for a particular medium.

A solenoid concentric with the Faraday core provides the magnetic field. The magnetic field generated by the coil is determined by

$$H = \frac{1.257ni}{L} \tag{2.7}$$

for H in oersteds

n = number of turns

i = current

L = length of windings.

Thus, application of an AC current generates an AC magnetic field parallel to the direction of light propagation which provides an AC rotation of the plane of polarization.

The Faraday effect is the result of the differential retardance between the two orthogonal circular components, right and left circularly polarized light. The amount of rotation, $\Delta\psi$, is equal to one-half the retardance, δ. The Faraday rotator can therefore be represented mathematically as a circular retarder. The Mueller matrix for a circular retarder of arbitrary retardance is represented by

$$\begin{bmatrix} 1 & 0 & 0 & 0 \\ 0 & \cos\delta & \mp\sin\delta & 0 \\ 0 & \pm\sin\delta & \cos\delta & 0 \\ 0 & 0 & 0 & 1 \end{bmatrix}$$

where the signs indicate counterclockwise and clockwise rotation respectively.

Two configurations are considered for providing polarization modulation. The Faraday modulator can be included between the sample and the analyzer; in this case the polarization azimuth of the reflected light is modulated. It is equivalent to modulating the azimuth of the analyzer (see Figure 2.1). Alternatively, the Faraday

PSMA Configuration

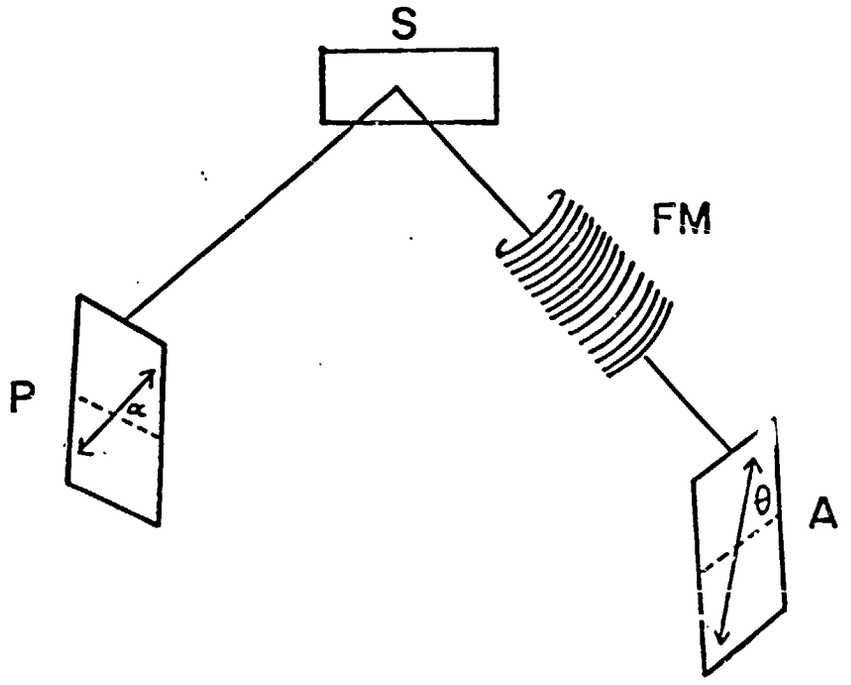

P polarizer at α

S sample

FM Faraday modulator

A analyzer at θ

Figure 2.1

modulator can be placed between the polarizer and the sample. This modulates the polarization of the incident light and is equivalent to modulating the polarizer azimuth (see Figure 2.2).

2.3 MATHEMATICAL DESCRIPTION OF PSMA ELLIPSOMETER

The Mueller calculus can be applied to the first configuration (PSMA) to determine the form of the intensity detected after the analyzer (constants of proportionality have been omitted for clarity).

$$\begin{bmatrix} (r_p^2+r_s^2) & (r_p^2-r_s^2) & 0 & 0 \\ (r_p^2-r_s^2) & (r_p^2+r_s^2) & 0 & 0 \\ 0 & 0 & 2r_pr_s & 0 \\ 0 & 0 & 0 & 2r_pr_s \end{bmatrix} \cdot \begin{bmatrix} 1 \\ \cos 2\alpha \\ \sin 2\alpha \\ 0 \end{bmatrix} =$$

reflection — linearly polarized light at α

$$\begin{bmatrix} r_p^2+r_s^2 + \cos 2\alpha (r_p^2-r_s^2) \\ r_p^2-r_s^2 + \cos 2\alpha (r_p^2+r_s^2) \\ 2r_pr_s \sin 2\alpha \\ 0 \end{bmatrix} \qquad (2.8)$$

PMSA Configuration

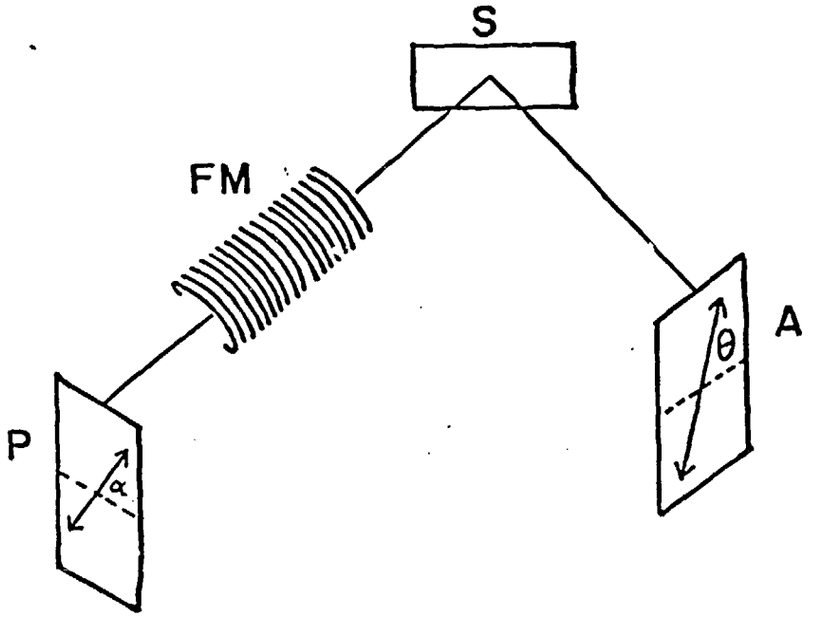

P polarizer at α

FM Faraday modulator

S sample

A analyzer at θ

Figure 2.2

$$\begin{bmatrix} 1 & 0 & 0 & 0 \\ 0 & \cos\delta & -\sin\delta & 0 \\ 0 & \sin\delta & \cos\delta & 0 \\ 0 & 0 & 0 & 1 \end{bmatrix} \cdot \begin{bmatrix} r_p^2+r_s^2+\cos2\alpha(r_p^2-r_s^2) \\ r_p^2-r_s^2+\cos2\alpha(r_p^2+r_s^2) \\ 2r_pr_s\sin2\alpha \\ 0 \end{bmatrix} =$$

Faraday rotator

$$\begin{bmatrix} r_p^2+r_s^2+\cos2\alpha(r_p^2-r_s^2) \\ \cos\delta\left[r_p^2-r_s^2+\cos2\alpha(r_p^2+r_s^2)\right] - 2r_pr_s\sin\delta\sin2\alpha \\ \sin\delta\left[r_p^2-r_s^2+\cos2\alpha(r_p^2+r_s^2)\right] + 2r_pr_s\cos\delta\sin2\alpha \\ 0 \end{bmatrix} \quad (2.9)$$

The intensity of the light is $r_p^2+r_s^2+\cos2\alpha(r_p^2-r_s^2)$ and the azimuth, β, is described as

$$\tan 2\beta = \frac{\sin\delta\left[r_p^2-r_s^2+\cos2\alpha(r_p^2+r_s^2)\right] + 2r_pr_s\cos\delta\sin2\alpha}{\cos\delta\left[r_p^2-r_s^2+\cos2\alpha(r_p^2+r_s^2)\right] - 2r_pr_s\sin\delta\sin2\alpha} . \quad (2.10)$$

$$\begin{bmatrix} 1 & \cos2\theta & \sin2\theta & 0 \\ \cos2\theta & \cos^2 2\theta & \cos2\theta\sin2\theta & 0 \\ \sin2\theta & \cos2\theta\sin2\theta & \sin^2 2\theta & 0 \\ 0 & 0 & 0 & 0 \end{bmatrix} \cdot \begin{bmatrix} r_p^2+r_s^2+\cos2\alpha(r_p^2-r_s^2) \\ \cos\delta\left[r_p^2-r_s^2+\cos2\alpha(r_p^2+r_s^2)\right] - 2r_pr_s\sin\delta\sin2\alpha \\ \sin\delta\left[r_p^2-r_s^2+\cos2\alpha(r_p^2+r_s^2)\right] + 2r_pr_s\cos\delta\sin2\alpha \\ 0 \end{bmatrix}$$

analyzer at θ (2.11)

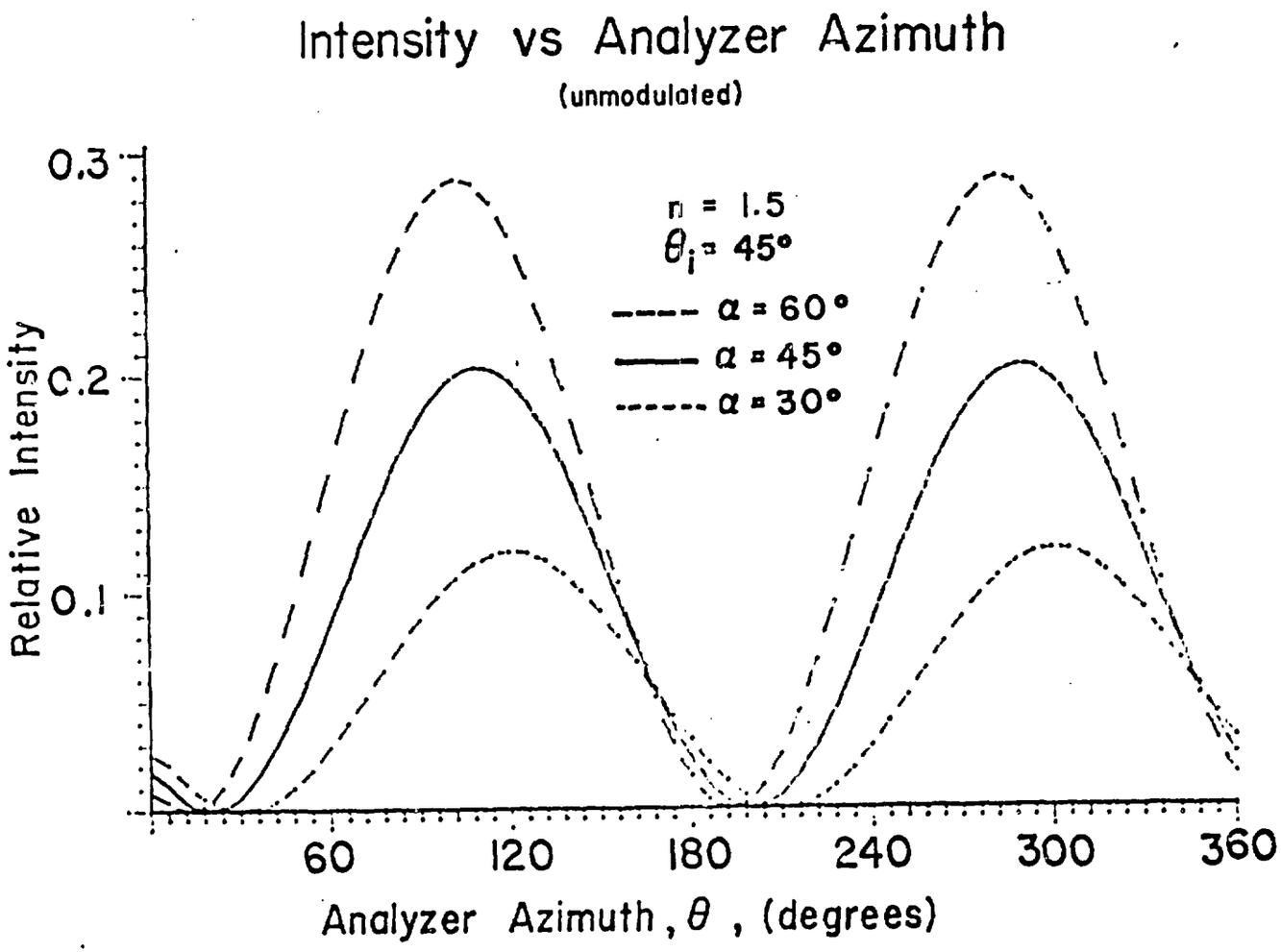
Intensity vs Analyzer Azimuth
(unmodulated)
n = 1.5
θ_i = 45°
α = 60°
α = 45°
α = 30°
Relative Intensity
0.3
0.2
0.1
60
120
180
240
300
360
Analyzer Azimuth, θ, (degrees)

Figure 2.3

The intensity out of the system is the first element of the resultant Stokes vector.

$$I = r_p^2+r_s^2+\cos2\alpha(r_p^2-r_s^2)$$
$$+\cos2\theta\left[\cos\delta\left[r_p^2-r_s^2+\cos2\alpha(r_p^2+r_s^2)\right] -2r_pr_s\sin\delta\sin2\alpha\right]$$
$$+\sin2\theta\left[\sin\delta\left[r_p^2-r_s^2+\cos2\alpha(r_p^2+r_s^2)\right] +2r_pr_s\cos\delta\sin2\alpha\right] \quad (2.12)$$

The intensity pattern as a function of analyzer angle is illustrated in Figure 2.3 for the simplified case of δ = 0 (unmodulated).

If a sinusoidal temporal modulation is applied, δ = Asinωt

$$I = r_p^2+r_s^2+\cos2\alpha(r_p^2-r_s^2)$$
$$+\cos2\theta\left[\cos(A\sin\omega t)\left[r_p^2-r_s^2+\cos2\alpha(r_p^2+r_s^2)\right]\right.$$
$$\left.-2r_pr_s\sin2\alpha\sin(A\sin\omega t)\right]$$
$$+\sin2\theta\left[\sin(A\sin\omega t)\left[r_p^2-r_s^2+\cos2\alpha(r_p^2+r_s^2)\right]\right.$$
$$\left.+2r_pr_s\sin2\alpha\cos(A\sin\omega t)\right] .$$

When this is expanded into a series of Bessel functions and

all terms higher than the first harmonic are deleted, the intensity becomes

$$I = r_p^2+r_s^2+\cos2\alpha(r_p^2-r_s^2)$$
$$+\cos2\theta\left[\left[J_o(A)+2J_2(A)\cos2\omega t\right]\left[r_p^2-r_s^2+\cos2\alpha(r_p^2+r_s^2)\right]\right.$$
$$\left.-2r_pr_s\sin2\alpha(2J_1(A)\sin\omega t)\right]$$
$$+\sin2\theta\left[\left[2J_1(A)\sin\omega t\right]\left[r_p^2-r_s^2+\cos2\alpha(r_p^2+r_s^2)\right]\right.$$
$$\left.+2r_pr_s\sin2\alpha\left[J_o(A)+2J_2(A)\cos2\omega t\right]\right]. \qquad (2.13)$$

The amplitude of the AC signal at frequency ω is equal to

$$-4r_pr_s\sin2\alpha\cos2\theta J_1(A) + 2\left[r_p^2-r_s^2+\cos2\alpha(r_p^2+r_s^2)\right]\sin2\theta J_1(A). \qquad (2.14)$$

This signal will go to zero only when

$$2r_pr_s\sin2\alpha\cos2\theta = \left[r_p^2-r_s^2+\cos2\alpha(r_p^2+r_s^2)\right]\sin2\theta$$

(provided $J_1(A)$ does not equal zero). This is the case when

$$\tan 2\theta = \frac{2r_p r_s \tan\alpha}{r_p^2 - r_s^2 \tan^2\alpha}$$

$$\theta = \tan^{-1}\left[\frac{r_s}{r_p}\ \tan\alpha\right]$$

or

$$\theta = \tan^{-1}\left[\frac{-r_p}{r_s \tan\alpha}\right]$$

which are the conditions for the azimuth of polarization and the null, respectively.

The amplitude of the AC signal at frequency 2ω is equal to

$$\cos 2\theta\, 2J_2(A)\left[r_p^2 - r_s^2 + \cos 2\alpha\,(r_p^2 + r_s^2)\right]$$

$$+ \sin 2\theta\, 2J_2(A)\, 2r_p r_s \sin 2\alpha\,.$$

At

$$\tan\theta = \frac{r_s}{r_p}\tan\alpha$$

this equals to

$$2J_2(A)\left[\frac{2r_p^4\cos^2\alpha + 2r_s^4\sin^2\alpha\tan^2\alpha + 4r_p^2 r_s^2 \sin^2\alpha}{r_p^2 + r_s^2\tan^2\alpha}\right]$$

and at

$$\tan\theta = \frac{-r_p}{r_s \tan\alpha}$$

i' equals to

$$\frac{2J_2(A)}{r_p^2+r_s^2\tan^2\alpha}\left[-2r_p^2\cos^2\alpha-2r_s^2\sin^2\alpha\tan^2\alpha-4r_p^2r_s^2\sin^2\alpha\right].$$

In both cases, the 2ω component never goes to zero at the point where the ω component does and hence can be used as a check that light is still passing through the system.

The condition for the fundamental term approaching zero is used to locate the null. This is possible to do automatically only if the amplitude of this term experiences a sign change going through the null. An analysis of equation (2.14) indicates that this is the case. This is also shown in Figure 2.5.

2.4 PHASE-SENSITIVE DETECTION

Using phase-sensitive detection, the amplitude of the fundamental component of the AC signal is checked. When this amplitude is non-zero, an error signal is used to add a DC bias to the coil. This adds a DC rotation to the polarization azimuth emerging from the Faraday cell and is equivalent to rotating the analyzer. The direction of

the biasing depends on which side of the null the analyzer is at. When the analyzer is located on a null, error signal goes to zero and the system is locked. At the same time, the amplitude of the first harmonic is monitored to insure that it is nonzero.

To obtain an absolute value of n using equations (2.4) and (2.5), the exact azimuth of polarization, ψ_r, must be determined. This is a combination of the physical position of the analyzer plus the equivalent rotation due to the Faraday cell. (90^o must be added if a null rather than a maximum has been located). Using equations (2.6) and (2.7) or by prior measurement of the coil, the DC current applied to the coil can be calibrated to read out as angle of rotation.

Once one value of n has been obtained, the sample is scanned to determine the gradient profile. As n changes, the position of ψ_r changes and the bias current changes in order to keep the system locked on a null. Change in current is thus a direct measure of change in ψ_r. Data reduction can then provide a measure of n across the sample.

2.5 MATHEMATICAL DESCRIPTION OF PMSA ELLIPSOMETRY

The second configuration is shown in Figure 2.2. In this case, the Mueller calculus provides the following results.

$$\begin{bmatrix} 1 & 0 & 0 & 0 \\ 0 & \cos\delta & -\sin\delta & 0 \\ 0 & \sin\delta & \cos\delta & 0 \\ 0 & 0 & 0 & 1 \end{bmatrix} \cdot \begin{bmatrix} 1 \\ \cos 2\alpha \\ \sin 2\alpha \\ 0 \end{bmatrix} =$$

modulator — incident light linearly polarized at α

$$\begin{bmatrix} 1 \\ \cos\delta\cos 2\alpha - \sin\delta\sin 2\alpha \\ \sin\delta\cos 2\alpha + \cos\delta\sin 2\alpha \\ 0 \end{bmatrix} =$$

$$\begin{bmatrix} 1 \\ \cos(\delta+2\alpha) \\ \sin(\delta+2\alpha) \\ 0 \end{bmatrix} . \qquad (2.15)$$

$$\begin{bmatrix} (r_p^2+r_s^2) & (r_p^2-r_s^2) & 0 & 0 \\ (r_p^2-r_s^2) & (r_p^2+r_s^2) & 0 & 0 \\ 0 & 0 & 2r_pr_s & 0 \\ 0 & 0 & 0 & 2r_pr_s \end{bmatrix} \cdot \begin{bmatrix} 1 \\ \cos(\delta+2\alpha) \\ \sin(\delta+2\alpha) \\ 0 \end{bmatrix} =$$

reflection from sample

$$\begin{bmatrix} r_p^2+r_s^2+\cos(\delta+2\alpha)(r_p^2-r_s^2) \\ r_p^2-r_s^2+\cos(\delta+2\alpha)(r_p^2+r_s^2) \\ 2r_pr_s\sin(\delta+2\alpha) \\ 0 \end{bmatrix} . \qquad (2.16)$$

The intensity of the light is $\left[r_p^2+r_s^2+\cos(\delta+2\alpha)(r_p^2-r_s^2)\right]$ and the azimuth, β, is described as

$$\tan 2\beta = \frac{2r_p r_s \sin(\delta+2\alpha)}{r_p^2-r_s^2+\cos(\delta+2\alpha)(r_p^2+r_s^2)} \quad . \tag{2.17}$$

$$\begin{bmatrix} 1 & \cos 2\theta & \sin 2\theta & 0 \\ \cos 2\theta & \cos^2 2\theta & \cos 2\theta \sin 2\theta & 0 \\ \sin 2\theta & \cos 2\theta \sin 2\theta & \sin^2 2\theta & 0 \\ 0 & 0 & 0 & 0 \end{bmatrix} .$$

analyzer at θ

$$\begin{bmatrix} r_p^2+r_s^2+\cos(\delta+2\alpha)(r_p^2-r_s^2) \\ r_p^2-r_s^2+\cos(\delta+2\alpha)(r_p^2+r_s^2) \\ 2r_p r_s \sin(\delta+2\alpha) \\ 0 \end{bmatrix} \tag{2.18}$$

The resultant intensity is given by the first element of the Stokes vector derived from the last operation.

$$\begin{aligned} I = {} & r_p^2+r_s^2+\cos(\delta+2\alpha)(r_p^2-r_s^2) \\ & + \cos 2\theta \left[r_p^2-r_s^2+\cos(\delta+2\alpha)(r_p^2+r_s^2) \right] \\ & + \sin 2\theta \left[2r_p r_s \sin(\delta+2\alpha) \right] \quad . \end{aligned} \tag{2.19}$$

Applying a sinusoidal modulation in time and expanding gives

$$I = r_p^2+r_s^2+(r_p^2-r_s^2)\left[(J_o(A)+2J_2(A)\cos2\omega t)\cos2\alpha - (2J_1(A)\sin\omega t)\sin2\alpha\right]$$

$$+ \cos2\theta\left[r_p^2-r_s^2+(r_p^2+r_s^2)\left[J_o(A)+2J_2(A)\cos2\omega t)\cos2\alpha - (2J_1(A)\sin\omega t)\sin2\alpha\right]\right]$$

$$+\sin2\theta\left[2r_pr_s\left[(2J_1(A)\sin t)\cos2\alpha + (J_o(A) + 2J_2(A)\cos2\omega t)\sin2\alpha\right]\right] . \quad (2.20)$$

The amplitude of the fundamental component of the AC signal is equal to

$$-(r_p^2-r_s^2)2J_1(A)\sin2\alpha - \cos2\theta(r_p^2+r_s^2)2J_1(A)\sin2\alpha$$

$$+\sin2\theta(2r_pr_s)2J_1(A)\cos2\alpha .$$

This term is zero when

$$2r_pr_s\sin2\theta\cos2\alpha - (r_p^2+r_s^2)\cos2\theta\sin2\alpha$$

$$- (r_p^2-r_s^2)\sin2\alpha = 0 .$$

One condition which satisfies this is

$$\theta = \tan^{-1}\left(\frac{-r_p}{r_s \tan\alpha}\right).$$

In this case, the fundamental term will go to zero at a null but not at a maximum (except for the case of normal incidence). The second zero point is undetermined. For the incident polarization, α, equal to 45^{o}, the second zero will be at the angle which is the negative of the null angle

$$\theta = \tan^{-1}\left(\frac{r_p}{r_s}\right).$$

The amplitude of the first harmonic is equal to

$$(r_p^2 - r_s^2)\,2J_2(A)\cos 2\alpha + \cos 2\theta\,(r_p^2 + r_s^2)\,2J_2(A)\cos 2\alpha$$

$$+\sin 2\theta\,(2r_p r_s 2J_2(A)\sin 2\alpha).$$

At the null

$$\tan\theta = \left(\frac{-r_p}{r_s \tan\alpha}\right)$$

this equals

$$2J_2(A)\left[-2r_p^2 r_s^2\cos^2\alpha - 4r_p^2 r_s^2 \sin^2\alpha - 2r_p^2 r_s^2 \frac{\sin^4\alpha}{\cos^2\alpha}\right]$$

which again is non-zero.

There are two interesting points about this arrangement. Because the AC modulation is initiated before the

sample, the form of the modulation is affected by reflection from the sample. This manifests itself in two ways. There is a DC shift of the modulation which can be seen in intensity equations (2.19) and (2.20). This can be traced back to the resultant of equation (2.16). The Stokes vector describing the light incident on the analyzer contains the modulation term (δ=Asinωt) in the intensity element as well as in the elements which indicate the azimuth of the polarization.

The second effect is a change in the amplitude of the modulation. Since

$$\tan\psi_r = \pm\tan\psi\tan\alpha$$

$$\frac{d\psi_r}{d\alpha} = \frac{\pm\tan\psi\cos^2\psi_r}{\cos^2\alpha} .$$

The attenuation of the modulation is affected by both the incident polarization azimuth, α, and the angle of incidence, θ_i (which affects ψ). Figure (2.4) shows this attenuation as a function of α for different θ_i. The attenuation is strongest near the Brewster angle (which is also where the best sensitivity for calculating n from ψ occurs) and increases with α. Even near the Brewster angle, gain in modulation amplitude occurs

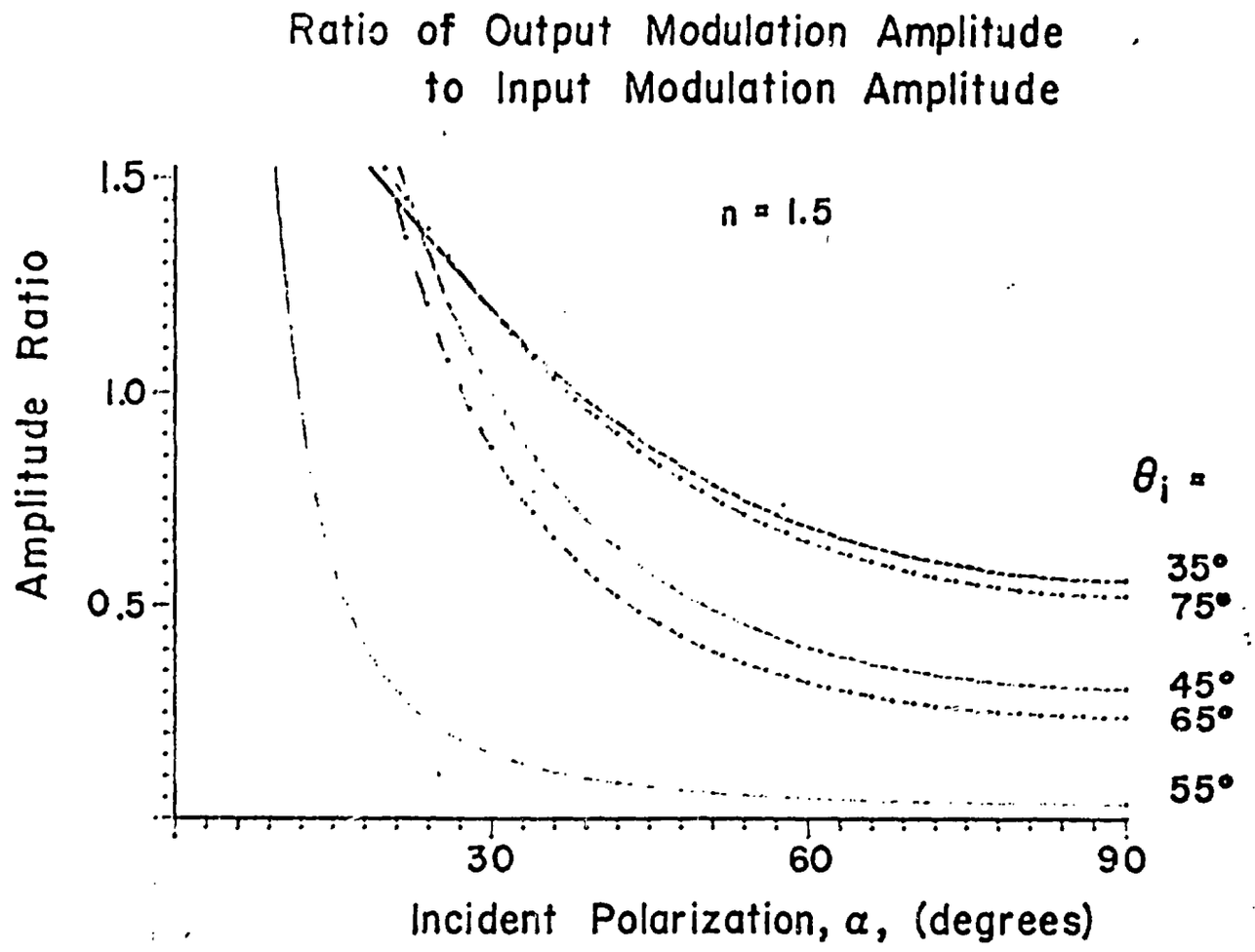
Ratio of Output Modulation Amplitude
to Input Modulation Amplitude
n = 1.5
Amplitude Ratio
1.5
1.0
0.5
θ_i =
35°
75°
45°
65°
55°
30
60
90
Incident Polarization, α, (degrees)

Figure 2.4

if α is chosen small enough.

2.6 COMPARISON OF THE TWO CONFIGURATIONS

Figures 2.5 and 2.6 are plots of the amplitude of the AC signal at frequency ω for the PSMA and PMSA configurations respectively. In the PSMA case, there are zeros at both the nulls and 90° to the nulls (maximum intensity). In the PMSA case, there are zeros at the nulls. The second zeros show up unsymmetrically; for the special case of $\alpha = 45^{\circ}$ they are symmetric about the x-axis. Figure 2.7 shows graphically the location of the zeros in each case.

A more detailed examination of the amplitude values near the null azimuth gives an indication of the sensitivity of the two methods in locating this point. For the PSMA method, sensitivity increases with increasing incident polarization azimuth, α, and with increasing angle of incidence, θ_i, (see Figure 2.8). For the PMSA case, sensitivity is independent of α and less than the optimum PSMA at the same θ_i. As θ_i is varied, the sensitivity decreases towards the Brewster angle and then increases again more rapidly at angles greater than the Brewster angle.

The above results taken by themselves can be misleading. They apply only to the determination of ψ_r. The

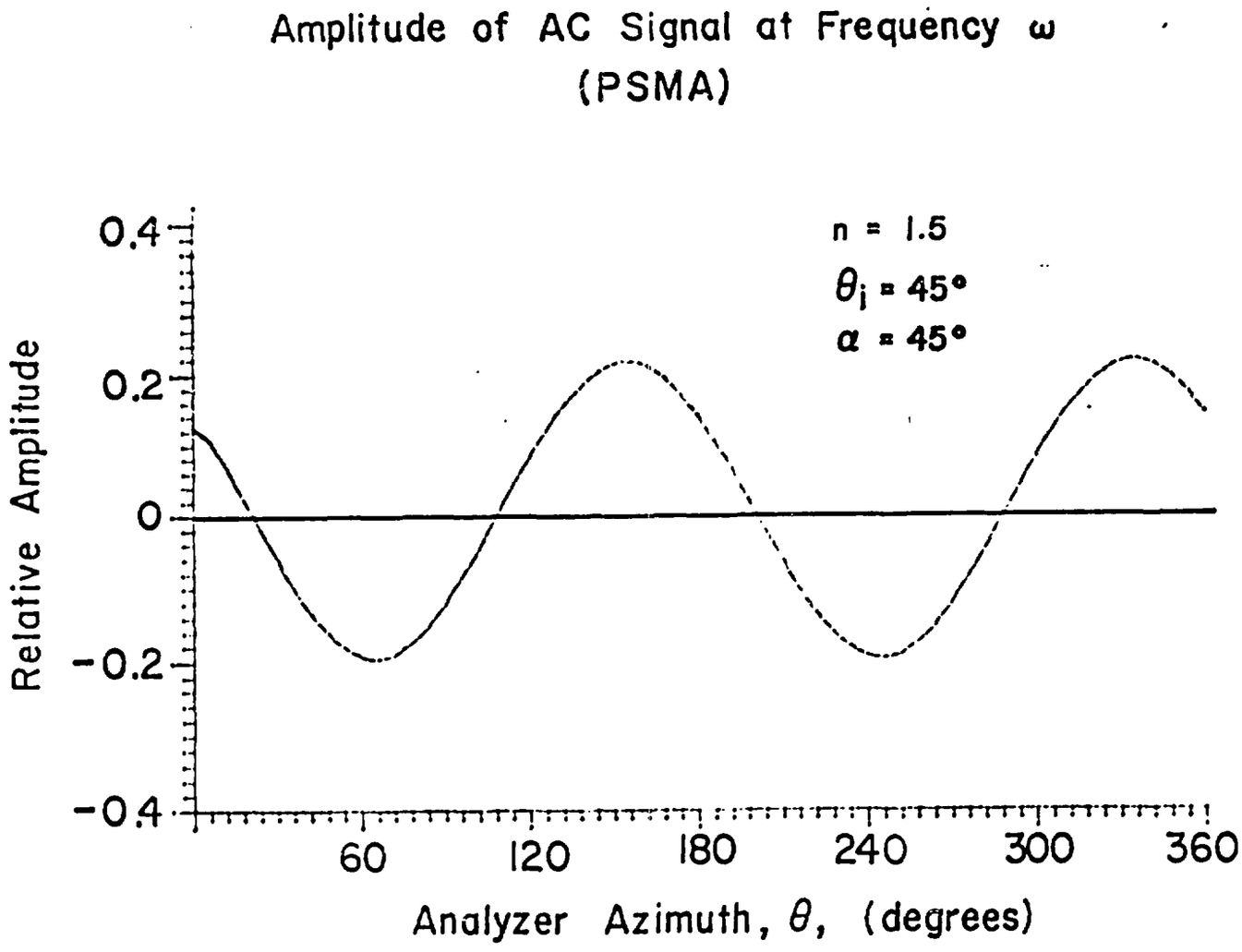
Amplitude of AC Signal at Frequency ω
(PSMA)
n = 1.5
θ_i = 45°
α = 45°
Relative Amplitude
0.4
0.2
0
-0.2
-0.4
60
120
180
240
300
360
Analyzer Azimuth, θ, (degrees)

Figure 2.5

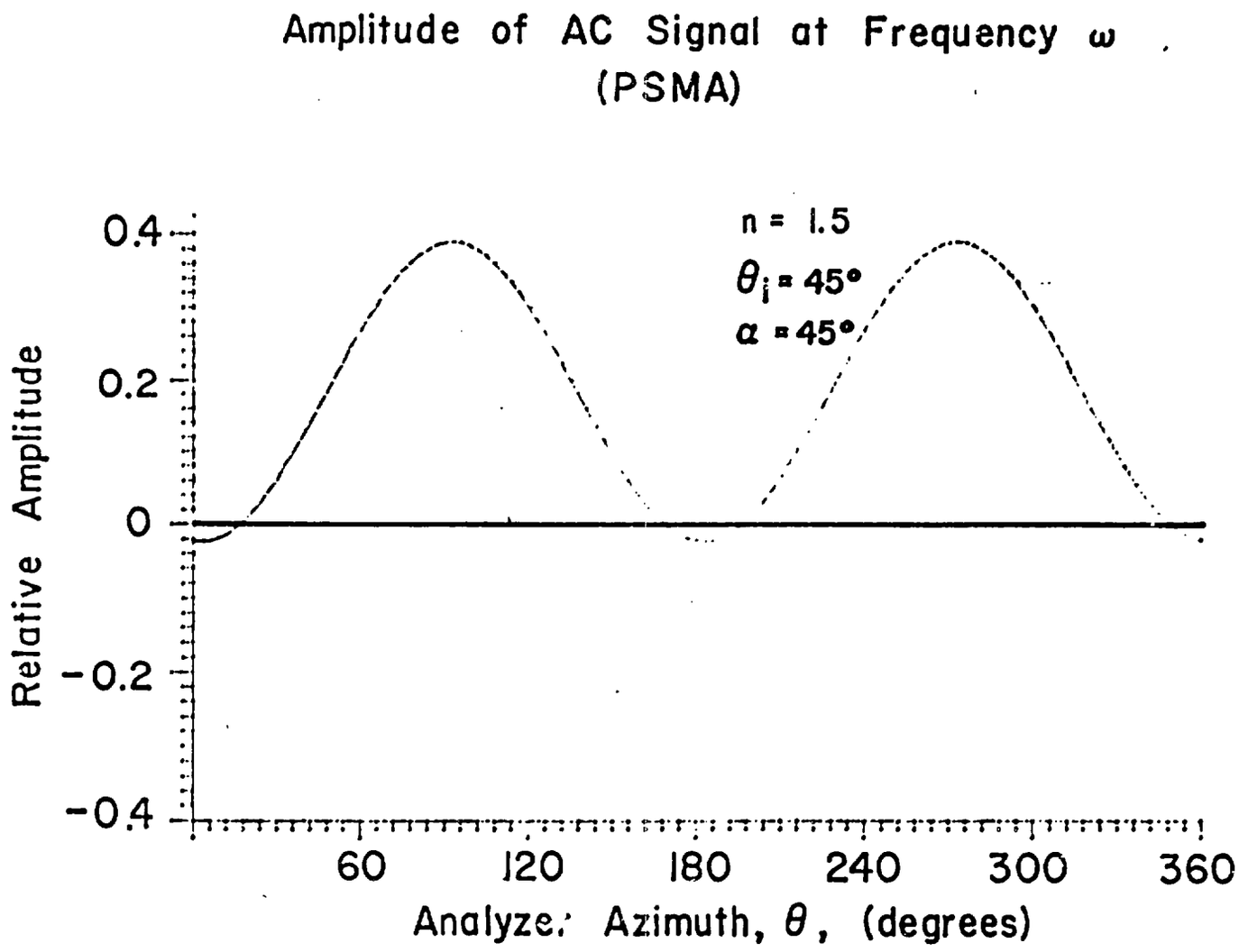
Amplitude of AC Signal at Frequency ω
(PSMA)
n = 1.5
θi = 45°
α = 45°
0.4
0.2
0
-0.2
-0.4
Relative Amplitude
60
120
180
240
300
360
Analyzer Azimuth, θ, (degrees)

Figure 2.6

Zero Positions of AC Signal

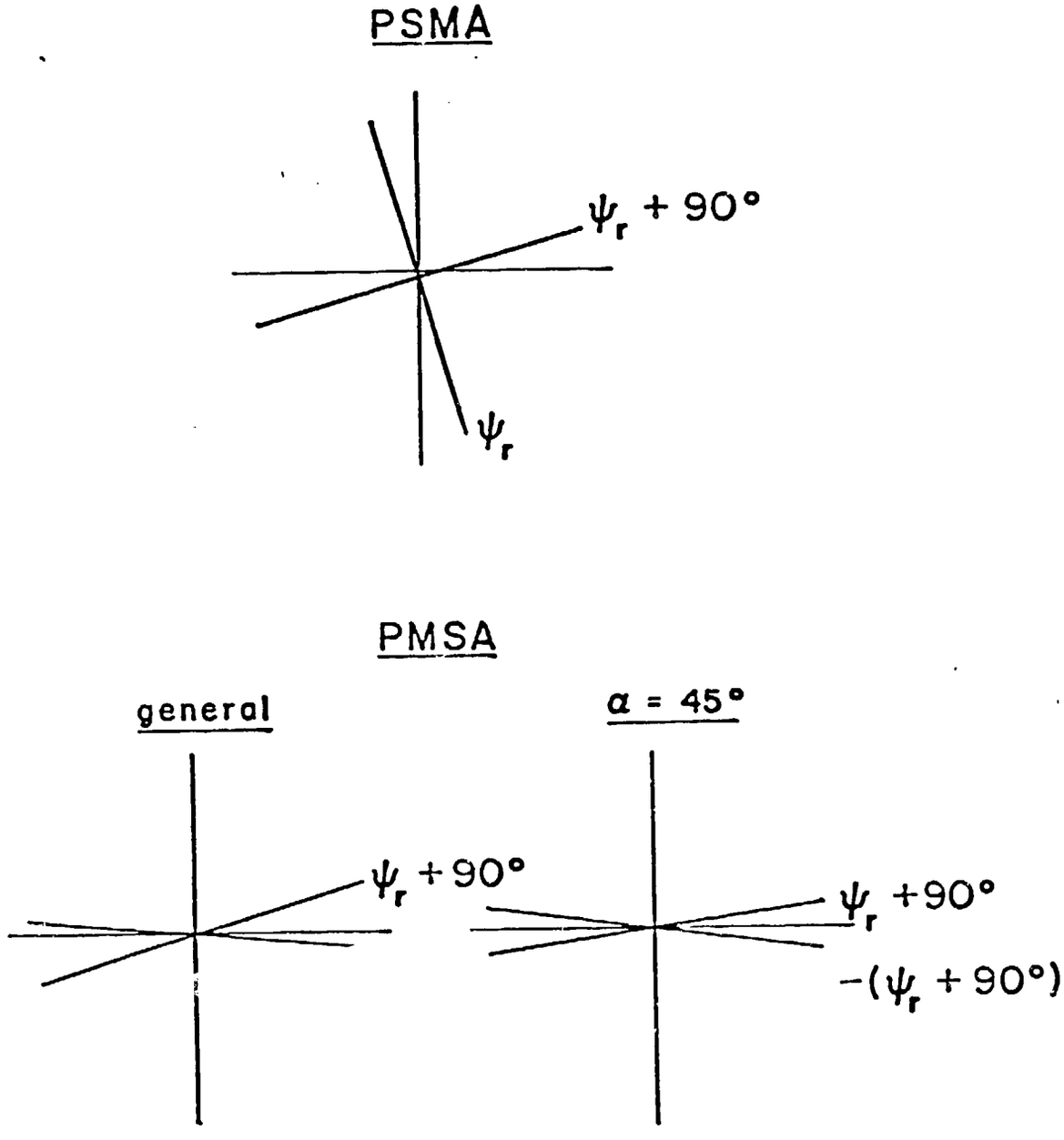

Figure 2.7

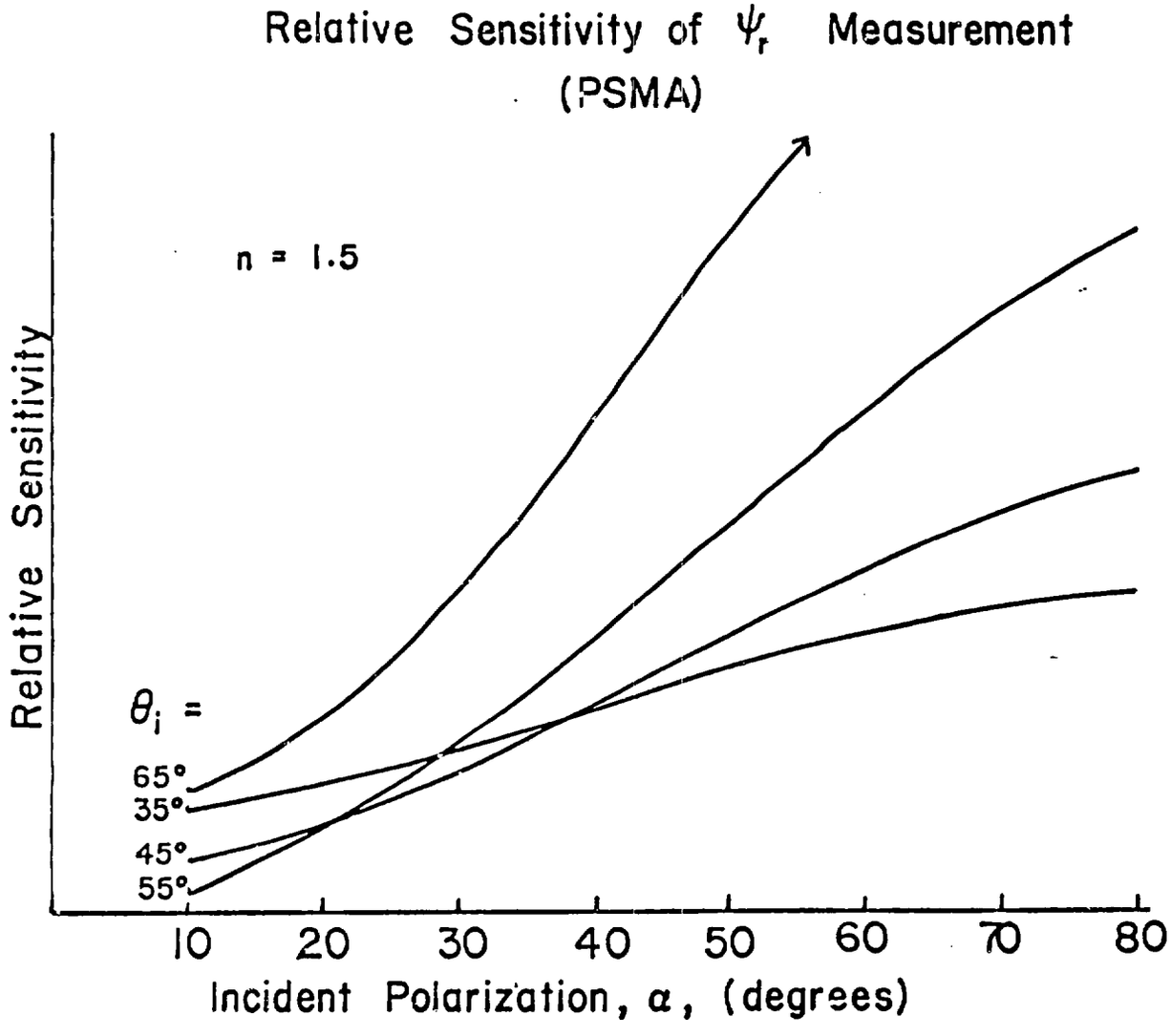
Relative Sensitivity of Ψ_r Measurement
(PSMA)
n = 1.5
Relative Sensitivity
θ_i =
65°
35°
45°
55°
10
20
30
40
50
60
70
80
Incident Polarization, α, (degrees)

Figure 2.8a

Relative Sensitivity of Ψ_r Measurement
(PMSA)

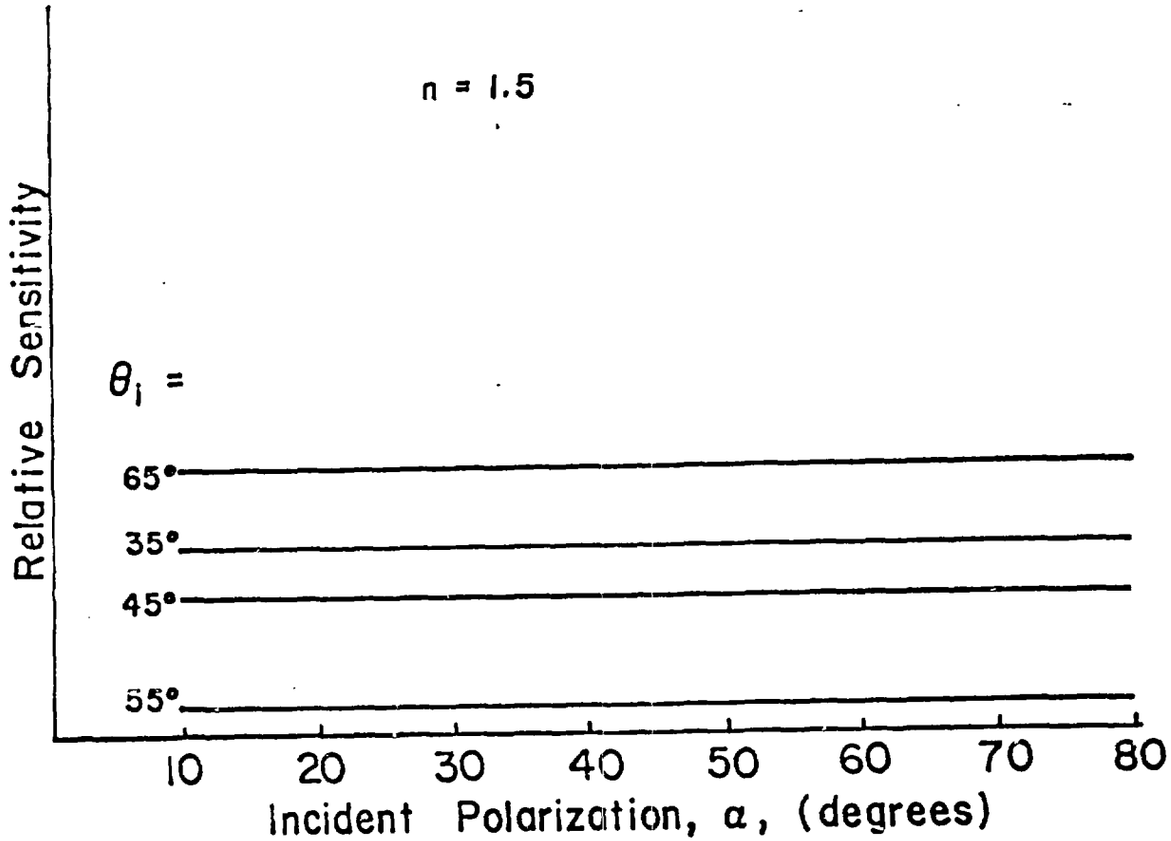

Figure 2.8b

value of n is calculated from ψ, where

$$\tan\psi = \left|\frac{\tan\psi_r}{\tan\alpha}\right|.$$

The effect of ψ_r on ψ differs with α.

$$\frac{d\psi}{d\psi_r} = \frac{\sec^2\psi_r}{\tan\alpha\sec^2\psi}$$

$$= \frac{1+\tan^2\psi\tan^2\alpha}{\sec^2\psi\tan\alpha} .$$

If this effect is combined with the values in Figure 2.8, a plot of the relative sensitivity of ψ as a function of α and θ_i is obtained (see Figure 2.9). This is a more useful result since the determination of n from ψ is the ultimate concern. The effects of θ_i on sensitivity remain the same, but those of α have changed considerably. In the PSMA case, sensitivity is now peaked at $\alpha = 45^\circ$. For the PMSA method, sensitivity decreases with α. For small α, a value higher than the optimum PSMA sensitivity can be obtained.

From the previous discussion it appears that both configurations of polarization modulation are reasonable. The change in amplitude of the modulation on reflection in the PMSA case can be controlled; it can be made to be greater than one by choosing the correct (small) value for the incident polarization azimuth, α. The sensitivi-

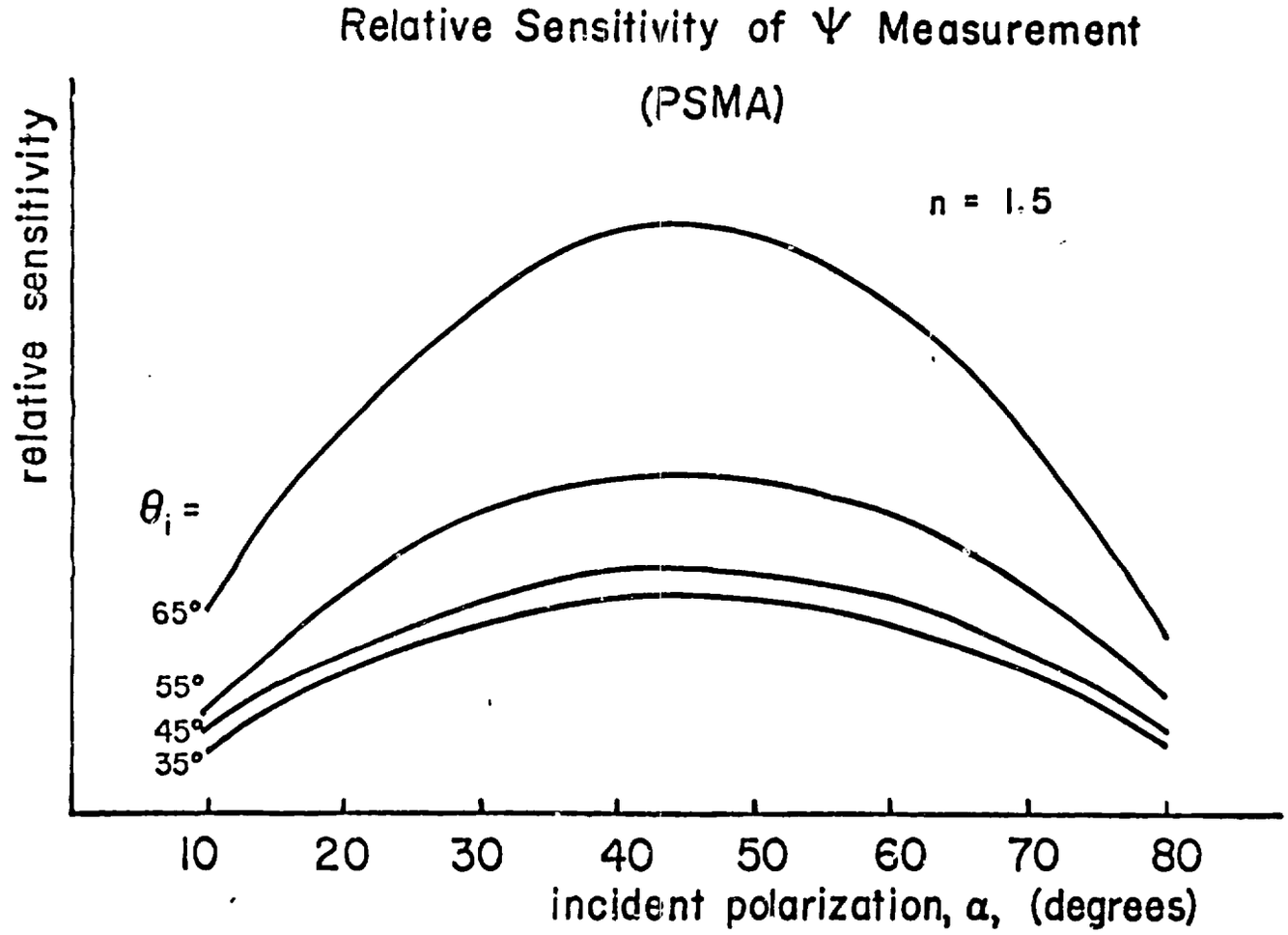
Relative Sensitivity of Ψ Measurement
(PSMA)
n = 1.5
relative sensitivity
θ_i =
65°
55°
45°
35°
10
20
30
40
50
60
70
80
incident polarization, α, (degrees)

Figure 2.9a

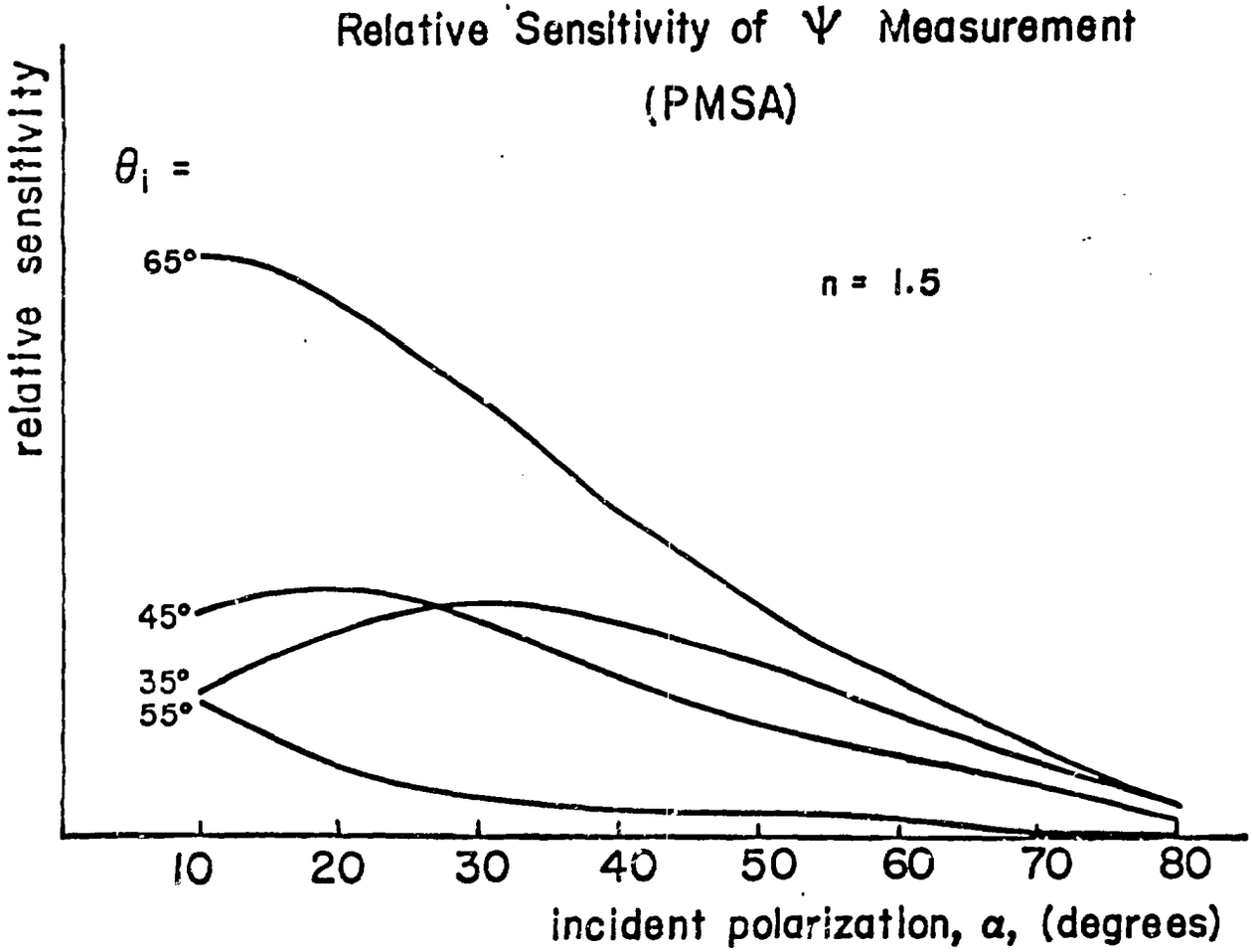
Relative Sensitivity of Ψ Measurement
(PMSA)
relative sensitivity
θi =
65°
n = 1.5
45°
35°
55°
10
20
30
40
50
60
70
80
incident polarization, α, (degrees)

Figure 2.9b

ties of determining ψ are generally similar, although that of the PMSA configuration can optimally be greater than that of the PSMA configuration for small α.

In the PSMA arrangement, the zeroes of the ac amplitude are all separated by 90^{o}, corresponding to intensity maxima and minima. In the PMSA arrangement, the zeroes are not uniformly spaced and spacing varies with different samples and setups. The positions of only half the zeroes can easily be related to index of refraction.

The PSMA configuration was chosen as the preferable method because all the zero positions are well known. However, the system was designed allowing for possible change to the PMSA arrangement.

Section III

Design of Infrared Imaging System

A gradient index, two-element, infrared camera objective has been designed. The lens operates at f/1.8 with a 44 mm. focal length. It was designed using germanium as a base material. The half field of view is 21.8°, with almost diffraction limited performance out to full field, for 10 μm. wavelength radiation. The index profile in each of the elements is identical and varies only in the radial direction.

The value of the refractive index of the two germanium elements depends only on the distance from the optical axis, r. This type of dependence can be represented by the following formula:

$$N(r) = N_{00} + N_{10}r^2 + N_{20}r^4. \qquad (3\text{-}1)$$

Several interesting features on radial GRIN design can be associated with the coefficients in Eq. 3-1:

(1) N_{00} is the index of the base material; it is the index that one specifies in an homogeneous design.

(2) N_{10} is the coefficient of the quadratic term. There are two important properties associated with N_{10}. First, the contribution to the power of a thin element

is given by:

$$\Phi_{grad} = -2N_{10}t \qquad (3\text{-}2)$$

where Φ_{grad} is the power due to the gradient, and t is the thickness of the element. This power contribution gives the designer two new effective degrees of freedom in controlling first-order properties: N_{10} and element thickness t.

Second, the contribution to Petzval field curvature due to the presence of the gradient is given by

$$\sigma_{4grad} = \frac{\Phi_{grad}}{(N_{00})^2} = \frac{-2N_{10}t}{(N_{00})^2}, \qquad (3\text{-}3)$$

in analogy with the contribution due to the surface curvatures in homogeneous design. Notice that this contribution is inversely proportional to the square of N_{00}. By using the gradient to increase the power of an element, the designer incorporates less Petzval field curvature than by using the equivalent surface curvatures.

(3) N_{20} is the fourth power coefficient. It has no effect on power or Petzval field curvature. It can be used to correct other aberrations without changing previously corrected Petzval field curvature or first-order properties. In this way spherical aberration can

be decoupled from Petzval field curvature etc.

The systems first order design is illustrated in the Figure 3-1. The aperature stop is located at the rear surface of the first element. The system was designed systematically in a two step process.

The back half of the system was designed first. The first curvature and the base index were fixed; the back curvature was used to control focal length. The third-order aberrations that could not be corrected by symmetry were eliminated in the half-system first; that is, third-order spherical aberration, astigmatism, and Petzval field curvature were brought to zero. Next, the whole system was assembled and scaled to the specified focal length. This was done by placing two of the single element lens back to back. Finally, the system was reoptimized (at unequal conjugates, object plane at infinity) such that all the third-order aberrations were eliminated.

Table 3-1 shows the dominant parameter used to control each aberration. The design of the half-system was as follows: The surface curvatures and the value of the quadratic coefficient N_{10} were used to produce the required power and to correct the Petzval field curvature to zero. The spherical aberration was eliminated next with the fourth power coefficient N_{20}. Stop position

does not affect power, Petzval field curvature, or spherical aberration; it was used to correct astigmatism. Coma and distortion were eliminated by symmetry. For the case of unequal conjugates, the parameters and aberrations could not be related so simply, but the design was close enough to the desired solution that convergence was rapid.

The third-order solution suffered from higher-order aberrations, so symmetry of the curvatures was broken, and an optimization based on ray positions was used to control spot size. A solution was generated this way.

The parameters for the final design are listed in Table 3-2. Both lenses have the same gradient composition which is radial and almost parabolic in its dependence of refractive index on radial position. This would mean that the samples could be fabricated in very long cylinders and the same rod could be sliced to form both of the elements. The required change in index of refraction from center to edge of the 12.5 mm radius cylinder is 0.13. This is a reasonable value for the fabrication of axial gradients using germanium-silicon alloys. As yet, it is beyond any radial component of re-

fractive index gradient which can be fabricated in germanium. The curvatures on the surface are shallow, but are still required to be non-zero to allow adequate correction of the aberrations in the imagery.

The lens system is diffraction limited over the full field of $\pm 21.8^{\circ}$ if used at 10 μm. The field curves are plotted in Figure 3-1. The migration at the off-axis field points occurs at the aperture stop which is located just past the back surface of the first element. The vignetting is not very severe even at full field as can be seen in the plots. The sagittel field is flat, and the tengential field curve exhibits an inward curving field.

The system tolerences are summarized in Table 3-3. The tolerence was determined assuming a point spread function twice that of diffraction limited performance. The tolerances are large when compared to tolerances for gradient index systems used in the visible. This is not surprising, since the wavelengths used are a function of 17 times larger than wavelengths in the visible portion of the spectrum.

Dominant Parameters Used to Correct Third Order Aberrations in the Symmetric System

Dominant Parameters	Aberrations
Quadratic coefficient, N_{10}	Petzval field curvature
Fourth power coefficient, N_{20}	Spherical aberration
Stop position	Astigmatism
Symmetry	Coma
Symmetry	Distortion

Table 3-1

Infrared Diffraction Limited Lens System

Lens Data

f/1.8 fl = 44 mm.

N_{00} = 4.003

N_{10} -0.85244×10^{-3} mm^{-2}

N_{20} $+0.14639 \times 10^{-6}$ mm^{-4}

CV_1 0.010356 mm^{-1}

CV_2 0.013431 mm^{-1}

CV_3 -0.008453 mm^{-1}

CV_4 -0.009340 mm^{-1}

Element Th = 10 mm

Sep = 27.65 mm

radius = 12.5 mm

Table 3-2

Infrared Diffraction Limited Lens System

Tolerance Analysis

f/1.8 f1 = 44 mm.

Decen	0.1 mm.
Tilt	0.01 radius
N_{10}	1%
N_{20}	2%
CV_1	2%
Th_1	2% Elements
Th_3	10% Air space

Table 3-3

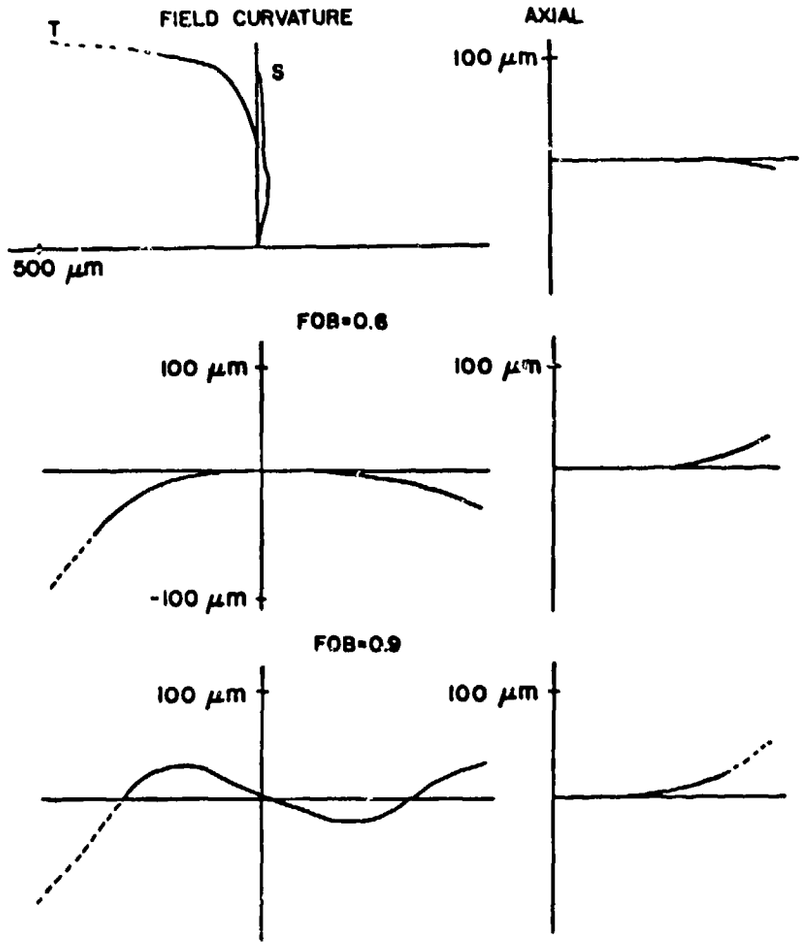

Figure 3-1

Ray Trace Plot of F/1.8 Infrared Lens System

The transverse aberrations are plotted as a function of relative aperture for the various fractional object heights (FOB); axial fan FOB equals 0.6 (13.1°) and FOB equals 0.9 (19.6°). It is seen that the maximum transverse aberrations of all rays are less than 20 micrometers. In addition, the field curvature is plotted showing the tangential field inward curving and the sagital slightly backward curving.

Section IV

INTRODUCTION

A general overview of the problems of making infrared gradient index materials was given in the previous contract report (see Research Contract Report DAAH01-80--C-1324 entitled Gradient Index Lens Research, Final Report, July, 1980 to July, 1981, Research Contract with The Department of the Army, Micom, Redstone Arsenal). In Section I of that report, are outlined some of the important parameters for determining which are suitable materials for making infrared transmitting gradients. Since that time, we have completed the manufacture of many gradient profiles. This is enclosed in the following section.

CRYSTAL GROWING

4.1 PHYSICAL DESCRIPTION

The main frame and some sub-assemblies of the crystal growing apparatus were donated to the University of Rochester by Corning Glass Works. The system had originally been used for the fabrication of sapphire tubing of various cross sectional shapes. Many of the system requirements for the fabrication of gradient materials are quite different from the requirements for sapphire. Consequently, the system was rebuilt at the University to meet these requirements.

Figure 4-1 is a diagram illustrating in further detail the actual crystal growing region, including crucible, pull-rod and heating coils. The crucibles and pull-rod end are enclosed in a double walled quartz jacket. The double wall allows cooling of the quartz cylinder by flowing water between the jackets. The growing is done inside of this quartz cylinder to facilitate a controlled environment. This is necessary for two reasons. The first is that the heating is done by the use of an induction furnace. This

CZOCHRALSKI CRYSTAL GROWING

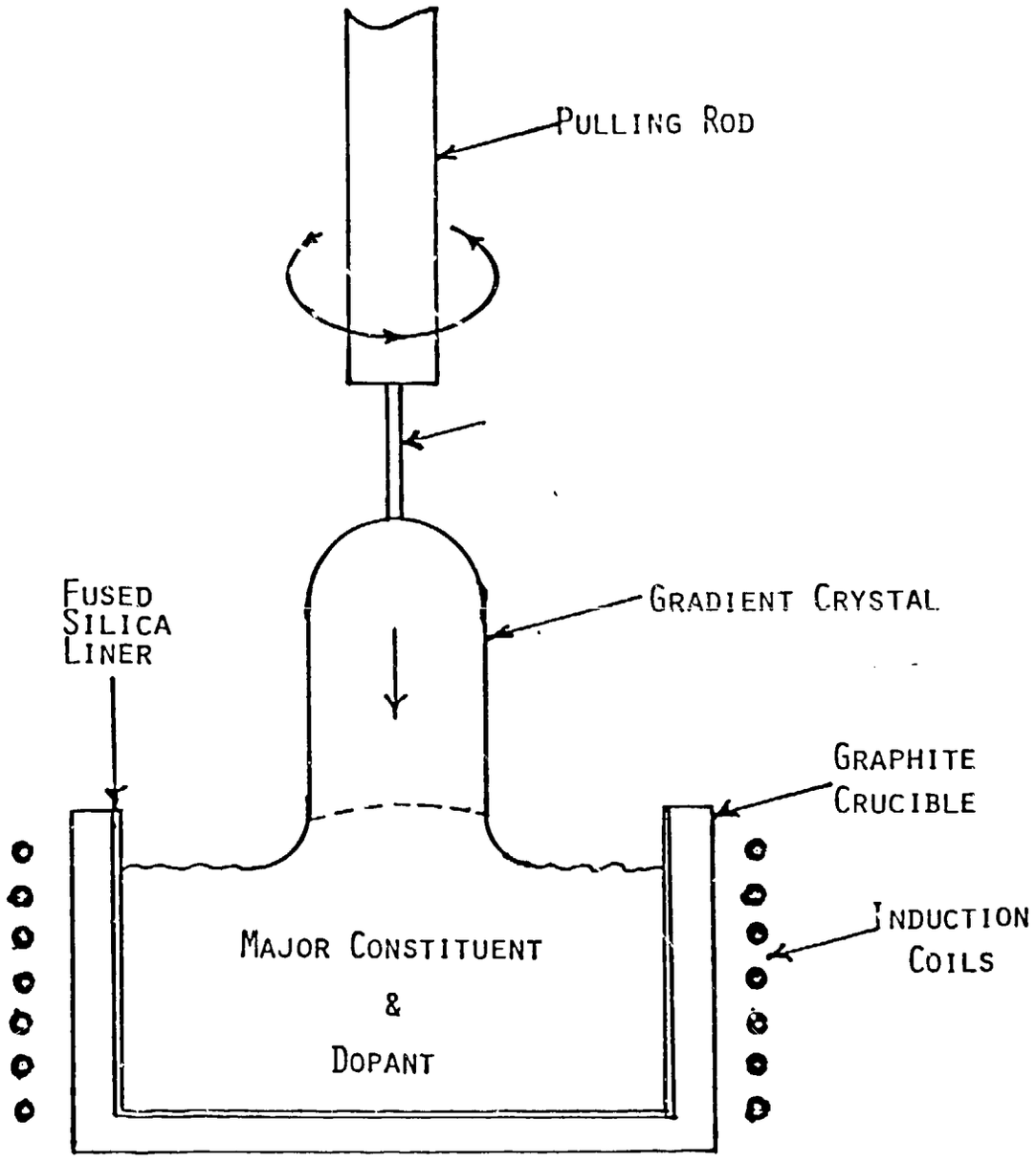

Detail of Crystal Growing Region

Figure 4-1

requires a susceptor material to absorb the R.F. energy in order to produce heat. The susceptor used is graphite. Since this material oxidizes at elevated temperatures, it must be maintained in an oxygen-free atmosphere. Secondly, the two materials being used to fabricate gradient index crystals, namely germanium and silicon also oxidize at elevated temperatures.

The upper and lower ends of the double walled quartz jacket are sealed to aluminum mounting rings with double o-ring seals. The upper aluminum cover plate has a teflon o-ring seal in the center for the pulling rod to pass through. This allows for pull-rod rotation and translation as well as allowing the pull rod temperature to become hotter than standard rubber o-rings could withstand. The pull-rod temperature is generally less than about 80°C at the point of passage through the upper cover.

During early experiments, attempts were made at running the system under a vacuum. This was a complication which was deemed unnecessary. Initial attempts at running the system under a vacuum met with problems primarily because of difficulties in maintaining adequate vacuum. Experiments with growing pure germanium were more successful while running the system under a positive pressure of nitrogen. The source of gas is boiling liquid nitrogen. This reduces

the chance of moisture being introduced into the system. This is a generally accepted practice in the growth of germanium crystals. The experiments which were performed under a vacuum were performed with a vacuum of only about 0.1 mm. of Hg. Much higher vacuums are generally used in vacuum type systems. Trying to modify the apparatus to run under these conditions would have required major reconstruction.

Since the system relies on the use of induction heating in order to melt the material, a susceptor material is required. The germanium, which is the major constituent of all crystals grown in this system, does not absorb sufficient R.F. energy in the solid state to heat itself. When the germanium is molten its conductivity at the applied frequency increases considerably. The germanium actually is heated directly from the R.F. energy once it is molten. The operating frequency for the R.F. generator is about 480 KHz.

For the growth of pure germanium crystals the susceptor is also used as the crucible. Graphite is one of the best and least expensive susceptor materials. Many pure germanium crystals were grown in crucibles machined from graphite rods. However, difficulties were encountered when even small amounts of silicon were added to the melt. It was determined that the silicon once dissolved in the germanium

was probably reacting with the carbon crucible. A quartz liner was then added to the inside of the graphite susceptor to eliminate this problem. The final crucible configuration is illustrated in Figure 4-2. The thermocouple leads can be seen in the diagram, and the actual thermocouple junction is located in the center of the crucible just below the bottom of the inner graphite surface.

A number of problems were encountered with temperature registration and control during the crystal growth process. The problems arise because of the sensitivity of the growth process to the melt composition, and because the required melt temperature changes as a function of time during the growth of a crystal. Another difficulty arises from an inability to directly measure the melt temperature. It is difficult to resolve this last problem due to restrictions in the system geometry.

Temperature measurement and control relies on the use of a Chromel-Alumel thermocouple junction as the sensing element. The junction is made by joining Chromel and Alumel wire of .010" diameter. It is formed using an oxygen-propane torch. The fine wire is necessary to reduce the amount of heat which is carried away from the thermocouple junction. This method was chosen because of the inability to use an optical pyrometer. A noncontact method would appear

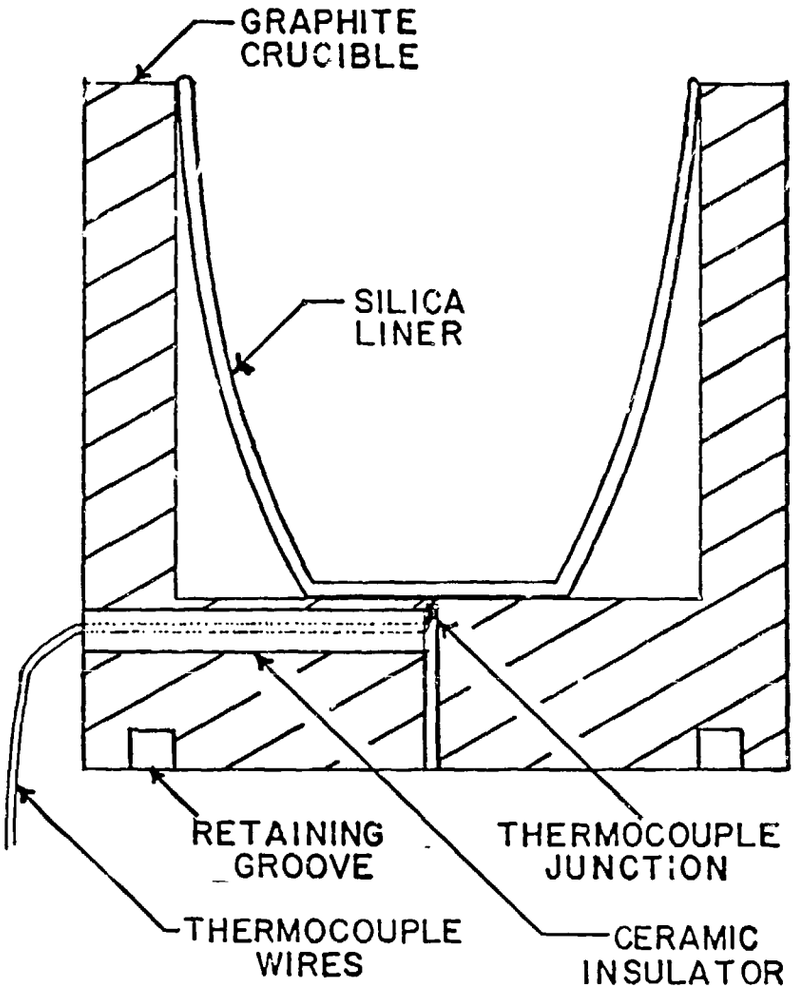

Crucible Diagram

Figure 4-2

ideal for this situation. In reality, it is difficult to get the pyrometer to "look" at a fixed region inside the crucible without any interference from the much cooler crystal. The limitation is more a function of the geometry than anything else, (i.e., the crucible's inside diameter is very close to the crystal's outside diameter.)

One of the major difficulties with the use of the thermocouple is in obtaining an adequate thermal contact to the melt. After trying different techniques of thermocouple placement, it was concluded that the most reliable measurements were made when the thermocouple junction was built into the bottom of the graphite susceptor. This is done by drilling a hole into the side of the susceptor just beneath the inner bottom surface and parallel to it. The thermocouple wires are then fed through a ceramic insulator to keep them from shorting except at the junction. This assembly is then cemented into the bottom of the crucible using a ceramic cement. The cement insures a good thermal contact. Results using this system are good.

On an absolute scale, there is always a discrepancy between temperature read and the actual temperature. No attempt is made to use the temperature measurement as an absolute measurement. The system works consistently on a relative scale, and this is adequate for the crystal growing

process. The absolute reference point for each run is determined from the temperature at which crystallization begins. Therefore, the fact that absolute temperature read varies from crucible to crucible or run to run is of no consequence as long as the readings are reliable on a relative scale. The temperature is computer controlled, and once the initial crystallization temperature is found, the computer follows a preprogrammed temperature cycle using this crystalization point for calibration.

When the original crystal growing apparatus was set up, there was concern that it should be possible to have some absolute measure of the crystal location. It was believed that this could best be done with a stepper motor drive geared to the crystal pull-rod. This system allows for the control of the crystal pulling speed and the crystal location either manually or by computer control. The mechanism which was installed allowed for a vertical movement of 0.050 inches per revolution, coupled to a stepper motor with 200 steps per revolution. This gave a minimum vertical increment of 0.00025 inches, or equivalently about 6.4 μm. This was coupled through appropriate electronics to keep track of position to this resolution.

The speed control for this mechanism consisted of a timer of variable rate to increment the stepper motor. The equip-

ment was set up to allow for a variable pulling rate of 1-255 mm./hr. This pulling rate as well as any larger displacements were all computer controlled. Initial experiments with this arrangement seemed to work well for growing homogeneous germanium crystals. There was evidence on the external surface of the crystals that pulling was done in discrete intervals. These individual movements were obviously having an effect on the crystal growth.

The hydraulic pulling mechanism was the method by which crystals were grown when the system was used for making sapphire rods. The problem of active control of pulling rate was not a problem for that system, and a single needle valve was used to adjust the hydraulic flow rate. Since this rate never needed to vary, it was set once and forgotten. Ideally, one would like to have three requirements satisfied: 1) vary the pull rate over a fairly wide dynamic range, 2) maintain precise control, 3) have the rate controlled by computer.

It was concluded that the best method for achieving the desired control was through the use of a digital hydraulic valve used in conjunction with the hydraulic pulling mechanism. The digital hydraulic valve took the place of the needle valve and is illustrated in Figure 4-3. Each valve is set for a flow rate of twice the value of the previous

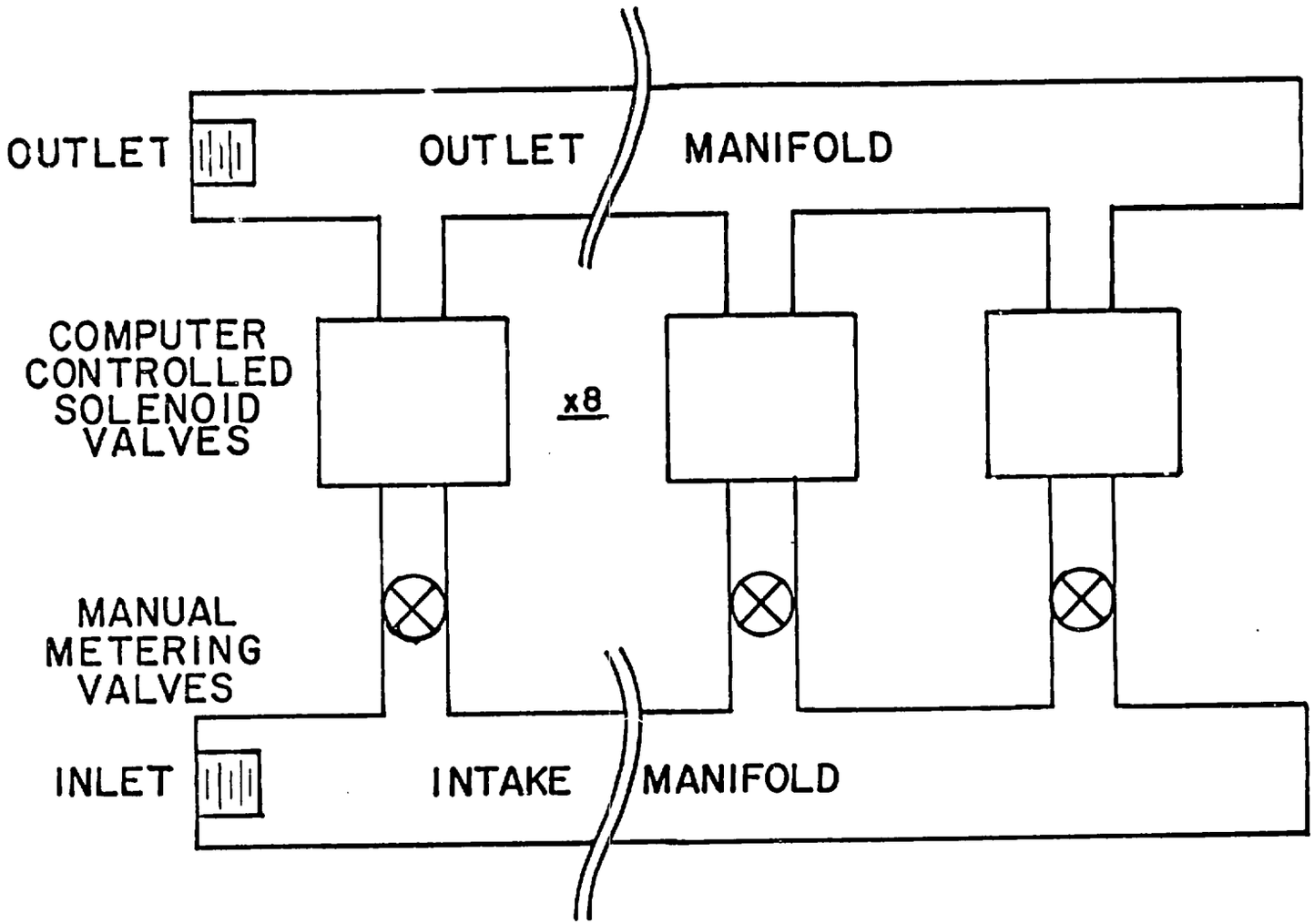

Digital Hydraulic Valves

Figure 4-3

one. The slowest needle valve is adjusted for a flow rate which corresponds to a crystal pull rate of 0.1 mm./hr. Each valve can then be turned on or off via the computer interface and the relays operating the electric solenoid shut-off valves. This system allows for any flow rate from 0-25.5 mm./hr. in 0.1 mm./hr. increments. There is no evidence of any problems of valve interaction.

Any number of valves can be opened without any noticeable effect on the flow rate of any neighboring valves. This is due to the fact that the flow rates involved are very slow. The flow rate through the fastest flowing valve is about 0.1 ml./min. The system is operated under a constant pressure of 50 p.s.i., driven by a regulator on a dry nitrogen tank. This pressure must be fairly well maintained since variations in the differential pressure cause different flow rates through the hydraulics. Temperature also has a small effect on oil viscosity and, subsequently, can effect the flow rates. The system runs very well to within an accuracy of better than 10% and has been reliable. This limitation is partially set by the accuracy of initial calibration. The only difficulty which has been encountered is that after a valve or valves are opened, it takes roughly 2-5 minutes for the system to stabilize at the proper rate. Also, when motion is first started, the system must be operated for a

few millimeters in the upward direction before proper operation can be attained. Even with these limitations this method of pulling has been more than adequate for meeting the requirements needed for control and smoothness.

The one other aspect of the grower which deserves a brief discussion is that of pull rod rotation. The rotation rate is manually controlled and is adjustable continuously from 0-60 revolutions per minute. All experiments were conducted with a fixed rotation rate and most were run at or near the maximum speed. This was done to increase the agitation in the melt, since the gradient crystal process depends to some extent on a homogeneous melt. This also helps in maintaining rotational symmetry within the crystal. Ideally, one would also like to rotate the crucible to help maintain rotational symmetry in the melt as well. The system, as it stood, could not be easily modified to allow for this extra nicety.

The crystal growing apparatus was interfaced to a Compucolor microcomputer, which is based on an 8080A microprocessor. The computer was not ideally suited to operation of experimental apparatus in the laboratory. Consequently, a great deal of effort went into interfacing the computer to the experiment. It is important that one have the ability to accurately control the temperature and pull rate as a func-

tion of time. Since this need can only be satisfied through the use of some type of automation technique, the effort of interfacing was worthwhile. The system hardware is illustrated in Figure 4-4.

The computer has control of temperature via a D/A converter and a modified Leeds and Northrup temperature controller. It has control of the pull rate via electronic interface to the stepper-motor drive and a digital 8 bit parallel output to the hydraulic valve assembly. There was also temperature feedback to the computer via an analog to digital converter. This was unnecessary because of the quick response of the controller and R.F. induction furnace. Temperature response rate is always better than 10°C per minute, and control rates driving the growth process are almost always less than 0.2°C per minute, and certainly never exceed about 5°C per minute. It was found that there is no real need to monitor the temperature any more accurately than a chart recorder. The chart recorder maintains a permanent record of the tempertaure cycle used.

The growing process is controlled by interupts within the computer. Therefore, the computer control of the system is made "invisible" to the operator of the computer. This has advantages. The major advantage is that one never has to interfere with the computer control of the experiment. That

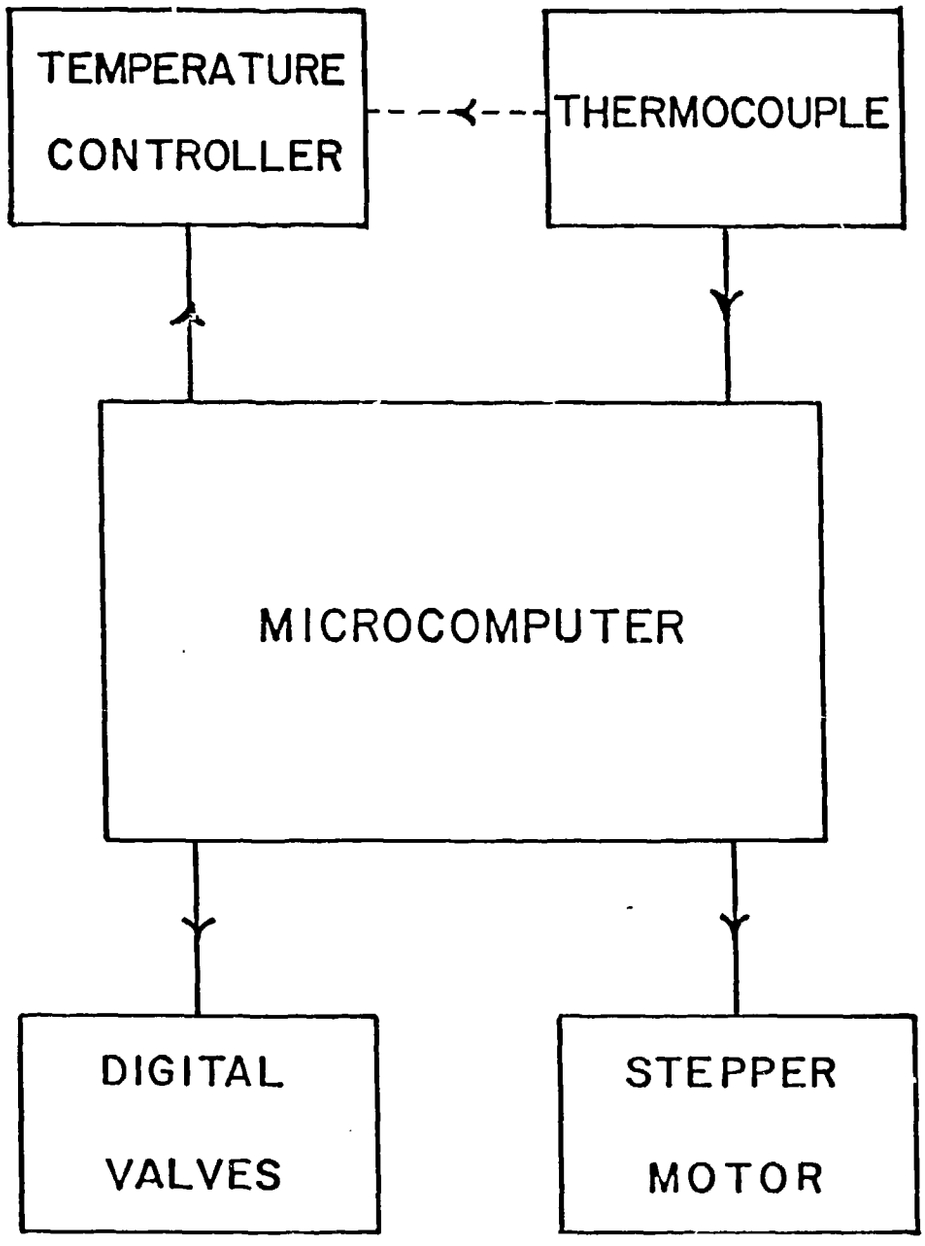

Compucolor-Crystal Grower Interface

Figure 4-4

allows one to alter the process during crystal growth. It also allows for manual take-over at any point, for any reason. It is definitely a very useful technique for controlling a process-control type system such as this because of the freedom of control.

Due to the nature of operation of the Compucolor computer system, the interrupt system of the computer is already being used at close to its limit of capability. There is one 8080-A interrupt address remaining for user use out of the eight which are built into the C.P.U. After using this remaining interrupt for an extended period of time (3-4 months), and experiencing occasional system failures at random times, it was determined that there was no method of using this interrupt without interfering with the internal timings of the machine. This situation arose due to the interrupt software which was used in the Compucolor. There was no way to modify the software since it was contained in the read-only portion of memory. Since this now meant that the present interrupt scheme would not work, a new method had to be found. The computer system is operated using a computer language called Forth. The language operates by repetitive execution of an inner-loop which circles through instructions, and an idle-loop which waits for terminal input during periods of non-execution.

4.2 GROWING TECHNIQUES

The first procedure which must be carried out before beginning any crystal growth is to etch the raw materials. The ingredients used to grow the crystals tend to pick up fairly large amounts of surface contaminants and oxides. These unwanted agents can interfere with the crystal growing process and must be eliminated. The accepted procedure is to etch the crystal in a material which actually dissolves the surface, thus eliminating the unwanted surface contaminants.

The etching process for germanium and silicon is slightly different. The etchant solution used for germanium consists of the following:

a) 1 part H_2O_2

b) 1 part HF

c) 4 parts H_2O

The germanium is etched in the above mixture while the mixture is heated to a boil. After etching, the material is washed in distilled water and dried before weighing and insertion into the crucible.

The etchant solution used for silicon consists of:

a) 1 part HF

b) 2 parts HNO_3

This etchant is used at room temperature and in a plastic crucible since this solution dissolves glass. The reaction is quite vigorous and must be done under a fume hood. If allowed to continue indefinitely, the etchant will dissolve all of the silicon. In general, very small amounts of silicon are used, therefore only a few small pieces are placed in 20-30 ml. of etchant. Adding 100 ml. of distilled water halts the reaction. The silicon is then removed, washed, weighed and placed in the crucible with the germanium.

The normal amount of germanium used with the system is 50-60 grams. The crucible will easily accommodate twice this amount, but it is advantageous to have crystal growth occuring slightly down inside the crucible and susceptor. This helps to grow flatter faces of constant index by flattening out the isothermal surfaces during growth. After the amount of desired germanium is determined, the required amount of silicon must be calculated to create the desired initial silicon concentration.

All references to percent concentration refer to atomic percents. Therefore, the percent silicon level can be found as follows:

$$\%Si = \frac{\text{\# of atoms of silicon}}{\text{\# of atoms of silicon \& germanium}}. \qquad (4\text{-}1)$$

The number of atoms of any element can be related back to its mass via its molecular weight and Avagadro's number. For any pure element:

$$\#\ \text{of atoms} = 6.02\text{x}10^{23}\ \text{x}\ (\text{mass in grams})\ \text{x}\ \frac{1}{\text{M.W.}}. \quad (4\text{-}2)$$

Now substitute Eq. (4-2) into Eq. (4-1). The molecular weight of silicon is 28.0869 A.M.U. and that of germanium is 72.59 A.M.U. This results in the following expression for the percent silicon in terms of the masses of silicon and germanium in the melt:

$$\%\text{Si} = \frac{M_{si}}{M_{si} + \frac{28.086}{72.59} M_{ge}}. \quad (4\text{-}3)$$

Most of the experiments of practical value are started with initial concentration of about 1% silicon, and average germanium masses of about 60 grams. This leads to the result

that the average initial silicon mass is about 250 mg. Therefore its mass must be measured on a very sensitive balance since this mass should be known to within one percent. Since the density of silicon is 2.33 grams/cm.^{3}, this requires only about 0.1 cm.^{3} of silicon. This calculation has been done to illustrate the small quantities of silicon involved in the process and to understand the importance of handling and controlling these small values very accurately.

After materials have been prepared and inserted into the crucible, the system is sealed and purged of oxygen by flushing with nitrogen. A thermos of liquid nitrogen is attached to an inlet port and allowed to boil away. A one liter thermos of liquid nitrogen is adequate for growing one crystal. After purging the system, the R.F. generator is started and the computer is activated to raise the temperature to about 1100°C. This is well above the melting point of germanium (935°C) and allows the silicon to dissolve in the molten germanium.

The system allows time for the silicon to dissolve and then begins it's prearranged cooling cycle. At a temperature of about 20°C above the crystallization point, the crystal seed is lowered. This allows the system to reach a thermal equilibrium. After crystallization begins, the computer operates a prearranged pulling and temperature

cycle. Figure 4-5 illustrates a typical temperature versus time plot for sample IR-5 and has the critical points labeled.

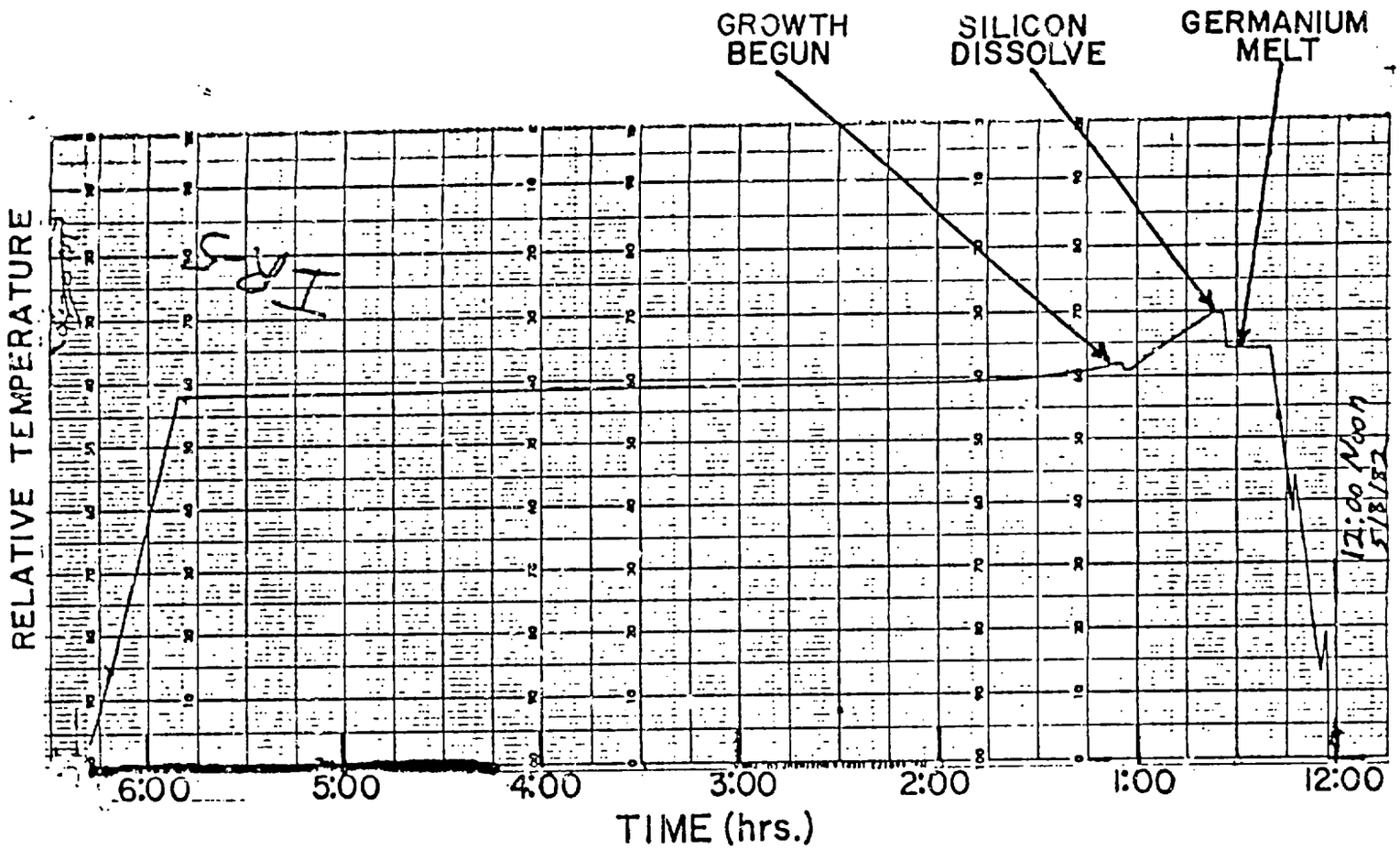

Temperature versus Time for Sample IR-5

Figure 4-5

4.3 PROBLEMS AND SOLUTIONS

It is interesting to briefly investigate how the crystal gradient growing system developed. The techniques evolved as different problems became evident. The last section briefly outlined how a crystal is grown. This section examines some of the early experiments, their problems, and subsequent solutions.

In early experiments, the oxidation of materials was a problem when heating to the required temperature. These early tests were done under a nitrogen atmosphere, but the system was not adequately sealed from the external atmosphere. Germanium-oxide formed on the melt surface and interfered with the growth process.

The sealing of the system was improved. The problem of adequately sealing the system for operation under vacuum was serious. The largest difficulty was a leak at the pulling rod entrance to the chamber. Attempts at vacuum techniques were abandoned, and again flowing a positive pressure of nitrogen from the liquid state was tried. The work done in attempting to seal the system for vacuum operation proved adequate for operation under positive nitrogen pressure. Thus, the oxidation problem was eliminated.

The next problem which was encountered was in the early stages of crystal growth. The original technique used for pulling a crystal consisted of a tungsten wire attached to a seed holder on the end of the pulling rod. This proved to be adequate at the beginning of crystallization, but large crystals (50 grams or larger) often broke from the seed wire and fell into the melt. This led to attempts at using germanium seeds as a starting point for crystalliztion.

The germanium seed technique is the current method used and has evolved into the form illustrated in Figure 4-6. The seed crystal is notched a few millimeters from one end to allow for easy clamping. The crystal shape is about 1 cm. square and about 5-10 cm. long. When it is initially lowered into the melt, the end melts off and since the pull rod is rotating, the seed "necks" into about a 2 mm. diameter cylinder. Crystallization then begins from this seed. This technique has been very successful but must be used with care since the melt temperature is usually about 25-30°C above the melting point of pure germanium. This requires that caution be used until crystallization has begun since it is very easy to melt off the end of the seed and lose contact with the melt.

The next problem arose when dissolving silicon in the germanium melt while using graphite as a crucible material.

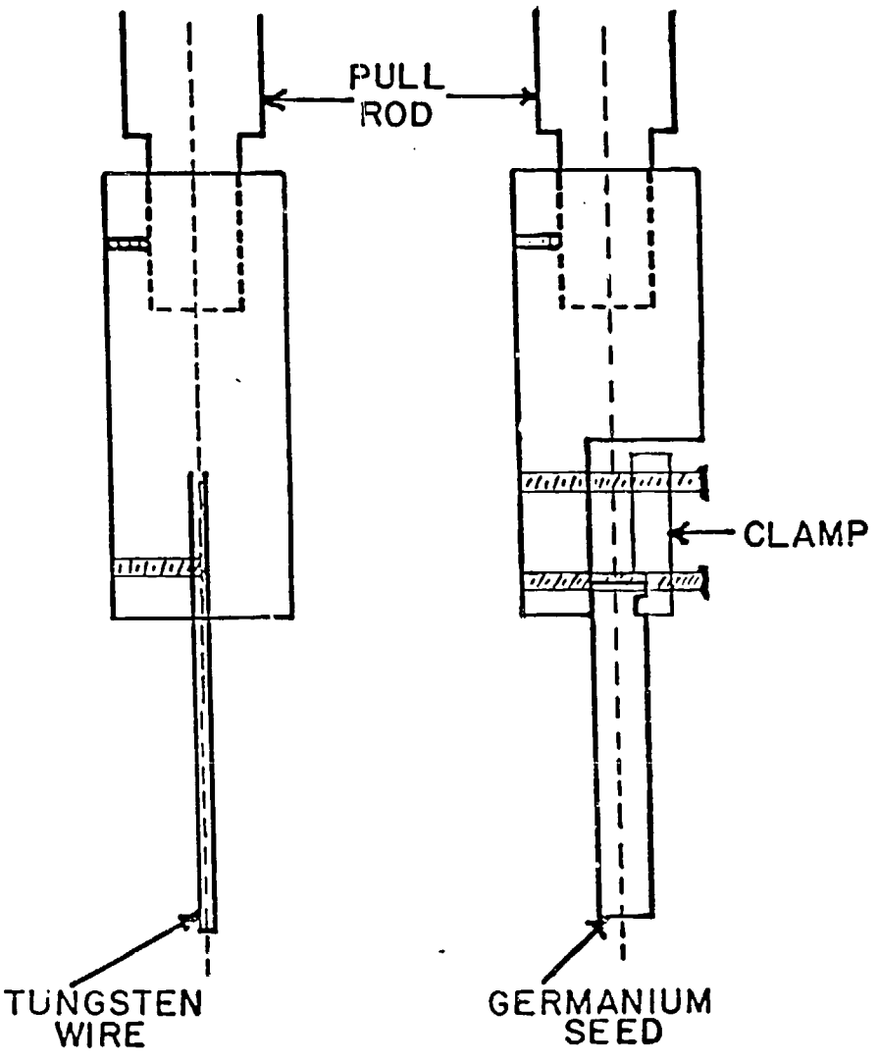

Seed Holders

Figure 4-6

This led to the formation of very small (1 mm. diameter) dendritic type crystals of varying length on the melt surface. These would not dissolve even at temperatures as high as 1250°C, which is well above the liquidus temperature for the concentration of silicon in the melts. Therefore, it was concluded that these may be silicon-carbide crystals, but no attempt was made to verify this analytically. This problem was alleviated by using silica crucible liners inside of the graphite, and only using the graphite as a susceptor. The problem has not been encountered since implementing this modification. This seems to indicate a reaction between the silicon and the graphite since germanium grows very well using graphite crucibles.

The last two difficulties are somewhat interrelated. They are the initial silicon concentration used and the crystal pull rate. Both of these problems can be related to an attempt at trying to crystallize silicon from the melt at a rate faster than the melt can maintain equilibrium. Silicon is rapidly depleted from the melt, especially during the beginning phases of crystallization. If material is forced to crystallize at a rate faster than feasible, a silicon depletion area forms near the interface between crystal and melt. This leads to the formation of very small crystals, all of which form silicon gradients. This phe-

nomena could be called micro-segregation. This led to crystals with large amounts of scatter, and in some cases led to opaque crystals.

These problems were eliminated by starting with no more than about 1% initial silicon concentration in the melt. Pulling speeds never exceed 3-4 mm./hr. near the homogeneous end of the crystal, and much slower pull rates are used while crystallization is beginning. This compares with pull rates for pure germanium with the same system and crystal size of about 20-50 mm./hr.

4.4 RESULTS

The experiments that resulted in crystals which were worth testing are summarized in Table 4-1. The samples listed are designated with IR prefixes. This designation applies only to samples which were cut, polished, and tested. Samples which were fabricated but not listed were regarded as failures. Generally, these were incomplete crystals and after experiment 24 the usual reason for failure was mechanical difficulty with the crystal grower. Prior to Experiment 24, there were many other problems which needed to be solved. These problems and solutions have been discussed in the preceding sections.

In the following discussion of crystals and results, the experimental and calculated index distributions are compared. The interferometric measurements, except in special cases which are stated, were all taken as a function of position along the axis of the crystal. This measurement is facilitated by slicing a 2 mm. thick sample from the center of the crystal and parallel to the axis of crystal rotation. This sample is then ground and polished to an optical quality surface. The parallelism between the two faces is maintained to within the accuracy of a an arcsecond. This resulted in wedges of less than two fringes at 10.6 μm., when measured in transmission. In samples which were grown

Sample Number	Exp. Number	(1) Initial Ge Mass (g.)	Initial Si Mass (g.)	Mass of Remaining Material (g.)	Initial Si Con. C_o (%)	(2) Growing Time/hr.	(3) Scatter	Expected Δn	Measured Δn	Useful Δn	Useful Gradient Thickness (mm)	Measured Sample Thickness (mm)
IR-1	15	178.8	1.4305	N/A	2.026	0:54	D,--	0.271	----	0	0	2.34
IR-2	19	68.1	0.4929	N/A	1.836	N/A	D,--	0.250	----	0	0	3.96
IR-3	24	57.2	0.2526	18.9	1.128	4:25	B,A	0.164	0.15	0	0	1.93
IR-4	26	54.65	0.266	28.7	1.242	3:36	B,--	0.179	----	0.02	2	1.91
IR-5	27	55.7	0.257	0	1.178	4:17	B,A	0.171	0.18	0.06	6	1.91
IR-6	28	56.17	0.259	0	1.178	4:55	B,A	0.171	0.18	0.06	6	1.93
IR-7	30	55.5	0.258	0.044	1.187	3:25	B,A	0.172	----	0	0	1.93
IR-8	31	55.3	0.260	N/A	1.196	N/A	B,C	0.173	----	0	0	1.96

(1) Includes addition of melted portion of germanium seed

(2) From time of initial crystallization to removing crystal from the melt

(3) The first code corresponds to high silicon region
The second code corresponds to high germanium region

(A) Little scatter, wavefront measured

(B) Some scatter, wavefront measured

(C) Some forward propagation, no wavefront

(D) No forward propagation

Crystal Growing Results Summary

Table 4-1

to completion, it is easy to align the interferometer so that the remaining wedge is not important. It is difficult to remove wedge error from the measurement of samples which do not contain large homogeneous regions. All samples were also measured with a test plate to assure that the surface irregularity was minimal. These types of errors must be eliminated when the sample is being prepared. No crystal had more than one wavelength of surface error when measured at visible wavelengths.

Figure 4-7 illustrates the cross-sectional shape of each of the crystals listed in Table 4-1. This information is important because there is no way to model the entire crystal growing process, and, consequently, it is difficult to predict apriori the shape of the crystal. After gaining experience in the process of the crystal growing process, it is now possible to now reproduce previous crystals. These programs can be altered to make predictable variations in the crystal's final form.

In order to do a realistic comparison between theory and experiment, it is necessary to have information about the radius of the crystal as a function of length. This information is obtained by laying the polished crystal on a piece of millimeter ruled graph paper and centering the crystal along some axis. The crystal shape can then be traced out

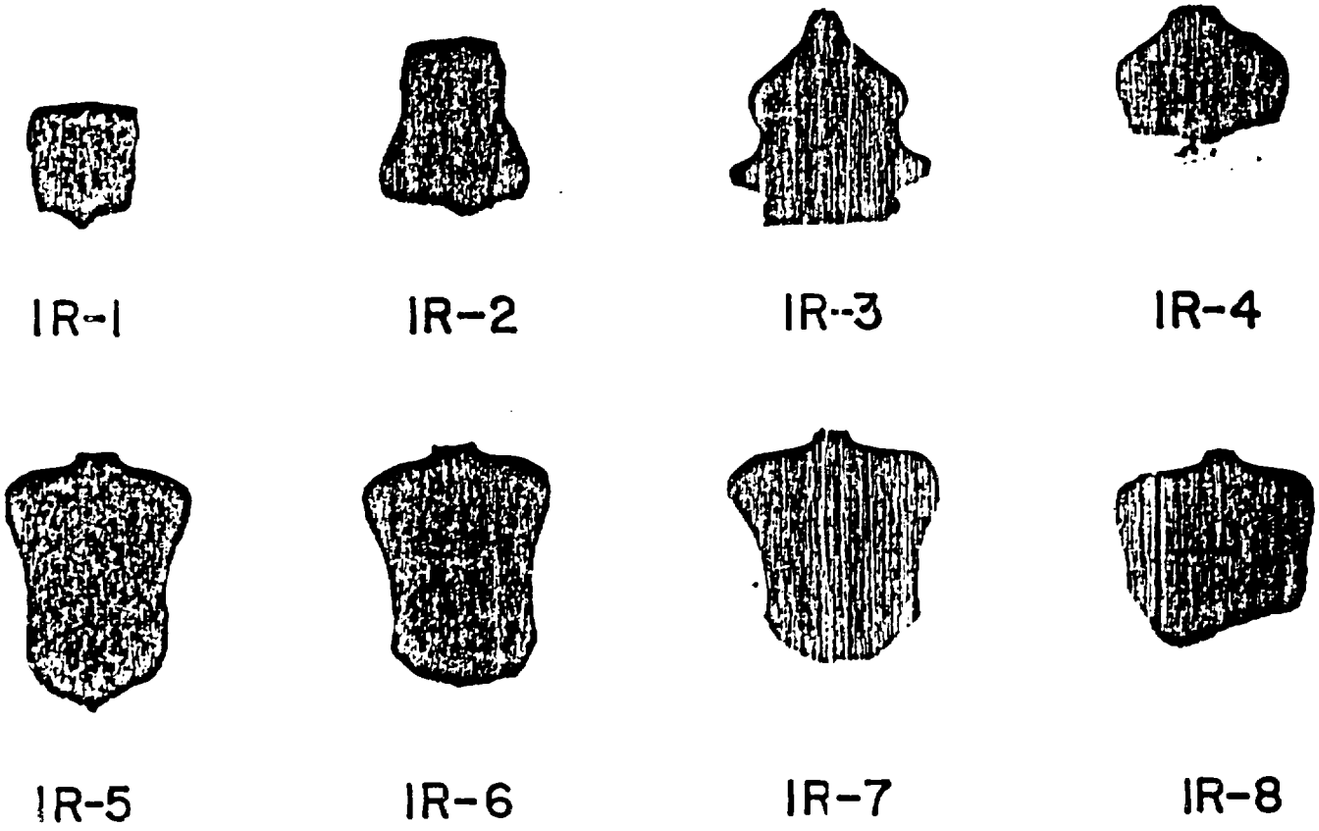

Crystal Cross Sections IR-(1-8)

Figure 4 -7

on the paper and the resulting crystal radius can be measured as a function of ℓ, the crystal length. A series of data for $R(\ell)$, where ℓ has integer values with units of millimeters.

The information obtained in this way can then be used to calculate $V(\ell)$, the total crystal volume as a function of length. $V(\ell)$ can be calculated at integer values of ℓ, by the following equation:

$$V(\ell) = \sum_{n=0}^{\ell} \pi R^2(n)\ \Delta\ell \quad \text{mm.}^3, \qquad (4-4)$$

where n, ℓ integers, and $\Delta\ell$ = 1mm.

The concentration profile in the crystal depends on the fraction of material crystallized. This quantity is related to the volume as a function of length by the following relation for $g(\ell)$:

$$g(\ell) = \frac{V(\ell)}{V_{total}}, \qquad \ell = \text{integer}, \qquad (4-5)$$

This quantity is very important, because it is used to derive the silicon concentration. In the previous chapter, it was shown that under the assumption of low initial silicon concentration in the melt, the concentration profile has the following form:

$$C(g) = 5.5\ C_0(1-g)^{4.5}. \qquad (4\text{-}6)$$

Upon substitution of $g(\ell)$ into the expression for $C(g)$, one obtains the series of numbers for $C(\ell)$ for integer millimeter values of ℓ. From this expression, it is a simple matter of substituting the expression for band gap as a function of concentration. This is given from experimental data taken by Johnson and Christian.[1] The expression has the following form:

$$\begin{aligned} EGAP(C) &= 0.72 + 1.467\ C_{si}\ \text{eV.}\quad C_{si}<0.15 \\ &= 0.894 + 0.306\ C_{si}\ \text{eV.}\quad C_{si}>0.15, \end{aligned} \qquad (4\text{-}7)$$

Since the concentration of silicon is always well below 10%, the first half of the expression given in the last equation is relevant. Substitution of the values for C(ℓ) into this equation now gives the expected value for band gap as a function of length. This can then be used in the expression for refractive index as a function of band gap derived in the previous chapter.

These calculations are all done in the computer by entering the original function R(ℓ), the volume of germanium remaining in the crucible after crystal growth, and the initial concentration of silicon. This results in a theoretical calculation of index as a function of length. The results can be plotted on the same scale as the experimental data which was taken by the interferometer. This is the method used to make the following plots. In each case, the theoretical curves are plotted as a series of points at 1 mm. intervals and superimposed on top of the measured index profile.

Samples IR-1 and IR-2 both have very high scattering and can not be measured interferometrically. It is assumed that the pulling speed and temperature cycling rates were too rapid to allow for large scale crystallization. This may have caused very small crystals to form, each of which has its own gradient. This causes scatter, and also eliminates any gradient formation on a large scale.

The first crystal with a verifiable gradient was sample IR-3. This crystal was grown with much operator interference during the growth process. This was caused by a lack of experience in growing gradient crystals and improper computer programming. The shape of the crystal testifies to the fact that there were many discontinuous variations in growing parameters at various points along the crystal. This can be seen in the crystal cross-section shown in Figure 4-7.

Figure 4-8 shows the calculated and measured indices of refraction as a function of position. The overall agreement is very good. There are deviations which occur at two obvious locations. These can be traced back to the two large changes made in the growth process as can be seen from the crystal profile in Figure 4-7. The overall change in index is within 5% of the predicted change in refractive index over the full length of the crystal. The surfaces of constant index have always been assumed to be planar when performing the theoretical calculations. This is the case for most crystals made later, but the rapid changes which occurred during crystal growth forced Sample IR-3 to have relatively steep curving surfaces of constant index. With the external heating system as it was, the general shape of the iso-index surfaces are generally curved so that they are

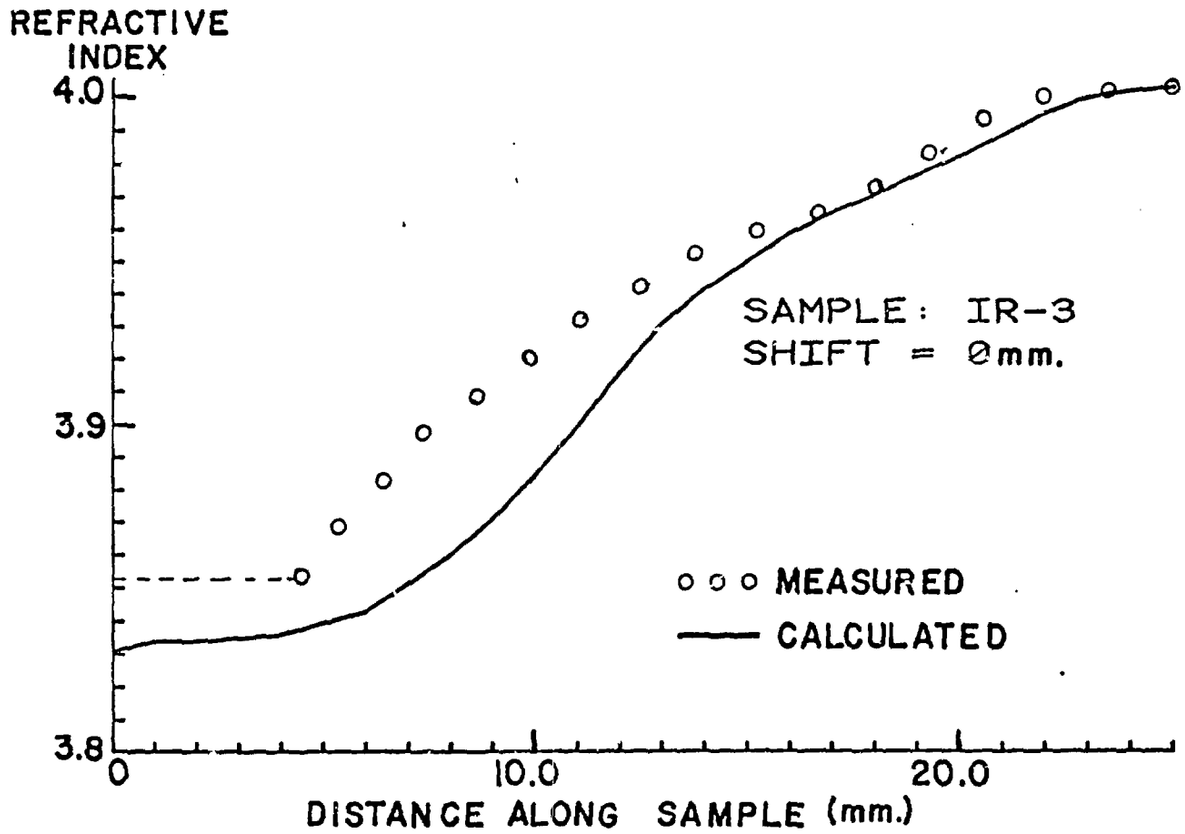

Calculated and Measured Refractive Index Profiles Sample IR-3

Figure 4-8

normal to the outer crystal surface. Figure 4-2 illustrates the curved surfaces of equal phase as seen in Sample IR-3.

The growth of sample IR-4 was an attempt at increasing the total change in index by increasing the initial silicon concentration slightly. This crystal has more scattering in the upper 3/4 of the crystal and it was very difficult to obtain any phase measurements in the upper 65%. The crystal was also not grown to completion, thereby not allowing one to adjust out any wedge which is present in the sample.

Sample IR-5 was a very succesful crystal. IR-6 was grown in an attempt to duplicate the index profile of IR-5. As can be seen in Figure 4-7, the $R(\ell)$ for the two crystals is very close. Figure 4-9 shows the calculated and experimental curves for sample IR-6. Figure 4-10 shows the deviation between samples IR-5 and IR-6. Again, it is seen that the agreement between the two is quite good. Figure 4-11 shows the variation in $n(\ell)$ for different radii from the center of the crystal. It can be seen that there is curvature present in the iso-index surfaces. This is mostly restricted to the upper 50% or less of the crystal. Once the process is stable and the diameter of the crystal is held constant as a function of ℓ, the curves seem to be very consistent. This would indicate that only the lower half of the crystal could be used in the fabrication of a gradient index element.

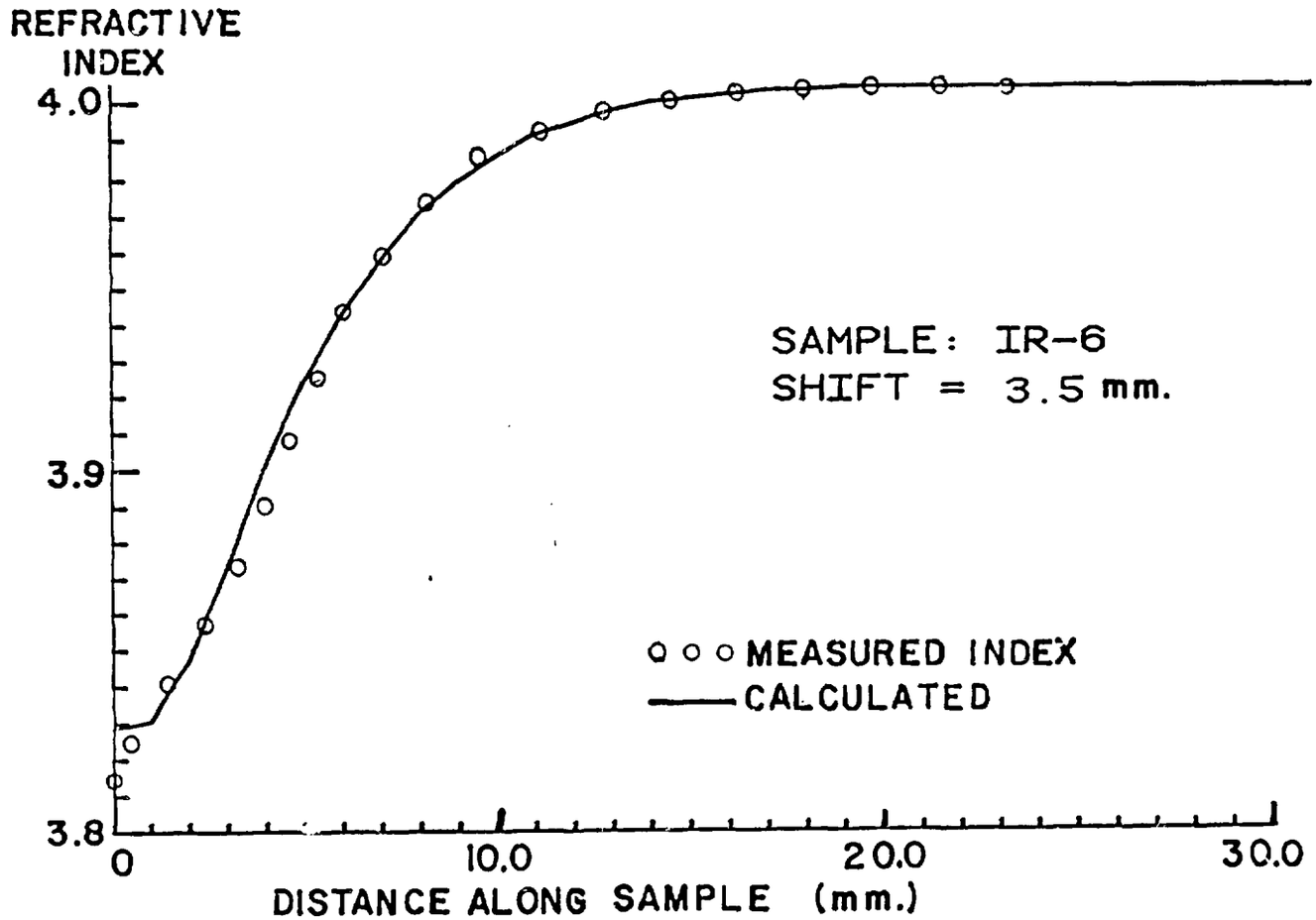

Sample IR-6 Calculated and Measured Index Profiles

Figure 4-9

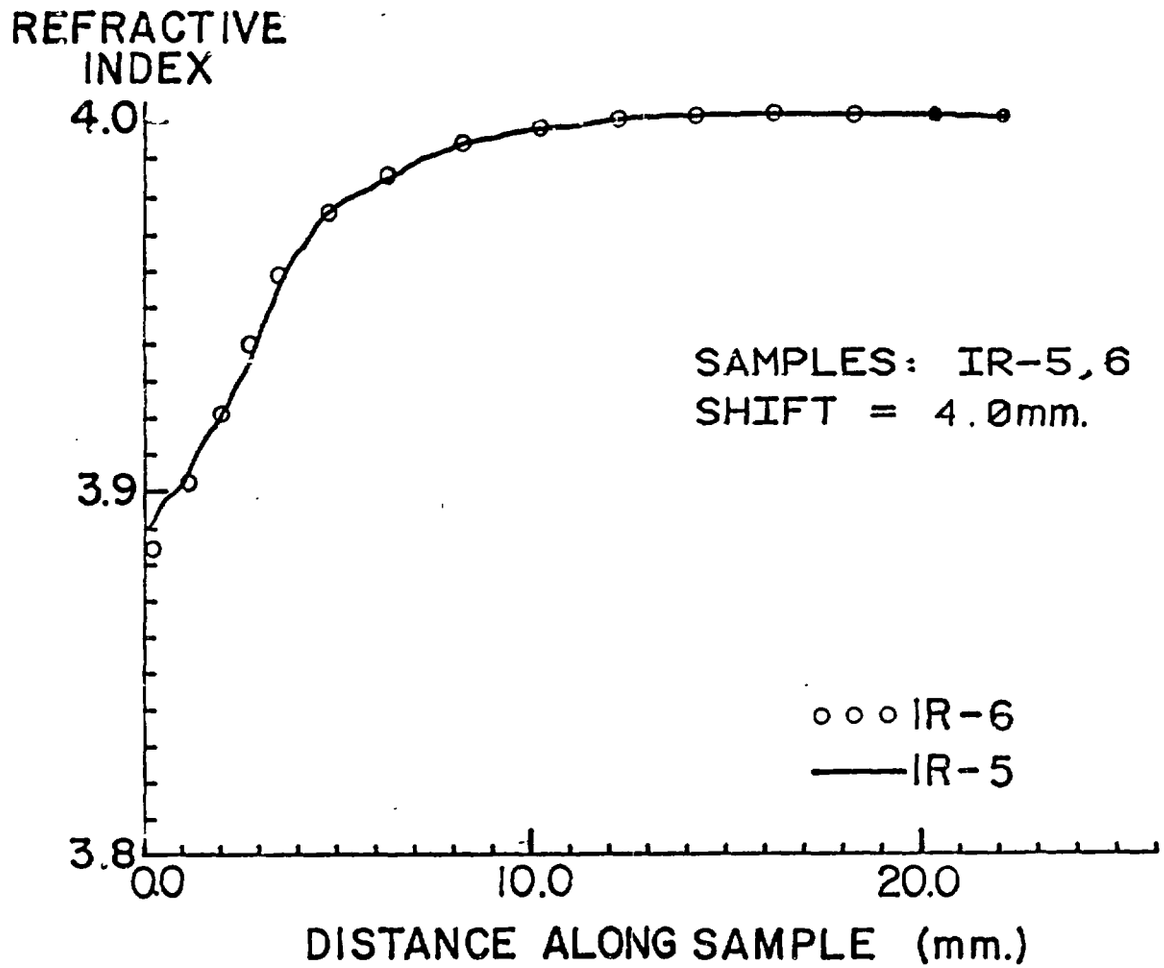

Comparison of Index Profiles for IR-5,6

Figure 4-10

This limits the useful Δn to about one third of the total or about 0.06, when a pure axial gradient is required.

Figure 4-12 shows the measured profile for Sample IR-7. After approximately one hour growing time, the crystal seed slipped in its holder. This allowed the crystal to be tilted and define a new axis of rotation. The crystal continued to grow normally except for this new axis. It was assumed that this would not have any serious effects on the lower half of the crystal and growth was continued. The result was the periodic index variation which is seen in the experimental data shown in Figure 4-12. The periodic index variation has a period of about 1 mm. with an amplitude of about 0.002 in refractive index.

In the case of sample IR-8, the entire seed holder fell off of the pull rod because it was not properly attached. This resulted in the crystal falling into the melt. The system was frozen in this form. The concentration in the melt was still fairly high, about 0.2%. The upper portion of the crystal had grown normally, but the lower "blob" as seen in Figure 4-7 was formed by a quick freeze. It is impossible to make phase measurements in this region although the upper half had expected properties.

The most important conclusion is that the index profile and total index change compare favorably with theory. The

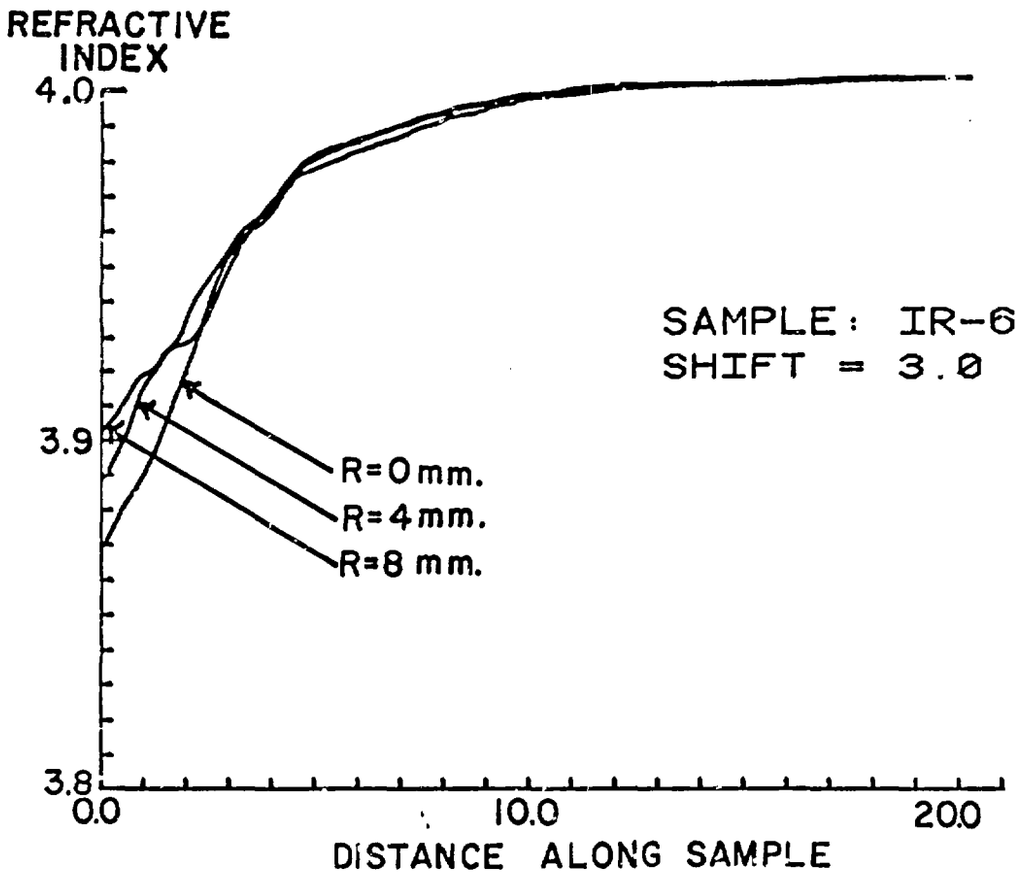

Sample IR-6 Variation of Gradient with Radius

Figure 4 -11

second important result is that with the techniques used, it generally took the first 30-50% of material to stabilize the growth process. There are two reasons for this. The first is that there are many transient effects occurring in the initial "necking out" and stabilization of crystal growth. The second reason is the rapid rate at which silicon is being depleted, thereby forming the steepest portion of the gradient.

Another important observation is that all crystals are polycrystalline in nature. At the high silicon end the number of individual crystal structures is greatest. This end contains the smallest polycrystals, usually on the order of 1 mm. in all dimensions. As growth continues only certain structures dominate, and the crystal structure progresses to a much larger polycrystalline structure. This probably accounts for the higher scattering at the top end of the crystals.

The conclusions regarding the use of this technique for optical material for use in actual optical elements is varied. It is definitely possible to get a change in index of refraction of sufficient magnitude to be practical. There are many improvements in technique which could produce very well controlled axial gradients. Discussion of actual conceived uses and actual suggested improvements are discussed in the following chapter.

References

[1]E. R. Johnson and S. M. Christian, "Some Properties of Germanium-Silicon Alloys," Phys. Rev. 95, 560 (1954).

Section V

Fabrication of Large Geometry Radial Gradients

Several methods have been suggested for manufacturing large geometry radial gradient optical elements. Generally, the method must allow for arbitrary profiles of index of refraction as a function of radius and be manufacturable in diameters of one to five centimeters. The normal diffusion techniques used for manufacturing axial gradients and small diameter radial gradients are not applicable for two reasons. First, the maximum diffusion depths are only five to ten millimeters and the profiles of index of refraction versus radius are limited by the geometry of the system. A number of techniques have been proposed. These include:

1) Phase separated glasses for enhancing diffusion depths
2) Electric field assisted diffusions
3) Vapor phase axial deposition
4) Chemical vapor deposition
5) Photopolymerization.

While the general thrust of this work was to investigate phase separated glasses, it is worthwhile to put this method in context. The electric field assisted diffusion method uses the prinicpal of a electric field established by a pair of conducting electrodes to modify the diffusion properties. This drives ions from the salt bath into the glass at a higher

rate. The diffusion rates can be enhanced by nearly an order of magnitude and it is possible to modify the index profile simultaneously. This technique appears to be a very viable method particularly in making large production runs of axial gradients. To date no work has been done on the use of electric field assisted diffusions in radial gradients.

The vapor phase axial deposition technique (VAD) was developed by the Japanese for low loss telecommunication fiber. The method is the deposition of material on the end of a cylindrical rod. If a temperature gradient is maintained between the center and edge of the rod, the deposition rates of various materials will be modified. Thus, it is possible to vary the composition of germanium oxide and silicon oxide as a function of radial coordinate by maintaining this temperature profile. This has been very successful and has led to the lowest loss optical communication fiber yet reported. In fact, it is within a few percentage points of the theoretical limit for loss. No work has been done on this technique for making optical components nor have the various materials been investigated which would allow one to determine which glasses can be deposited and which can not.

The chemical vapor deposition technique (CVD) is a deposition method similar to the VAD method, except the

deposition is done inside or outside of a cylindrical rod. In this method, layers of material are built up, each one of which is homogeneous but each one of which has an index of refraction different from its previous value. This leads to a series of discontinuous steps in index of refraction as a function of radial coordinate. It is expected that this technique will not be very useful for normal imaging components, however, a new method of analysis for these types of systems has been developed by Delano. In this analysis, it is possible to consider these systems as gradient index Fresnel optics. Therefore, it is possible to use these in Fresnel systems where it is difficult to fabricate grooves.

A final method is that of photopolymerization in which the index of refraction is changed by incident radiation. In this technique, a laser beam is incident on the material. The absorbtion of the photons from the beam then changes the energy state of the polymer and, thus, changes the index of refraction locally. This has the potential to make very large radial gradients of arbitrary index profiles. Currently this technique is being investigated under other contracts.

During this contract, we investigated the possibility of using phase separated glasses for manufacturing large geometry radial gradients. The technique is to take a

normal optical material, such as glass, raise the temperature above the transition point, and to cool it down so that the materials in the glass separate into two phases. One of the phases is normally a sodium rich phase which is soluable in some sort of acid and, thus, can be dissoved out. The resulting glass net-work is similar to a sponge. The open structure then allows diffusion of other ions into the material. After the new ions or molecules have been diffused into the material, the glass must be reconsolidated to form an optically clear glass.

The basic problem in this technique is to obtain a completely interlocking hole structure. During the initial phase separation, it is important that each of the holes to be eventually dissolved be interconnected so that the molecules can flow into the cavities during the diffusion process. If they do not completely interconnect, there will be large voids in the material, which will inhibit the diffusion and cause irregularities in the index of refraction profiles.

A second problem is the temperature at which the glass must be reconsolidated to form an optically transparent material. This value is highly dependent upon the size of the holes present and is in the range of 1400° for 50 angstrom holes. However, at these temperatures the glass begins to flow and therefore its shape will change.

We investigated a number of phase separated glasses

manufactured by Corning and by Hoya of Japan. In the case of the Corning glass, we were unable to consolidate it because of the high temperature involved (1450^{o}). In the case of the Hoya glass, a boundary layer existed in the center which inhibited diffusion through it. In discussions with Hoya representatives, it was not clear whether this could ever be eliminated.

At this point, we do not feel that the phase separated glass technique for making large geometry radial gradients is currently viable. Two technologies will have to be improved before it is usable. The first is to create glasses with such high homogeneity that the phase separation occurs throughout the material and, secondly, a thorough study will have to be undertaken to determine the dynamics of the phase separation process and the reconsolidation process. This work is currently being conducted by other groups, particularly for optical communications.

Appendix I

Ellipsometry
Experimental Apparatus

A polarization modulated ellipsometer has been built to measure absolute index profiles of gradient index samples. Figures I-1 and I-2 are respectively a schematic and a photograph of the optical system.

A Krypton ion laser, operating at λ = 6471 Å is used as the light source. Two microscope objectives and a pinhole are used as a spatial filter and beam expander. The beam diameter is increased by a factor of four. This is large enough to cover any existing gradient regions without wasting a large portion of the beam. A Glan-Foucault prism polarizer is used to provide linearly polarized light at a known azimuth. After reflecting from the sample, the light passes through the Faraday rotator and another polarizing prism used as an analyzer. Two lenses are used to image the sample face onto the detector with magnification. The detected signal is then processed by the electronic system.

I.1 ANGLE OF INCIDENCE

The angle of incidence has substantial effect on the accuracy and sensitivity of ellipsometric measurements. The optimum angle varies for different samples. Most commercial ellipsometers have built in capability for

Layout of Optical System

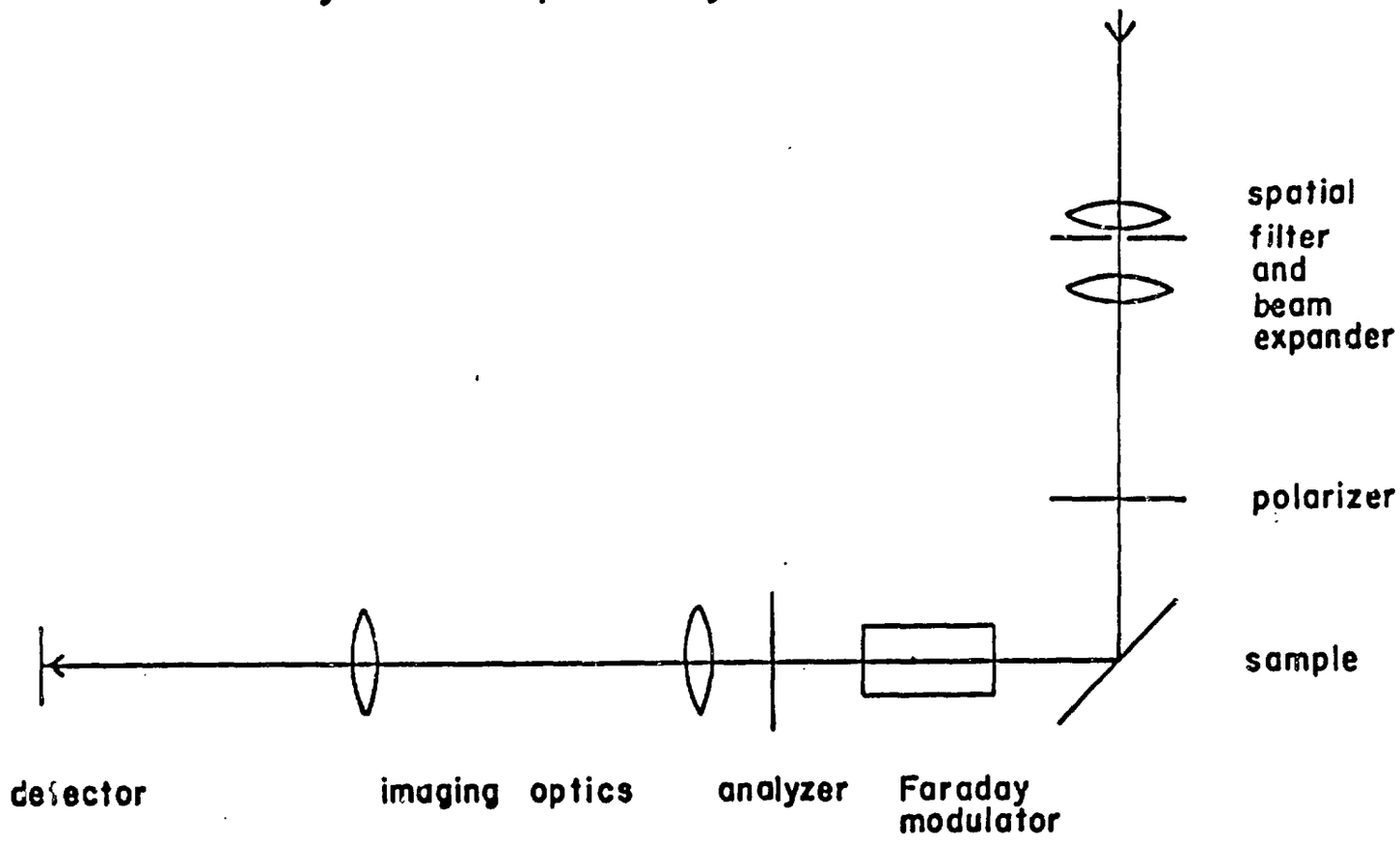

Figure I -1

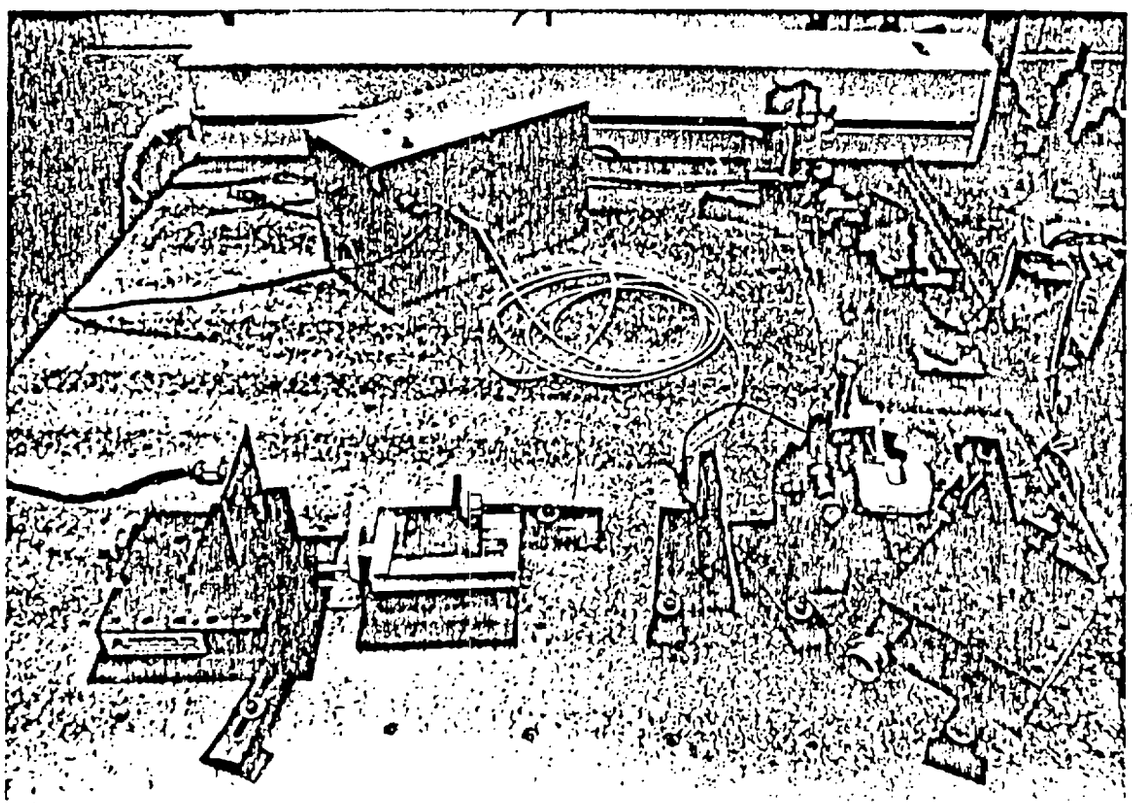

Figure I-2

adjustment of angle of incidence. This instrument has been designed to study the feasibility of measuring gradient index samples using ellipsometry and for simplicity operates at a fixed angle of incidence. This necessitates careful consideration of angle of incidence effects and types of samples to be measured; an angle must be chosen which will work reasonably for all cases.

The angle of incidence, θ_i, affects the precision of the measurement of ψ and, therefore, the accuracy of calculating n from ψ. Figure I-6 is a plot of $\frac{dn}{d\psi}$ vs. θ_i and demonstrates that the error in n is smallest when θ_i is near the Brewster angle, θ_B. In addition, the total signal strength increases with increased θ_i (see Figure I-3).

Figure I-9 shows that the sensitivity (and therefore precision) of measuring ψ increases with θ_i for the PSMA configuration. If the PMSA configuration is used, both the sensitivity of measuring ψ and the amplitude of the polarization modulation are greatly reduced near θ_B. These effects can be controlled with proper choice of incident polarization, α, but this requires constant monitoring as samples are changed. To accommodate the general case without much difficulty, an angle of incidence not too close to the Brewster angle is desired. This approach is a compromise. It is not

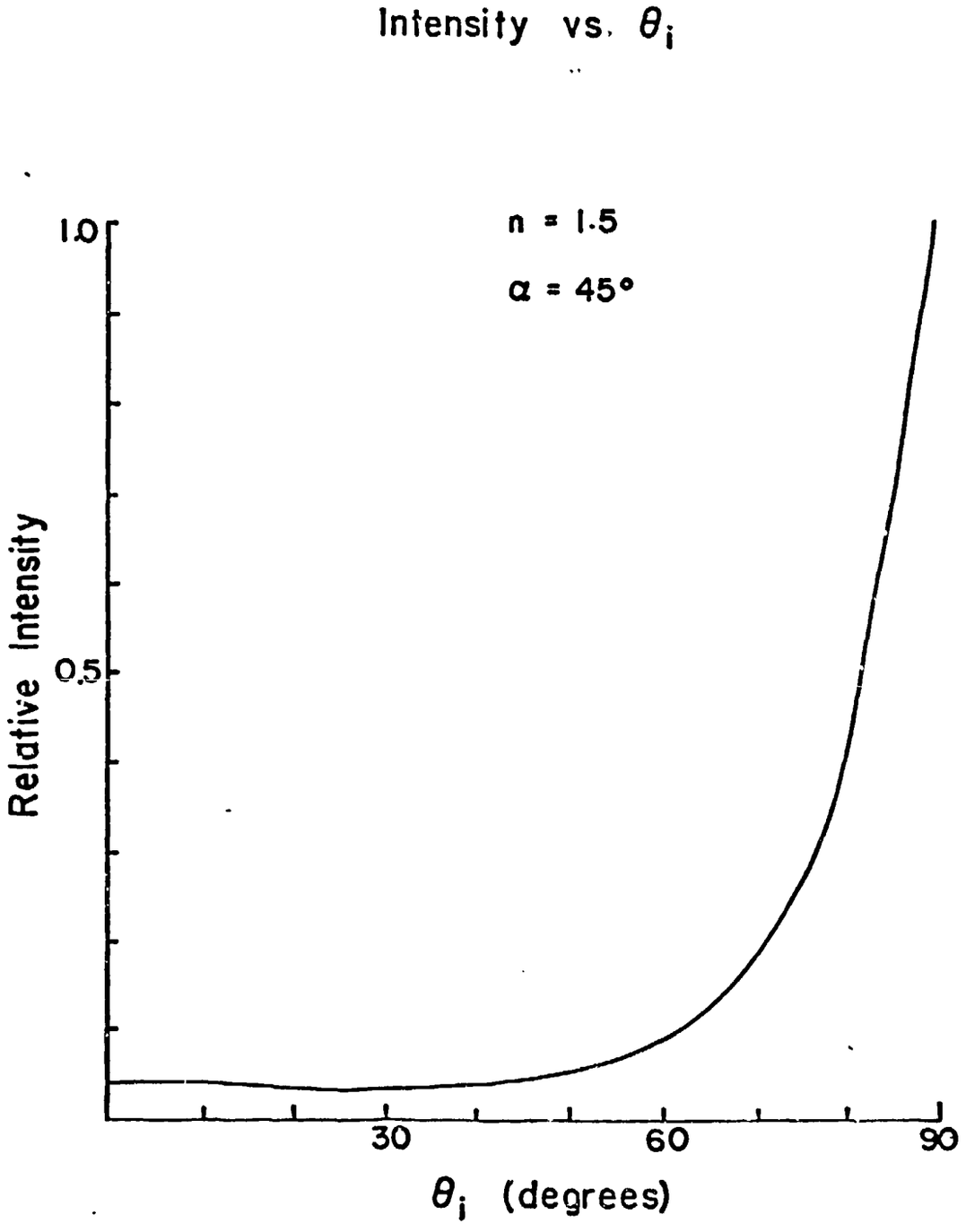
Intensity vs. θ_i
n = 1.5
α = 45°
1.0
0.5
Relative Intensity
30
60
90
θ_i (degrees)

Figure I-3

the optimum solution but prevents any effects from becoming too deleterious. The range of refractive indices being considered is approximately 1.5 to 2.6; the Brewster angle varies from 56° to 69°. An incidence angle of 45° was chosen as a reasonable compromise. In addition, the relative ease of setting 45° accurately reduces the amount of error introduces into the system.

I-2 COMPONENT DESCRIPTION

Polarizers

Both polarizer and analyzer are air-spaced calcite polarizing prisms made by Optics for Research. The extinction ratio specified is 10^{5}, and the end faces have been aligned parallel to one-half minute of arc. A broadband anti-reflection coating centered at 6000 Å has been applied to each end face.

Each prism is mounted in an Oriel precision polarizer rotator. These mounts allow 360° rotation with readings to 0.1°. In addition, a fine adjust micrometer drive operates over a range of 16°. Micrometer divisions represent approximately 1 minute of arc; angle resolution is 1 arc second.

Faraday rotator

The Faraday rotator consists of the core glass with a concentric solenoid. The glass is Hoya FR-5, a

terbium-doped silicate, with n_d = 1.6862. The optical path change due to the birefringence of this glass is nominally less than 10 mm/cm. Absorption is appreciable because of the presence of the terbium. At λ = 6471 Å, the absorption coefficient is approximately $85m^{-1}$.[29] Transmission is only 7% for the thickness of 31 mm. The Verdet constant is 0.23min/Oe-cm at 6328Å and the dimensions of the core are 6.35mm diameter by 31 mm long.

The Faraday core is centered in a coil 58 mm long with inner radius equal to 11 mm. With these dimensions, the magnetic field over the length of the core is uniform to within 2%.[1] The coil consists of several concentric layers with approximately 2600 windings total. The resistance is 48 ohms and the inductance approximately 0.08 henries. The coil was chosen with both DC and AC response in mind. The largest possible DC and AC magnetic fields are needed for a substantial range of polarization rotation and a reasonable amplitude of the rotation modulation. A high value of inductance will provide a large DC magnetic field for a given applied voltage, but will degrade the AC field amplitude because of its high impedance value. A DC response of 0.14 degrees/volt is measured. To obtain a range of rotation of ± 2^o, more than that required over the gradient regions measured, a DC bias of ± 15v is required. With

a modulation of 500 Hz, a ± 10v modulation amplitude yields a ± 0.25 rotation modulation. This corresponds to a maximum DC field of 0.3 amps and 170 Oe and an AC amplitude of 0.04 amps and 22 Oe. These magnetic fields are small enough that cooling of the coil is not required.

Imaging Optics

Figure I-4 is a schematic of the imaging system. A 93 mm focal length, f/2.6 doublet is used to image the sample face through the rotator and polarizer. A 10x microscope objective then enlarges and relays this image to the detector.

Image magnification and therefore resolution across the sample are limited by the light intensity at the detector. Since this system operates in a narrow intensity band centered on a null, light levels are consistently low. The magnification at the detector is approximately 7x. The detector has an active width of 1.27mm; detector resolution is therefore 180 μm. The gradient is scanned by translating the sample along a line 45° to the incident and reflected light. The detector remains fixed and is always conjugate to the on-axis portion of the field. This eliminates the problem of imaging a large field through the rotator and polarizing prism.

Imaging Optics

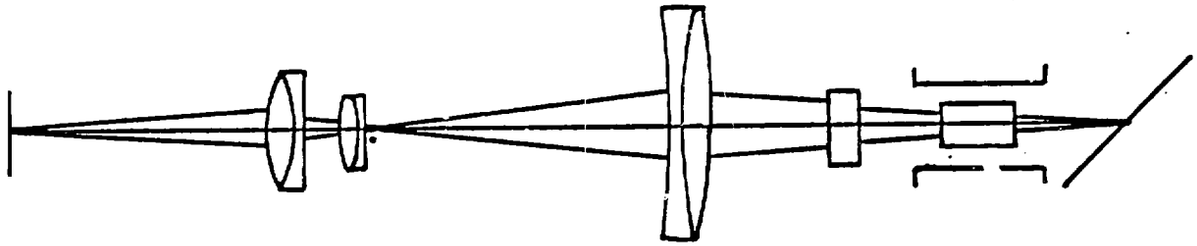

Figure I-4

Detector

The detector used is a PIN-3DP, a planar diffused silicon photodiode manufactured by United Detector Technology. This photodiode is optimized for photovoltaic mode of operation and has a linear response over ten decades of light level. At λ = 6471 Å, responsivity is 80% of peak response. The active area is 1.27mm x 2.54mm.

Electronics

Portions of the electronics in current use in phase-locked interferometry [2,3,4], have been utilized in this system. Because of the limited response of the Faraday rotator coil at high frequency, these electronics have been modified to operate at 500 Hz rather than the original 20 KHz.

Figure I-5 is a block diagram of the system.

The coil is driven by a 500 Hz signal; this modulates the polarization of the light reflected by the sample. The amplitude of the AC driving signal is 10 volts, corresponding to a modulation amplitude of approximately 0.25 degrees. The intensity as a function of time seen by the detector consists primarily of the driving frequency and first harmonic. This signal is amplified and filtered for 500 Hz, the driving frequency.

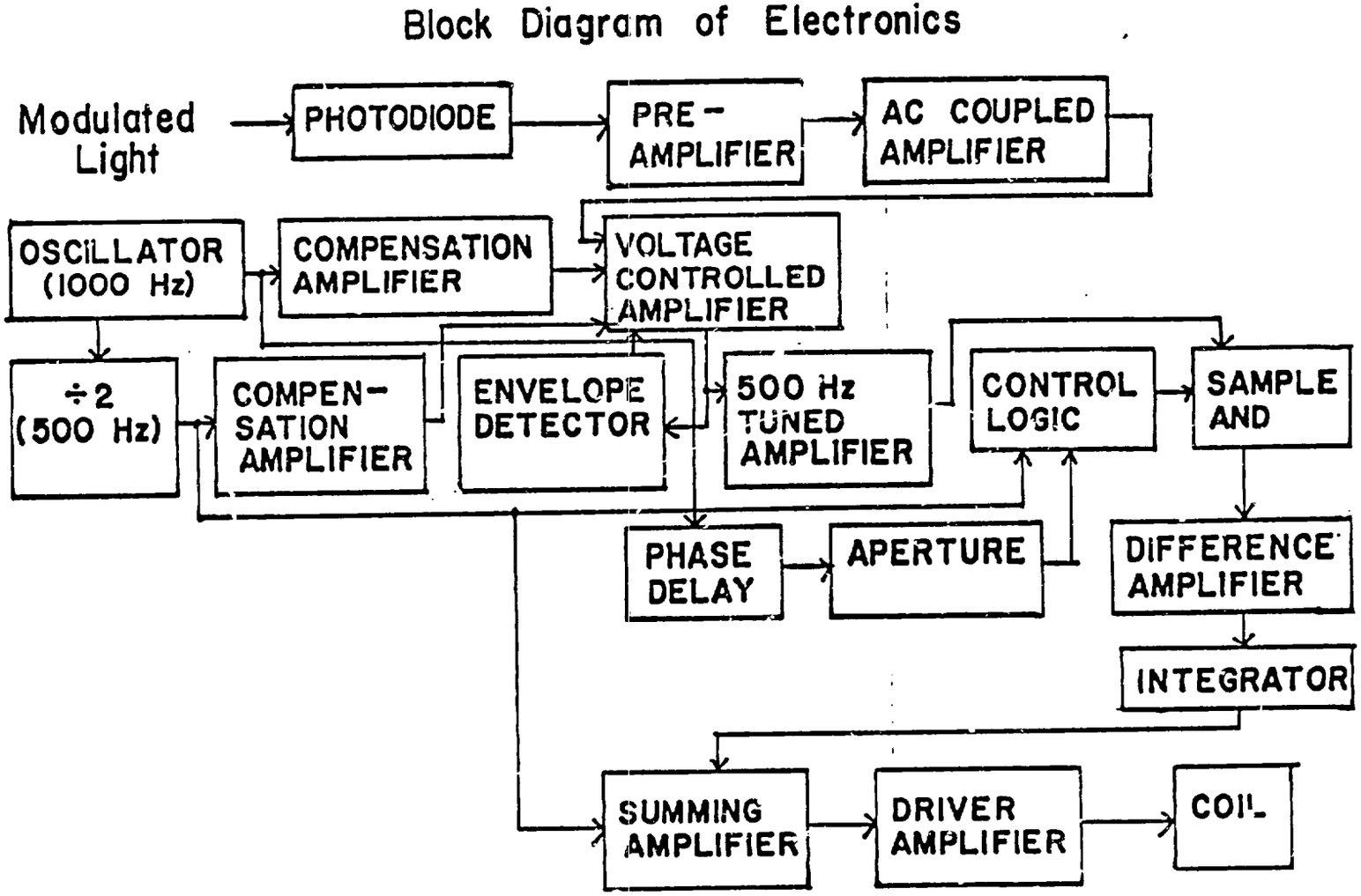
Block Diagram of Electronics
Modulated Light
PHOTODIODE
PRE-AMPLIFIER
AC COUPLED AMPLIFIER
OSCILLATOR (1000 Hz)
COMPENSATION AMPLIFIER
VOLTAGE CONTROLLED AMPLIFIER
÷2 (500 Hz)
COMPEN-SATION AMPLIFIER
ENVELOPE DETECTOR
500 Hz TUNED AMPLIFIER
CONTROL LOGIC
SAMPLE AND
PHASE DELAY
APERTURE
DIFFERENCE AMPLIFIER
INTEGRATOR
SUMMING AMPLIFIER
DRIVER AMPLIFIER
COIL

Figure I- 5

Two sets of sampling pulses, 180° out of phase, are created by the control logic and used to operate an analog switch. This switch, together with a difference amplifier, serves to rectify the 500 Hz signal. After passing through a DC filter, this error signal is integrated and fed back to a summing amplifier to bias the driving signal. This adds a DC bias to the coil, which rotates the plane of polarization of the exiting light. The sign of the bias voltage is such that it will decrease the magnitude of the error signal until it reaches zero. Because the range of the driving signal is limited, the analyzer is previously adjusted so that the intensity signal reaching the detector is close to a minimum. When the condition of zero error signal is reached, the system is locked on a minimum, 90° to the plane of polarization. As the sample is scanned, the bias voltage level to the rotator will change to change the effective angle of the analyzer and remain locked on a null.

The DC voltage is linearly related to change in polarization angle. Over a small range of angles, such as those corresponding to index changes in a gradient index sample, change in polarization angle is approximately linearly related to change in index of refraction. The output DC voltage, calibrated to Δn, is used to drive the vertical axis of an x-y

recorder. The recorder used is an Omnigraphic 2000, manufactured by Houston Instruments. As the gradient is scanned, horizontal position is monitored by a linear transducer manufactured by Schaevitz Engineering. The AC voltage produced by the transducer as a function of position is rectified and fed to the horizontal drive of the recorder. The output of the recorder is a plot of Δn versus position.

I-3 ALIGNMENT AND CALIBRATION PROCEDURE

Angle of Incidence

A 45° right angle prism is used to set the angle of incidence. The prism is placed in the sample holder, hypotenuse parallel to the sample position. One leg of the prism is silvered, and the incident light is retroreflected. The prism has an angle error of approximately 10 seconds of arc.

In practice, the accuracy desired in angle of incidence cannot be obtained entirely by this means because of the limited retroreflection distance. An angle as close as possible to 45° is obtained and then a more accurate value determined by calibrating with a sample of known index of refraction.

Polarizer and Analyzer

The absolute positions of the transmission axes

of the polarizer and analyzer must be determined and related to the scales on the rotary mounts. This is accomplished in two steps.[5] First the polarizer and analyzer, positioned one behind the other, are crossed. Then, inserted in their correct positions in the ellipsometer, they are rotated equal amounts until the emerging light is again extinguished. This will only occur when one polarizer is parallel and the other perpendicular to the plane of incidence. Because the light striking the sample contains only one component of linear polarization, no rotation occurs on reflection and the crossed analyzer extinguishes the beam.

The entire procedure is actually performed iteratively to make best use of the precision of the rotator mounts. When crossing the polarizers in consecutive positions, the fine adjust can always be used for good precision. But for the initial rotations with a reflecting surface in place, the gross adjustment must generally be used because of the limited range of the fine adjust micrometers. The polarizers are then returned to consecutive position and recrossed, since the accuracy of their crossed positions is affected by this last adjustment. When returned to ellipsometer position, the concurrent rotations can now be performed using only the fine adjust. Before this last set of adjustments is made, the position of the first polarizer

relative to the incident light is noted. If its transmission axis is more than 45^{o} from the plane of the incident light, both polarizers are rotated 90^{o}. This insures the maximum signal at the detector, allowing greater sensitivity for the remaining adjustments.

The entire calibration procedure is performed using a modulated input signal and taking advantage of most of the electronics of the operating ellipsometer. The automatic biasing is kept inoperative in order that the signal be only dependent on polarizer and analyzer positions. Two additional changes in the ellipsometer are made in order to increase the intensity level at the detector. A mirror is used in place of the sample to be measured, and the imaging optics are eliminated, leaving a narrower, more concentrated beam.

Coil Calibration

The polarization azimuth, ψ_r, of the reflected light is determined by adding together the analyzer angle (scale setting of null + calibration to actual azimuth + 90^{o}) and the equivalent angle due to any bias voltage applied to the coil. The analyzer angle is read directly from the scale of the mount after manual adjustment to a null (feedback voltage not operating). This provides a measure of absolute azi-

muth and hence absolute **n**, at one position. The most accurate method of calibrating change in voltage with change in angle is to do so directly with the feedback electronics operating. The analyzer is rotated a known amount. The feedback voltage to the coil corresponding to this change in angle produces a vertical line on the x-y recorder. The height of this line, which can be converted from $\Delta\psi_r$ to Δn for a specific sample, is used to calibrate the y-axis for plots of Δn versus position.

I-4 ERROR

Error Analysis

The two values directly used to calculate n are the angle of incidence, θ_i, and the previously defined ellipsometric parameter, ψ. Using the equation

$$n^2 = \sin^2\theta_i + \frac{\sin^2\theta_i \tan^2\theta_i \cos^2(2\psi)}{(1+\sin 2\psi)^2} \qquad \text{(I-1)}$$

it can be shown that

$$dn = \left| \frac{\cos^2(2\psi)}{n\left[1+\sin 2\psi\right]^2} \left[\sin^2\theta_i \tan\theta_i + \tan^3\theta_i\right] + \sin\theta_i \cos\theta_i \right| d\theta_i +$$

$$\left| \frac{2\sin^2\theta_i \tan^2\theta_i}{n} \left[- \frac{\cos 2\psi \sin 2\psi \left[1+\sin 2\psi\right] - \cos^3(2\psi)}{\left[1+\sin 2\psi\right]^3} \right] \right| d\psi \quad . \tag{I-2}$$

For ease in calculation, the $\mp$ in the original equation (I-1) has been eliminated. To provide consistent results, $\psi e^{-i\Delta}$ is actually used in place of ψ.

The actual measured quantities relating to ψ are α and ψ_r, the incident and exiting polarization azimuths. Going one step further,

$$\tan\psi = \frac{\tan\psi_r}{\tan\alpha}$$

$$d\psi = \left| \frac{1+\tan^2\psi\tan^2\alpha}{\sec^2\psi\tan\alpha} \right| d\psi_r + \left| \frac{\sin\psi\cos\psi}{\sin\alpha\cos\alpha} \right| d\alpha \quad . \tag{I-3}$$

Combining (I-2) with (I-3) allows analysis of the error in n as a function of angle of incidence and incident polarization azimuth.

Figure I-6 shows a plot of dn vs. θ_i for fixed

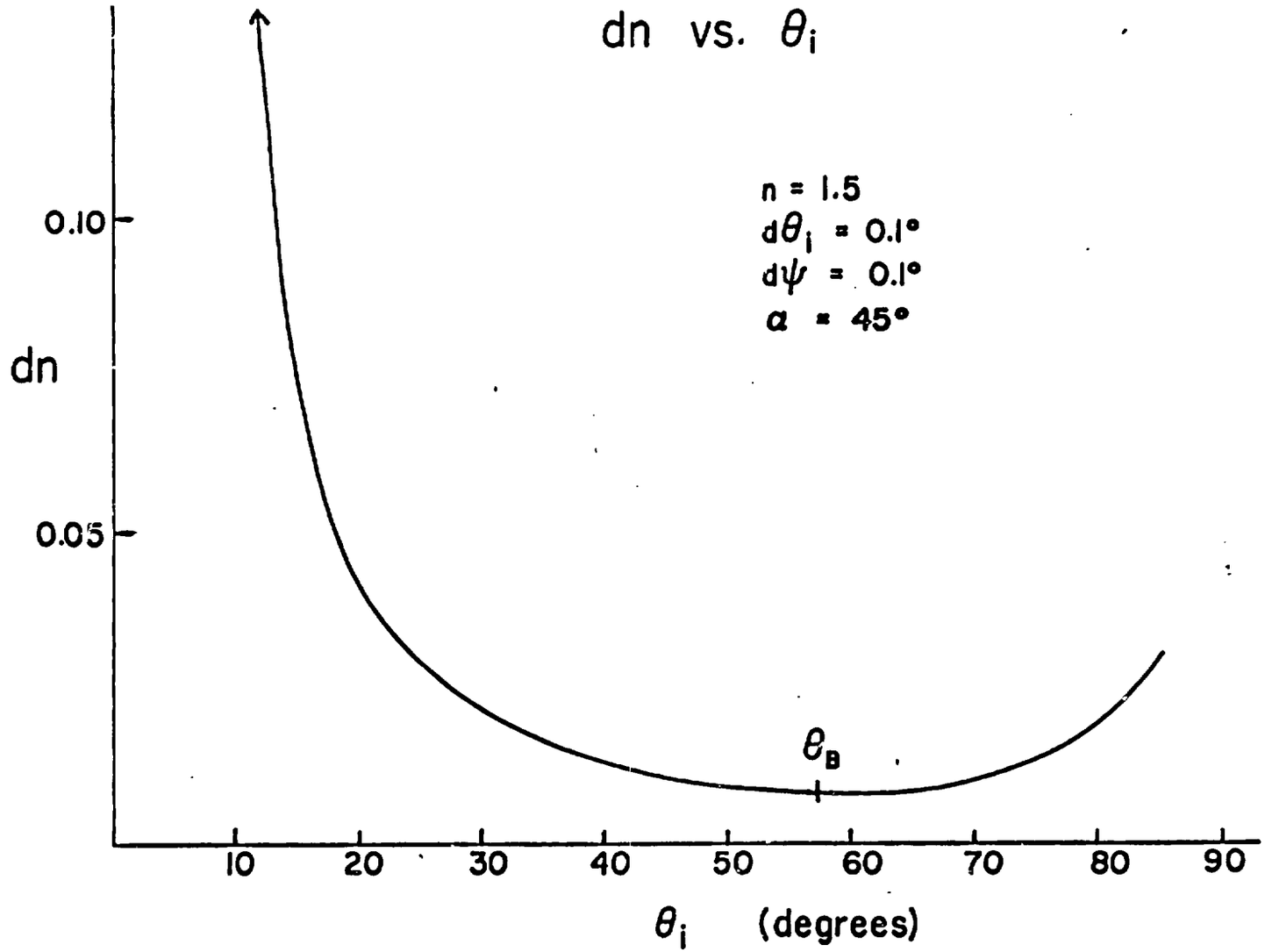
dn vs. θ_i
n = 1.5
$d\theta_i$ = 0.1°
$d\psi$ = 0.1°
α = 45°
dn
0.10
0.05
θ_B
10
20
30
40
50
60
70
80
90
θ_i (degrees)

Figure I-6

error in θ_i, ψ_r, and α. As already noted, dn is smallest for $\theta_i = \theta_B$. For θ_i not too far from θ_B, the increase in dn is not great.

The minimum position for a curve of dn vs. α varies with θ_i and n; for $n = 1.5$ and $\theta_i = 45^\circ$, it occurs at $\alpha = 30^\circ$. This relation is for fixed errors in the measured values; change in α actually affects the level of the AC signal which in turn affects the accuracy of the measurement. It is therefore difficult to separate the effect of α on error in n.

The calculation of n is approximately equally sensitive to errors in angle of incidence and in incident and emerging polarization azimuths. Tables I-1 and I-2 show how the value of n is affected for some typical errors in θ_i and in α and ψ_r.

Sources of Error

The accurate determination of index of refraction in an ellipsometer is strongly dependent on measurement capabilities. For instance, to calculate n in a glass sample to better then 0.5%, both angle of incidence and polarizer and analyzer angles must be known to 0.01°. In addition to the limitations of the particular setup and hardware in measuring these angles, there are many inherent sources of system error.

Effect of Error in θ_i on n

($\theta_i = 45^o$)

$d\theta_i$ (deg.)	dn (n=1.50)	dn (n=2.00)
0.01	0.0007	0.0013
0.02	0.0013	0.0026
0.05	0.0033	0.0064
0.10	0.0067	0.0129
0.20	0.0134	0.0257
0.50	0.0335	0.0643
1.00	0.0669	0.1287

Table I-1

Effect of Error in α and ψ_r on n

($\theta_i = 45^o$, $\alpha = 45^o$)

$d\alpha$, $d\psi_r$(deg.)	dn (n=1.50)	dn (n=2.58)
0.01	0.0008	0.0029
0.02	0.0015	0.0059
0.05	0.0038	0.0146
0.10	0.0076	0.0293
0.20	0.0152	0.0586
0.50	0.0381	0.1464
1.00	0.0761	0.2929

Table I- 2

Beam deviation due to imperfect components is a common source of trouble. A slight amount of wedge between the end faces of the polarizing prisms can be significant. The prisms used in this system have been aligned parallel to 0.5 minutes of arc. The rotating mounts and adapters holding the prisms are not very well engineered, however, and make it difficult to orient the polarizers perpendicular to the beam with a high degree of precision. This causes some problems with angle of incidence, beam rotation, and efficiency of polarization.

Variation among samples is another cause of angle of incidence error. The initial calibration of this angle is to the back of the sample holder. Any wedge in the sample causes the actual angle of incidence at the front surface to differ. This system is thus limited to measuring samples with plane parallel faces.

Measurement of polarization azimuth can be divided into two problems: location of the transmission axes of the polarizers and the experimental determination of the null condition. Initial alignment of the polarizer transmission axes can be done quite accurately. The limitation of the mount adjustments is 1 minute of arc and the electronics are

operating under more ideal conditions than in sample measurement. The actual calibration can only be done to 0.1^{o} because this is the smallest division that can be read on the circular scale. Precision is also lost when the polarizers are rotated to their desired positions because this must generally be done with the gross adjustment. The inadequate precision of the polarizer mounts is the primary limitation in measuring absolute azimuth; experimental noise is small compared with this.

The situation changes when considering relative azimuth measurements. Change in azimuth from one portion of the sample to another is monitored either with a voltage output (electronic biasing) or with the fine adjust on the analyzer (manual biasing). In either case, optical and electronic noise limits the accuracy of the measurement rather than component inadequacies.

Other potential problems to consider in ellipsometry are multiple reflections, residual birefringence in the optical components, surface roughness, polishing phenomena, and surface changes due to aging. Multiple reflections and birefringence both affect the polarization azimuth of the emerging light; in addition,

any birefringence in the system adds ellipticity to the form of the polarization. The present system has a small number of optical components; there are no sources of any significant birefringence. The biggest problem concerning multiple reflections was found to be reflection off the back surface of the sample. Interference fringes cause intensity variations which can be picked up by the detector if the electronics are not working perfectly. The back surfaces were rough ground or index matching fluid used to eliminate this problem.

Large-scale surface roughness causes scattering of light, decreasing the signal to noise ratio. Fenstermaker and McCrackin[6] have done a theoretical study of the effects of roughness $<< \lambda$. The apparent value of n for glass showed very little variation from the actual value compared to the other materials measured.

Surface polishing affects the measured index of refraction of optical materials when a surface dependent technique is used. The index of the polish film can be considerably different from that of the bulk material.[7] The slurry medium can cause leaching of metal ions out of the surface layer, thus decreasing the index. This is particularly true in alkali glasses. In some cases, high local pressures

exerted on the surface may increase the index through densification.

Experimental Procedure and Results

I-5 ABSOLUTE INDEX MEASUREMENT

Measurement of absolute index of refraction is a simple matter once the instrument has been aligned and calibrated. The polarizer is adjusted to the desired input polarization azimuth. Based on the discussions in the previous sections, 45° is used in most cases. The sample is cleaned with acetone and then placed in its holder, being careful to align it against the back of the holder. The automatic locking (nulling) feature of the electronics is turned off in order that the signal can be nulled by analyzer adjustment. The AC signal at the driving frequency is observed on an oscilloscope. The analyzer is rotated back and forth in order to check signal response and phase shifting at the null. Once an adequate signal is insured, the analyzer is rotated until the amplitude of the signal reaches zero. The analyzer angle corresponding to this null condition is read from the scale of the analyzer mount. The previously determined calibration factor is added to this angle to obtain the absolute null angle; 90° is then added to get ψ_r, the emerging polarization azimuth. The

ellipsometric parameter, ψ, is calculated from

$$\tan\psi = \frac{\tan\psi_r}{\tan\alpha}$$

if the incident polarization is not at 45°. The above relationship allows ψ to take on either sign (the $e^{i\Delta}$ factor has been omitted from the right hand side of the equation). With this convention, n can be calculated for any θ_i using

$$n^2 = \sin^2\theta_i + \frac{\sin^2\theta_i \tan^2\theta_i (\cos^2 2\psi)}{(1+\sin 2\psi)^2} \quad . \qquad \text{(I-4)}$$

I-6 ABSOLUTE INDEX RESULTS

Absolute index of refraction was measured on three known samples to test the performance of the ellipsometer. These are Schott SF64 glass, a Bausch & Lomb alumina silicate glass, and ZnSe manufactured by CVD, Inc. Measurements were taken on many different occasions to insure a representative sampling of error.

Table I-3 summarizes the results. Values which are grouped together represent measurements at different input polarizations; the sample was not

Absolute Index Measurements

($\theta_i = 45^\circ$)

material	actual n	measured n
SF64 Glass	1.700	1.701
		1.710
B & L Glass	1.500	1.450
		1.475
		1.471
		1.492
		1.495
		1.480
ZnSe	2.583	2.550
		2.516
		2.654
		2.573
		2.623
		2.571
		2.532
		2.573
		2.560

Table I-3

realigned between these readings. Error in θ_i and the absolute calibration of α and ψ_r remain constant. A comparison of any set of these values provides information on the repeatability of adjusting the polarizer and analyzer. Values which are spaced correspond to measurements between which the sample was reinserted in position. Angle of incidence is not constant for these and adds a considerable amount of error. All of the results quoted are based on assuming $\theta_i = 45^o$.

Another set of measurements were taken consecutively on six different samples. These were two different samples of the Bausch and Lomb glass, the ZnSe sample, a piece of CdS manufactured by CVD, Schott BK-7 glass, and the homogeneous region of a fiber preform manufactured by Corning. The results are averaged over six to nine readings at two to three input polarizations each. The first set of index values is calculated assuming $\theta_i = 45^o$. These values are all quite low. This implies a systematic error. The polarizer calibrations are not affected during the measurement procedure and previous measurements showed both high and low values of index. It therefore seems that the angle of incidence significantly differs from 45^o and is adding

this error to all the measurements.

For each sample, the θ_i needed to obtain the correct n was calculated. The average of these values was then used as the calibrated θ_i to recalculate n in each case. Table I-3 summarizes these results. The need to calibrate θ_i from measurement of known samples is obvious.

I-7 ERROR ANALYSIS - ABSOLUTE INDEX

Equations I-2 and I-3 are used to calculate predicted error in n based on estimated errors in the measurement of θ_i, α, and ψ_r. The results are based on $\theta_i = 45^\circ$ and $\alpha = 45^\circ$. The error in α and ψ_r is on the order 0.15° as the scales can only be read to 0.10°. Error in θ_i can be as large as 0.25°, even with calibrations to known samples, because of variation in the parallelism of the samples and in how they are set in the holder. Table I-4 lists the expected errors in n for the different indices measured based on these estimates. Figures are also given based on an error of 1.0° in θ_i to cover the examples in which θ_i was assumed to be 45°. The values of n given in Tables I-2 and I-3 mostly fall within these errors.

The absorption coefficients for ZnSe and CdS

Absolute Index Measurements

(calibrated θ_i)

material	actual n	measured n (before calibration)	measured n (after calibration)
B & L (1)	1.500	1.436	1.522
B & L (2)	1.500	1.436	1.521
BK-7	1.515	1.434	1.518
Corning	1.470	1.412	1.495
ZnSe	2.583	2.373	2.532
CdS	2.440	2.215	2.363

Table I-3

Predicted Error in Absolute Index

n	dn ($d\theta_i = 0.25^o$)	dn ($d\theta_i = 1.0^o$)
1.470	0.027	0.076
1.500	0.028	0.078
1.515	0.029	0.080
1.700	0.036	0.095
2.440	0.069	0.159
2.583	0.076	0.172

Table I-4

are approximately $14m^{-1}$ and $88m^{-1}$ at $\lambda = 6471$ Å. The values of $n\kappa$, the imaginary part of the complex index of refraction, are approximately 1.4×10^{-6} and 9.5×10^{-6}. These are small enough to assume a real index of refraction and allow calculation of that index from Equation I-4. If κ were not negligible, determination of Δ in addition to ψ would be necessary to calculate n and κ.

I-8 INDEX PROFILE MEASUREMENT

To measure index of refraction profiles, the gradient region of the sample is scanned across the field of view of the detector. Preliminary scans are done to determine an appropriate analyzer setting. Because the range of the DC biasing of the coil is limited, the analyzer must be set so that the signal can be nulled electronically at all positions along the gradient. The sample stage is then adjusted so that the detector is conjugate to the edge of the gradient region. The sample stage is scanned to produce a plot of Δn versus position as described in section I-2. Multiple scans are done for each gradient to insure repeatability. Calibrations of $\Delta\psi_r$ to voltage (see section I-3) are performed periodically and whenever any adjustments are made

in the electronics.

I-9 INDEX PROFILE RESULTS

Figures I-7 through I-9 are plots of Δn versus position for a ZnSe - ZnS gradient. This sample was manufactured by Raytheon and consists of deposited layers of varying composition ranging from pure ZnSe to pure ZnS. The Δn at 6471 Å is 0.23 and extends approximately 1.2 mm into the sample.

Figures I-7 and I-8 are gradient scans at two different positions on the sample. The shape of the gradient varies considerably. This is partly because the deposited layers are not uniform. There is also some variation due to the fact that there is no mechanism for translating either the sample or the detector vertically. The sample is manually adjusted in the holder to change position; this allows for differences in how parallel the gradient is to the scan direction. It is also apparent that there is considerable variation in the homogeneous region of the sample. This is primarily a result of surface effects such as polishing; there may also be a small degree of detectable intensity variations. The total measured Δn is correct to within the errors of the homogeneous region. The

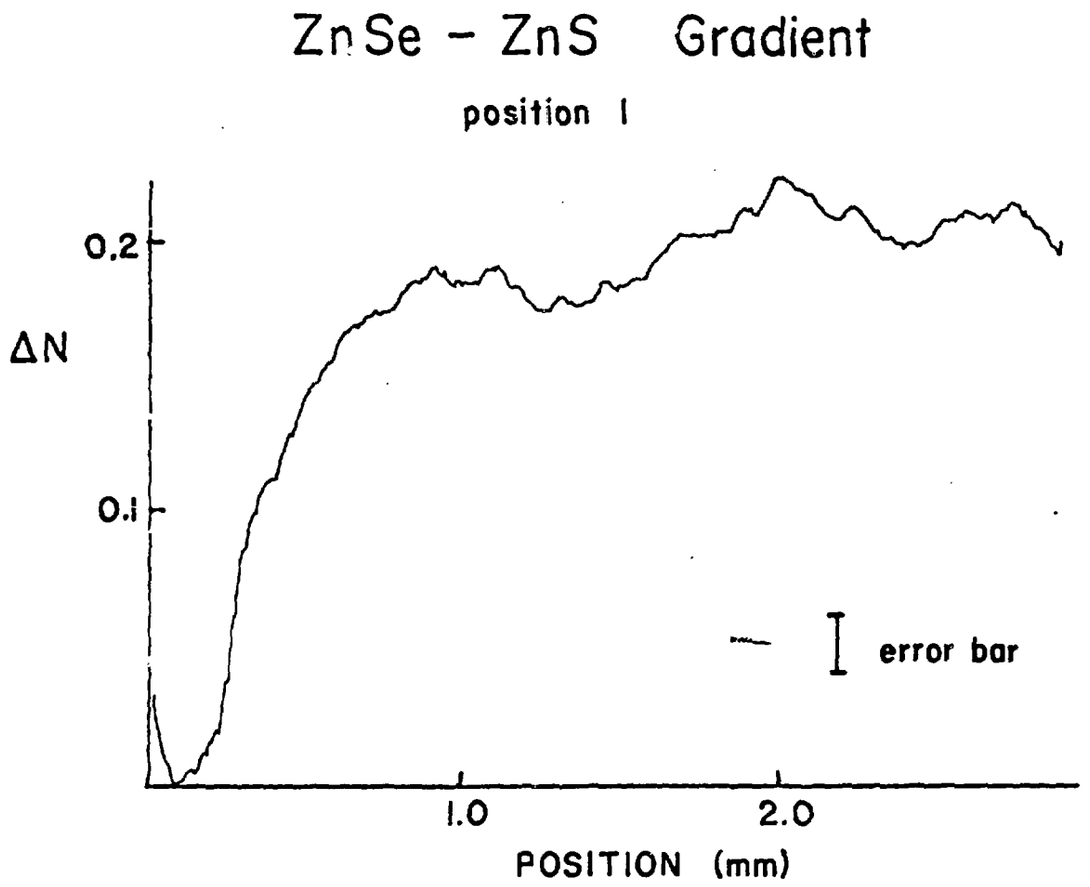
ZnSe - ZnS Gradient
position 1
0.2
ΔN
0.1
error bar
1.0
2.0
POSITION (mm)

Figure I-7

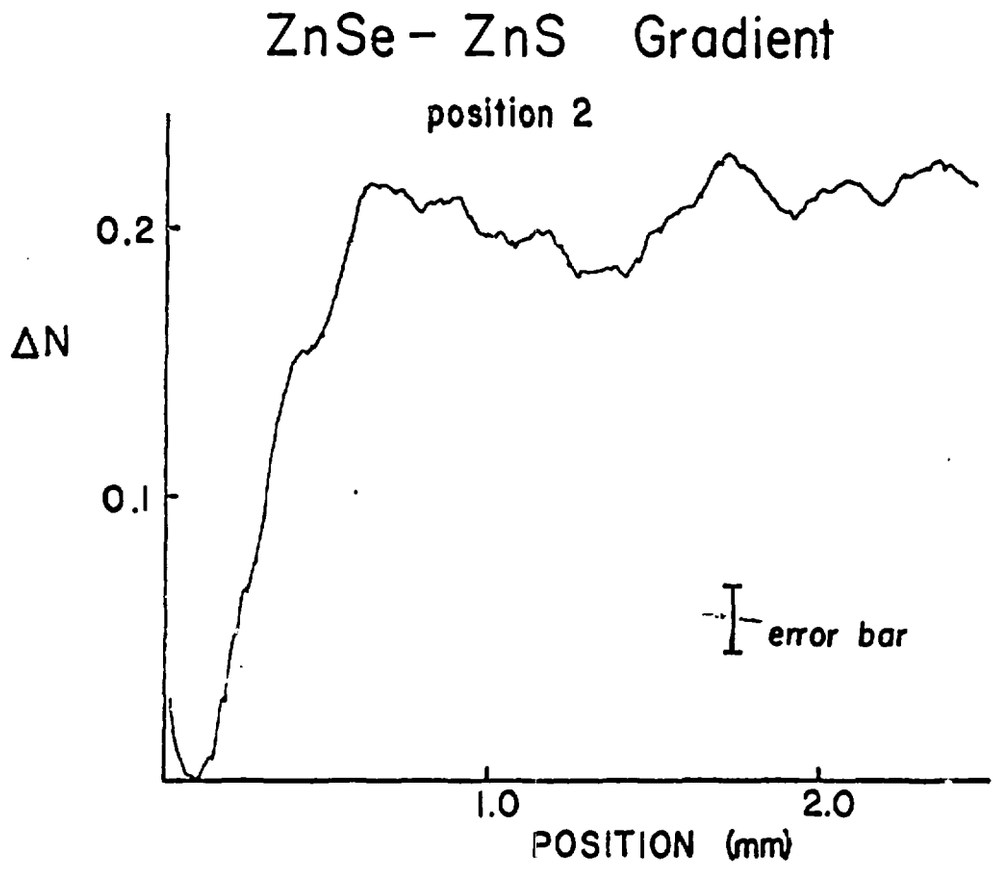
ZnSe - ZnS Gradient
position 2
0.2
ΔN
0.1
error bar
1.0
2.0
POSITION (mm)

Figure I-8

actual layers of constant index are smaller than the resolution of the system. There is thus considerable averaging in the profiles.

Figures I-9 and I-10 demonstrate repeatability of the gradient scans at a particular position.

Figure I-11 is a plot of a radial gradient in a fiber preform manufactured by Corning. The gradient has a parabolic profile with a measured Δn of 0.017 from the homogeneous outer region to the center. The scan does not necessarily traverse the exact center of the gradient because of the limited adjustability of the components.

Figure I-12 illustrates a radial gradient produced at the University of Rochester. It is the result of a lithium diffusion into a Bausch and Lomb alumina silicate glass. The gradient extends to the center of the sample. Previous measurements indicate a Δn of 0.013 from the center to the edge, the radius being 5.0 mm. Measurement on this system is done in pieces because of the limited range of the position sensor. Over a distance of 4 mm from the center, the Δn measured is 0.011.

Index profile measurements were attempted on gradient samples made by silver diffusion into Bausch

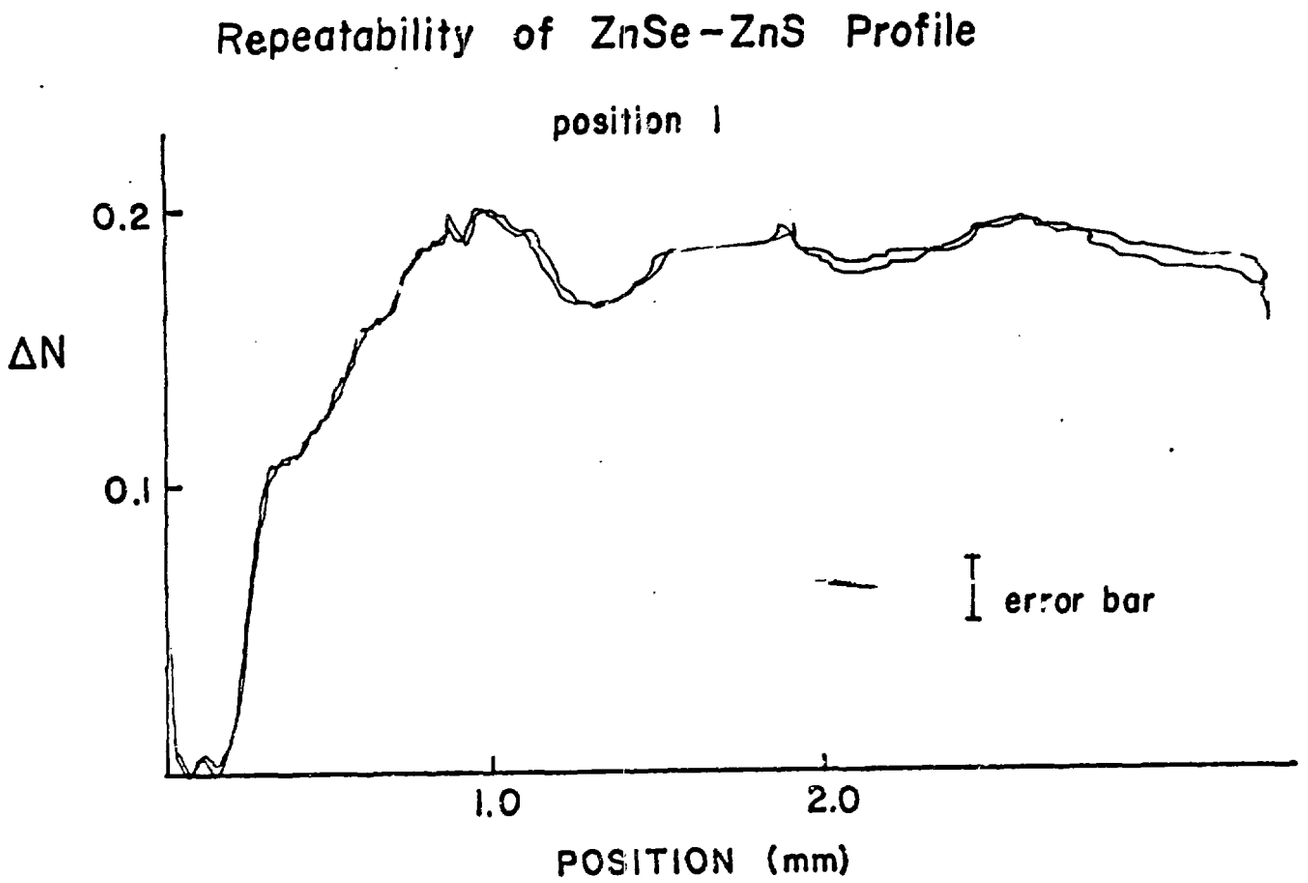
Repeatability of ZnSe-ZnS Profile
position 1
0.2
ΔN
0.1
error bar
1.0
2.0
POSITION (mm)

Figure I-9

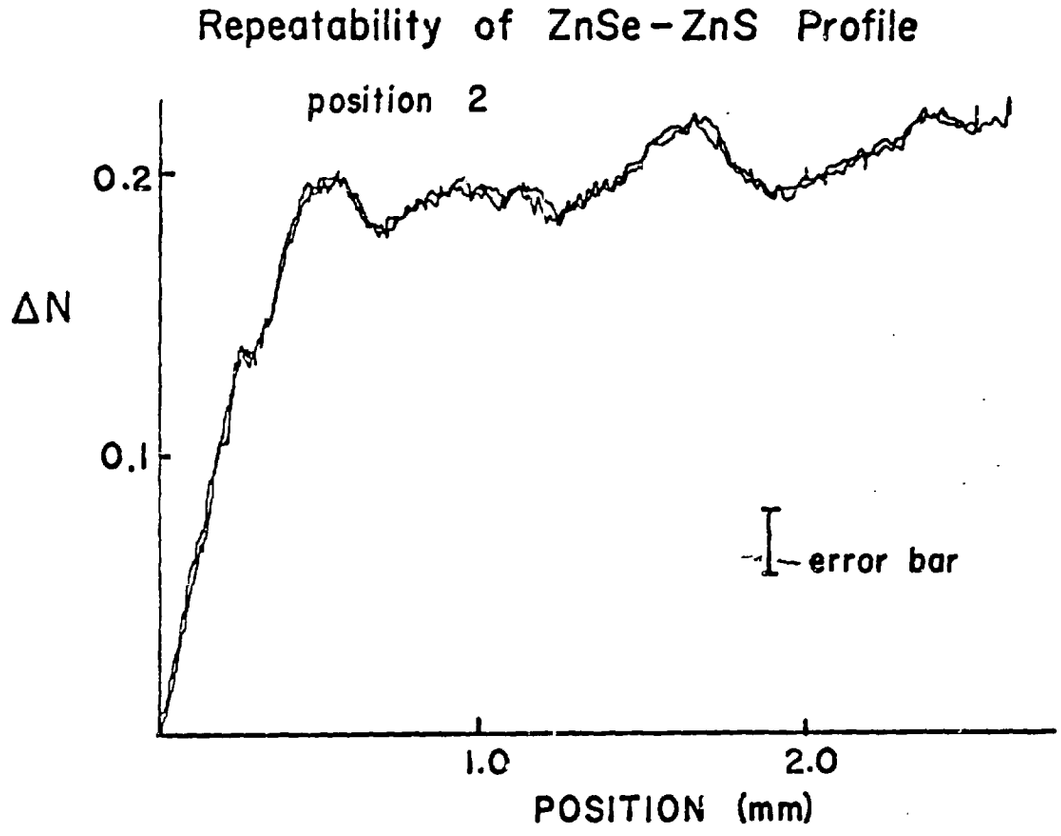
Repeatability of ZnSe-ZnS Profile
position 2
0.2
ΔN
0.1
error bar
1.0
2.0
POSITION (mm)

Figure I-10

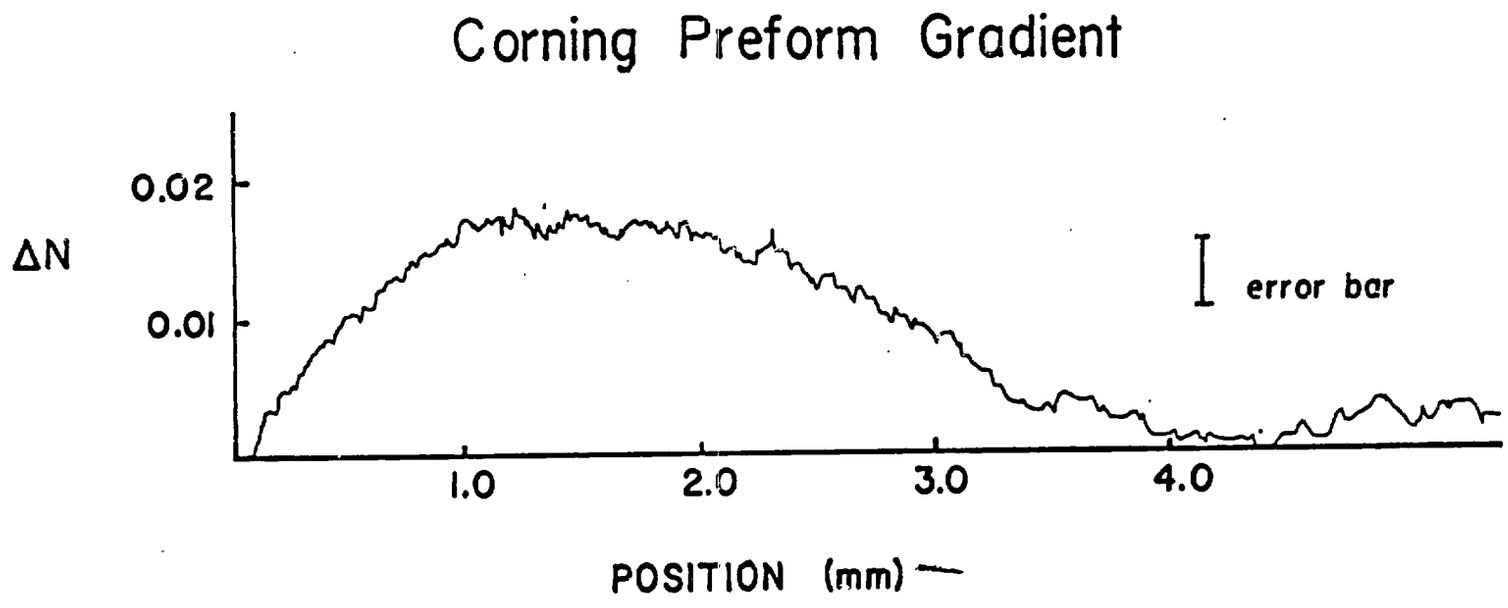
Corning Preform Gradient
ΔN
0.02
0.01
error bar
1.0
2.0
3.0
4.0
POSITION (mm)

Figure I-11

DPR-01 Radial Gradient

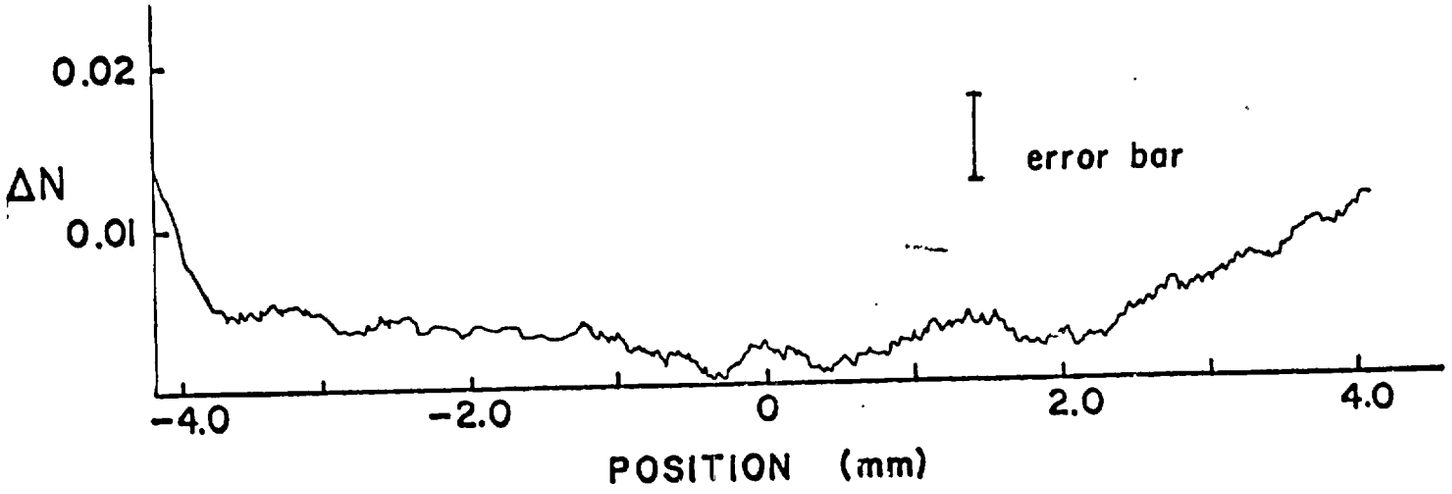

Figure I-12

and Lomb glass. The results did not agree with the expected profiles. These samples appear to have surface degeneration problems, i.e. leaching of the diffused silver ions and possibly the original sodium ions. The surface changes make it impossible to measure bulk index of refraction by this method.

I-10 ERROR ANALYSIS - RELATIVE INDEX

When measuring relative index, only the error in relative azimuth needs to be considered. Relative index, Δn, is not directly related to relative azimuth, $\Delta\psi_r$. To estimate errors in Δn, the relative error in ψ_r as the gradient is scanned is used in Equations I-2 and I-3. The result is then considered to be $d(\Delta n)$ rather than dn.

The accuracy of $\Delta\psi_r$ measurement depends on the ability of the electronics to follow changes in polarization and the accuracy of the calibration of the change in the bias voltage to $\Delta\psi_r$. The change in polarization azimuth over a gradient region is quite small. In the case of the ZnSe-ZnS gradient it is approximately 1.6°; for gradients in glass this change is generally 0.5° or less. The changes over a small portion of the gradient are very difficult to detect, even under ideal conditions. Because there is some

tendency to detect intensity variations, the noise in the bias voltage is even worse. This imperfection also affects the calibration of the change in the bias voltage to $\Delta\psi_r$. Under the current experimental conditions, the error in $\Delta\psi_r$ is estimated to be at least 0.1°. This corresponds to a Δn error of approximately 0.005 for glass gradients and 0.015 for the ZnSe-ZnS gradient. In a glass gradient with a total index change of 0.025, this error is 20% of the index change, and for the ZnSe-ZnS gradient, it is 6% of the total index change.

The accuracy of the calibration of Δn to $\Delta\psi$ depends on absolute n and the magnitude of Δn. For n = 1.5 to 1.52 the linearity of Δn with $\Delta\psi$ is approximately 3% (total Δn error = 0.0006). For n = 2.58 to 2.35 the error in linearity increases to 20% (total Δn error = .0015). The proportionality factors between Δn and $\Delta\psi$ were averaged over the index range for each gradient. This should eliminate error due to this calibration in determining total Δn; the actual Δn profile could have errors up to half the above figures from this source. In the case of a glass gradient, this is negligible compared to noise error. For the ZnSe-ZnS gradient, it can add substantially to the error in profile shape.

Table I-10 summarizes the above discussion. For a base index of 1.5 and Δn of 0.020, measured Δn can vary from 0.015 to 0.025. For n = 2.58, Δn = 0.23, Δn may range from 0.215 to 0.245.

Under normal test conditions, the magnitude of Δn and the base index are not known a priori. Change in index cannot be plotted directly, at least for high index samples, because of the $\Delta\psi$ to Δn calibration problem. The determination of Δn is more dependent on accurate absolute n measurement. Instead of determining Δn directly from $\Delta\psi_r$, $\Delta\psi_r$ is added to an initial absolute ψ_r for each point. The total ψ_r at each point is then used to calculate corresponding values of absolute n.

I-11 SYSTEM LIMITATIONS AND IMPROVEMENTS

This system demonstrates feasibility of measuring gradient index samples using ellipsometry. To be useful, however, much greater accuracy is needed in both Δn and n measurements. In particular, absolute index should be measurable with less error than the degree of gradient to be resolved. This would allow determination of absolute index profiles of unknown samples. As it stands now, change in index can be measured only if the base index is known.

Predicted Error in Relative Index

	n = 1.50	n = 2.58
noise error	0.0050	0.015
calibration error	0.0003	0.007
error in total Δn	0.0050	0.015
error in Δn shape	0.0053	0.022

Table I-5

There are three major areas of improvement needed in this system. The first is improvement in the measurement of angle of incidence and polarization azimuths for more accurate determination of ...ute index. Incorporation of the system into a commercial ellipsometer would provide much greater accuracy and also adjustability of angle of incidence. A more precise sample holder should be designed to allow for better consistency when changing samples. The polarizers should be mounted in rotators with more sensitive large scale adjustment for more accurate measurement of polarization azimuth. In addition, there should be better adjustability of the polarizer in the mount, to insure that the polarizers are perpendicular to the incident beam.

The second improvement needed is in gradient resolution. There are two conflicting problems: spatial resolution, which requires greater magnification, and polarization (and hence Δn) resolution, which requires higher AC signal level. With enough increase in signal modulation, both can be improved over the current system. The first step is to redesign the coil. Separate coils for DC rotation and AC modulation should be used. A low inductance coil for AC modulation will

greatly increase the amplitude of the AC signal; the increased signal to noise ratio will allow for detection of smaller changes in polarization. The amplifier for the coil can also be stepped up for signal improvement.

A third problem in this system is the limited adjustability of the sample holder and detector. One or the other, preferably the sample holder, should have two-dimensional precision translation. This is needed to control what area of the sample is being measured and is particularly important for radial gradients.

References

[1] B. D. Cullity, Introduction to Magnetic Materials, (Reading, Massachusetts: Addison Wesley Publishing Co., 1972), p. 26.

[2] D. C. Leiner and D. T. Moore, "Real-time phase microscopy using a phase-lock interferometer," Rev. Sci. Instrum., 49, 1701, (1978).

[3] G. W. Johnson, D. C. Leiner and D. T. Moore, "Phase-locked interferometry," Opt. Engr., 18, 46, (1979).

[4] D. C. Leiner, Phase-lock Interference Microscopy, M. S. Thesis, University of Rochester, 1977.

[5] M. J. Dignam and M. Moskovits, "Aximuthal misalignment and surface anisotropy as sources of error in ellipsometry," Appl. Opt., 9, 1868, (1970).

[6] C. A. Fenstermaker and F. L. McCracken, "Errors arising from surface roughness in ellipsometric measurement of the refractive index of a surface," Surf. Sci., 16, 85, (1969).

[7] H. Yokota, H. Sakata, M. Nishibori, and K. Kinoshita, "Ellipsometric study of polished glass surfaces," Surf. Sci., 16, 265, (1969).

DISTRIBUTION

	No. of Copies
IIT Research Institute ATTN: GACIAC 10 West 35th Street Chicago, Illinois 60616	1
US Army Materiel Systems Analysis Activity ATTN: DRXSY-MP Aberdeen Proving Ground, MD 21005	1
DRSMI-LP, Mr. Voigt	1
DRSMI-X	1
DRSMI-R, Dr. McCorkle	1
-RG	1
-RGC	20
-RGT	1
-REO	1
-REI	1
-RE	1
-RR, Dr. Hartman	1
-RR, Dr. Guenther	1
-RR, Dr. Gamble	1
-RN	1
-RPR	15
-RPT (Record Set)	1